Estimation of atmospheric land-surface interactions of irrigated broad-acre agriculture in inland Australia

Camilla Vote

BAppSc (Wine Science) / BAppSc *(*Environmental Science) (Hons)

Charles Sturt University

A thesis submitted to Charles Sturt University for the degree of Doctor of Philosophy

School of Environmental Sciences

Faculty of Science

Charles Sturt University

September 2013

TABLE OF CONTENTS

LIST OF FIGURES

LIST OF TABLES

CERTIFICATE OF AUTHORSHIP

I hereby declare that this submission is my own work and to the best of my knowledge and belief, understand that it contains no material previously published or written by another person, nor material which to a substantial extent has been accepted for the award of any other degree or diploma at Charles Sturt University or any other educational institution, except where due acknowledgement is made in the thesis. Any contribution made to the research by colleagues with whom I have worked at Charles Sturt University or elsewhere during my candidature is fully acknowledged. I agree that this thesis be accessible for the purpose of study and research in accordance with normal conditions established by the Executive Director, Library Services, Charles Sturt University or nominee, for the care, loan and reproduction of thesis, subject to confidentiality provisions as approved by the University.

Name: Camilla Vote

Date:

Signature:

ACKNOWLEDGEMENTS

Firstly, I would like to formally acknowledge the financial support for this study which was provided by Charles Sturt University through the Australian Post-Graduate Award. Top-up funding was also received from the National Water Commission of Australia as part of the Coleambally Water Smart Australia project. An additional post-graduate travel scholarship was received from the National Climate Change Adaptation Research Facility (NCCARF) to attend the Climate Adaptation Futures Conference in 2010.

Secondly, I would like to thank my Principal Supervisor, Mohsin Hafeez, for granting me the opportunity to undertake this study. I would also like to thank my co-supervisors, Philip Charlton and Andrew Hall, for their constant availability, assistance and guidance with respect to data processing, analysis and interpretation.

Thirdly, I would like to thank Rolf Faux for his assistance with instrument deployment and data collection; James Cleverly, Peter Isaac and Ray Leuning and all members of the OzFlux community who have helped me along the way; without this critical assistance, I would still be processing data.

I would also like to thank the landholders in the Coleambally Irrigation Area who assisted in this study by providing unlimited access to their properties; other staff and students of the former International Centre of Water for Food Security (IC Water) who collated ancillary data; and Michael Wilson and Austin Evans of Coleambally Irrigation Co-Operative Limited who provided access to essential crop water use information for the region.

And finally, I would like to thank the Stranger for all her support, particularly for shifting from London to Wagga Wagga so that I can complete this study. I know it sounded like a curse at the time, but it appears you quite like the country life, no?

RESEARCH PUBLICATIONS AND CONTRIBUTIONS

Journal publications

Vote, C., Charlton, P. & Hall, A. (2013). Geo-statistical regression analysis of water and carbon flux response of irrigated broad-acre crops to climatic drivers grown in an Australian semi-arid environment in a year with record high precipitation. *Manuscript submitted for publication.*

Vote, C., Hall, A. & Charlton, P. (2013). Seasonal water, carbon and energy fluxes of irrigated broad acrecrops in an Australian semi-arid climate zone. *Manuscript submitted for publication.*

Liu, G., Hafeez, M., Liu, Y., Xu, D., & **Vote, C**. (2012a). A novel method to convert daytime evapotranspiration into daily evapotranspiration based on variable canopy resistance. *J. Hydrol., 414–415* (0), 278-283. doi: 10.1016/j.jhydrol.2011.10.042

Liu, G., Liu, Y., Hafeez, M., Xu, D., & **Vote, C**. (2012b). Comparison of two methods to derive time series of actual evapotranspiration using eddy covariance measurements in the southeastern Australia. *J. Hydrol., 454–455* (0), 1-6. doi: 10.1016/j.jhydrol.2012.05.011

Conference proceedings and publications

Vote, C., Hafeez, M., Charlton, P., & Hall, A. (2012). *Carbon capture of irrigated Australian broad-acre crops*. Paper presented at the Climate adaptation in action 2012, June 26 – 28, Melbourne, Australia.

Vote, C., Hafeez, M., Charlton, P., & Faux, R. (2011). *Estimation of water and carbon footprints of Australian irrigated agricultural systems.* Paper presented at the IUGG Earth on the Edge: Science for a Sustainable Planet, June 28 - July 7, Melbourne, Australia.

ABSTRACT

With increasing climate variability and decreasing water resources, the productivity of global agricultural systems is uncertain. This is particularly relevant in semi-arid regions dependent on irrigation where the response of the water and carbon balance to changes in temperature and increasing levels of atmospheric carbon dioxide is unclear.

In Australia, many irrigation systems exist in the semi-arid, southern regions of the Murray Darling Basin and are of significant economic value, accounting for 31% of the gross value of agricultural production (ABS, 2012a). These same systems also account for the majority (54%) of national water consumption (ABS, 2012c). As agricultural production is sensitive to changes in climate, the forecast increased magnitude and frequency of disruptive climatic variability due to the enhanced greenhouse effect may negatively impact productivity through alterations of crop physiology, decreased yield and increased incidence of pests and disease. Furthermore, the behaviour and response of the water and carbon balance to increasing temperatures and atmospheric carbon dioxide concentration in these systems is unknown. Therefore, this study aims to quantify water and carbon dioxide fluxes of commonly irrigated broad-acre crops in Australia and investigate the influence of environmental variables on the mass and energy exchange of these systems.

The Coleambally Irrigation Area in south-western New South Wales was selected for this study. The mass and energy exchange of three of the major summer and winter crops (maize, rice and wheat) commonly grown in this region were investigated through the use of eddy covariance technologies. The impact of environmental variables on water and carbon dioxide flux was examined through the application of geostatistical regression models. These modelling techniques in conjunction with an estimation of biophysical water

productivity enabled the investigation of the relationship between water and carbon dioxide fluxes of these particular cropping systems.

In terms of evapotranspiration, the results showed that the largest amount of water lost to the atmosphere was through the production of rice; the cumulative total over the growing season was 783 mm. According to the Food and Agriculture Organisation, the approximate values of seasonal water use of rice generally ranges from 400 – 700 mm (Brouwer & Heibloem, 1986). Winter wheat production accounted for the least amount of water lost; the cumulative total over the growing season was 389 mm and was typical of seasonal water use of irrigated maize grown in Australia (Sadras & McDonald, 2012).

As a C4 plant, maize was found to account for the greatest amount of total carbon accumulation, or gross primary productivity, over the course of the growing season; the cumulative total of gross primary production was 1952 g C/m^2/year and were higher the range of values reported globally (789 g C/m^2/year – 1796 g C/m^2/year; Suyker & Verma, 2012; Yan et al., 2009b). Due to decreased incoming solar radiation and air temperature, and thus, decreased biomass production, winter wheat accounted for the least amount of total carbon capture; the cumulative total of gross primary production was 1367 g C/m^2/year and is within the reported range of 778 g C/m^2/year and 1716 g C/m^2/year (Dufranne et al., 2011; Gilmanov et al., 2003).

The results of the geostatistical regression modelling showed that net radiation, air temperature, wind speed and rainfall all had an impact on evapotranspiration rates of the two summer crops, maize and rice. It was found that net radiation was primarily responsible for the evapotranspiration rates of the winter wheat crop. Carbon uptake during the summer was primarily driven by wind speed and evapotranspiration rates. Net radiation was the major driver of gross primary production of the winter wheat crop.

In terms of biophysical water productivity, maize proved to be the most productive (14.4 g C/m^2); winter wheat was the least productive (2.1 g C/m^2).

The results of this study serve to fill the knowledge gap with respect to the effect of the climate on mass and energy exchanges of broad-acre cropping systems in Australian dryland irrigation areas. The estimation of the water and carbon dioxide fluxes of these systems and the investigation of their environmental influences provide some understanding of the behaviour of these systems.

1 INTRODUCTION

1.1 Overview

Increases in population and income per capita are leading to a demand for food twice the volume of what is currently consumed (Clay, 2011). With this increased demand for agricultural production, croplands and grazing pastures are fast becoming one of the largest terrestrial biomes, occupying about 40% of the Earth's surface (Foley et al., 2005; Hatala et al., 2012b; Ramankutty et al., 2008) with some studies predicting that the future global cropland area will need to double in size to compensate for this demand (Yu et al., 2012).

Inevitably, changes in land cover and land use to enable agricultural expansion will affect local surface mass and energy exchange by influencing the way in which radiative fluxes are partitioned at the surface, leading to a local temperature change (Foley et al., 2005; Krishnan et al., 2012; Scott et al., 2012). Changes to surface albedo and wind field modification properties of the land cover/land use will affect atmospheric circulation processes which will ultimately have an effect on local, regional and global climates, and thus atmospheric-land surface interactions of water and carbon dioxide fluxes. For example, at the continental scale, the annual area of Australian forest conversion to croplands and grasslands in 2009 was 186 383 ha and accounted for 7% of net greenhouse gas emissions (564.5 million tonnes carbon dioxide equivalent) (DCCEE, 2011). At the local scale, annual changes in land cover due to crop selection may also have a large impact on energy partitioning at the surface. For example, in irrigation areas, the availability of water is the major factor in determining crop selection. In years when water is limited, the total area of crops planted, particularly those with greater water requirements (e.g. rice) may be much less.

With the additional disturbance to the natural hydrological cycle as a result of freshwater resource diversions for irrigation, industry and

domestic consumption (Foley et al., 2005), these issues become increasingly significant in regions dependent on irrigation for their agricultural output (Rowan et al., 2011; Vermeulen et al., 2012; Yu et al., 2012). Without irrigation, natural variability in climate processes would otherwise limit agricultural production in these often semi-arid environments (Rowan et al., 2011), and it is these regions that are under increasing pressure to provide goods and services to the global community (Scott et al., 2012).

The forecast increased magnitude and temporal distribution of variability in climatic conditions due to the enhanced greenhouse effect is likely to have further detrimental effect on many of these agricultural regions (Easterling et al., 2007). For example, in regions where water resources are already limited, increasing irrigation requirements due to greater potential evapotranspiration and lower rainfall could lead to a significant decrease in agricultural productivity (e.g. crop yield, biomass accumulation, increased water use) by way of the impact on mass and energy exchanges (Rowan et al., 2011; Scott et al., 2012). This is compounded by the sensitivity of agriculture to increasing climate variability (Yu et al., 2012), where the response of the water and carbon balance of agro-ecosystems to unprecedented increases in temperature and atmospheric carbon dioxide concentrations is uncertain (Domingo et al., 2011; Kanniah et al., 2011). Additionally, the level of contribution of agricultural broad-acre cropping systems to the carbon cycle as a source or a sink of atmospheric carbon dioxide compared to other ecosystems such as forests, tundras and wetlands remains relatively unknown (Gilmanov et al., 2010).

In order to adapt to a changing climate that may have lasting effects on regional, continental and global carbon and water cycles, accurate and up-to-date information regarding energy, water vapour and carbon dioxide fluxes of agro-ecosystems is required (Kalfas et al., 2011; Yu et al., 2012). By quantifying carbon dioxide exchange in conjunction with evapotranspiration, a comprehensive review of agro-ecosystem

processes and the functions that drive them can be made (Suyker & Verma, 2010; Xiao et al., 2012). The measurement of these fluxes can be achieved through the implementation of eddy covariance technologies which have become the standard tool to investigate atmospheric land-surface interactions (Baldocchi, 2003).

While there have been many eddy covariance studies reporting the estimation of the mass and energy balance of broad-acre agricultural cropping systems world-wide (some more recent examples include Dufranne et al. (2011), Hatala et al. (2012b), Leahy et al. (2012), Kueppers & Snyder (2012) and Mudge et al. (2011)), very few publications reporting the interaction between atmospheric land-surface fluxes of Australian broad-acre agricultural systems have been produced. With the aim of obtaining observation-based estimates to determine the role non-forest ecosystems as net sources or sinks of atmospheric CO_2, Gilmanov et al. (2010) conducted a synthesis of 118 eddy covariance flux tower sites representative of non-forest ecosystems which included savannas, grasslands and croplands. Of these 118 sites, only one was located in Australia and was representative of the tropical shrub lands and savannas found of the Northern Territory. In the southern regions of Australia, the only significant body of work was conducted in 1994 and 1995 (see Isaac, 2004; Isaac et al., 2004; Leuning et al., 2004). Better known as the OASIS campaign, this study was designed to investigate the spatiotemporal variation of heterogeneous dryland, rain-fed agricultural systems at field and regional scales with the aim of resolving some of the issues related to spatial scaling of land-surface fluxes. More recent applications of eddy covariance methodologies to quantify the mass and energy exchange of Australian broad-acre farming were presented by Ward et al. (2012). Like OASIS, this study focused on the water and carbon balances of dryland, rain-fed broad-acre cropping systems in relation to adjacent tree belts, which are being increasingly adopted by land managers to reduce salinity as well as sequester carbon. The primary focus of this study was not to

quantify the mass and energy exchange, but to determine whether the application of eddy covariance techniques was suitable in these 'belt and alley' ecosystems. Until now, in-depth and up-to-date information regarding the estimation of water, carbon and energy cycles of Australian irrigated broad-acre cropping systems are yet to be reported.

In Australia, the majority of agricultural production systems (including broad acre cropping) exist within arid or semi-arid climatic regions. This is particularly true of the irrigated areas that exist mainly in the south-central region of the Murray Darling Basin (MDB) and have significant economic value. For example, irrigated agriculture contributes to 31% of the gross value of agricultural production in the MDB (ABS, 2012a). At the same time, it accounts for 54% of the total national water consumption (ABS, 2012c). With the unknown effects of unprecedented changes in climatic conditions and increased atmospheric carbon dioxide concentrations and further diversions of irrigation water for industrial, domestic and environmental use, future irrigated agricultural production in these areas may be unsustainable.

The information obtained in this study will provide an insight into the vegetation/climate feedbacks of Australian broad-acre cropping systems within these semi-arid environments. The directly measured estimates of latent heat flux could also be used to test previously established hydrological model assumptions (e.g. Penman-Monteith methods to determine evapotranspiration). Furthermore, the information could be used to parameterise these models for the specific climatic conditions experienced in the study area which may improve water use efficiency and water productivity in these regions. Targeted eddy covariance studies of different irrigation application methods may also assist in design optimisation to further increase water use efficiencies of these systems. The data obtained will also provide a source of much-needed, defensible data required for modelling purposes. For example, the estimates of water vapour and carbon fluxes of commonly-grown irrigated broad-acre crops (e.g.

maize, rice and wheat) could be used to calibrate agricultural models such as the Agricultural Production Systems Simulator (APSIM; http://www.apsim.info/), which may provide greater understanding of the trade-off between greenhouse gas emissions and water conservation efforts in Australian irrigated broad-acre agricultural systems. In addition, the data would be a useful contribution to the baseline information used to inform outputs of various Government climate change mitigation and adaption initiatives. For instance, under the 'Carbon Farming Futures' program, Australian farmers can earn carbon credits by reducing their emissions and storing carbon within the landscape, including soil and vegetation. Currently, the carbon balance of agricultural systems is determined through the use of various calculators, including the National Carbon Accounting Toolbox (NCAT). Some of the inputs used to model greenhouse gas emissions are derived from remotely-sensed estimates and climate and soil data (Department of Climate Change, 2008). As eddy covariance technologies can directly measure the net carbon capture of the land-surface, substitution of the remotely-sensed data with the EC data would provide greater confidence in estimation of the carbon balance.

1.2 Objectives

To date, few studies have reported an integrated quantitative assessment of energy, water vapour and carbon dioxide fluxes of irrigated broad-acre agricultural cropping systems, especially in Australia. Therefore, in order to determine the role of irrigated agro-ecosystems as net sources or sinks of carbon dioxide, and identify the processes that drive mass and energy exchange within them, a more comprehensive assessment of land-surface interactions particular to these systems must be obtained.

The broad objectives of this thesis are as follows:

1. To determine whether irrigated agro-ecosystems in Australian semi-arid climate zones are net sources or sinks of carbon dioxide.

2. To determine which of the common broad-acre cropping systems (i.e. maize, rice and wheat) grown in these environments are most productive.
3. To determine the major environmental drivers of water vapour and carbon dioxide exchange of these systems through non-traditional methods of Bayes Information Criterion model selection and geostatistical regression.

A complete audit of the carbon and water balance of an agricultural production system should consider the cycle of carbon and water into and out of the system through other mechanistic processes such as direct carbon emission through fossil fuel use and indirect carbon emission through energy-intensive processes e.g. irrigation application and fertiliser use. Therefore, it is important to emphasise that this study is representative of atmospheric mass and energy budgets only; additional losses of carbon through, for example, management practices, grain export and biomass decay beyond the scope of this study.

1.3 Thesis Outline

A significant portion of this study is dedicated to the field collection and subsequent processing, quality control and analysis of high-frequency time series eddy covariance data. As such, Chapter 2 is a general introduction to the greater study area. Chapter 3 details the theoretical background of micrometeorology and the application of eddy covariance methodologies to determine the mass and energy balance of land-surface interactions. Chapter 4 outlines the research methodology adopted to achieve the stated objectives. An assessment of quality control parameters specific to the successful application of eddy covariance technologies within an agricultural environment is given in Chapter 5. This chapter also characterises the site specific details and micrometeorological conditions that affect the quality control parameters at each flux tower location. Chapter 6 presents the distribution of fluxes and the relationship between the dependent (i.e.

the fluxes) and independent variables (e.g. air temperature, net radiation) in order to understand the processes that regulate mass and energy exchange within the study area. The water productivity of each cropping system is also presented here. Comparisons of the results of this study and similar eddy covariance studies of agro-ecosystems elsewhere are discussed in Chapter 7. Limitations of this particular study and the potential impacts that they may have had on the outcome are also addressed in this section. The final chapter presents the summary, conclusions and possible directions for further research.

2 COLEAMBALLY IRRIGATION AREA

2.1 General overview

The focus of this study will be the Coleambally Irrigation Area (CIA), which is a gravity-fed irrigation system located 650 km west of Sydney in the lower parts of the Murray-Darling Basin in the Riverina district of New South Wales (NSW), Australia. The study area is one of two major irrigation areas located within the larger Murrumbidgee catchment that form the Riverina (see Figure 2.1). In 2010/11, the total value of agricultural commodities produced in the Riverina was $1834 million, with broad-acre crops accounting for $1399 million (ABS, 2012b).

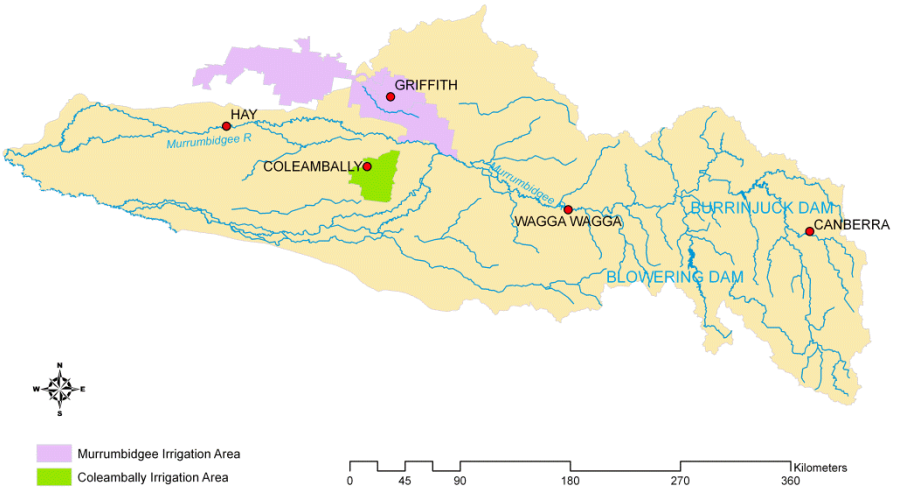

Figure 2.1 The Murrumbidgee catchment and major irrigation areas, townships and surface water storages.

The CIA was developed between 1958 and 1970 for the sole purpose of irrigated agriculture. It was designed to make use of the water that was diverted from the newly constructed Blowering and Burrinjuck dams built to service the Snowy Hydro-Electric Scheme and transmitted along the Murrumbidgee River (Watt, 2008).

Originally, the distribution and management of all irrigation water across the state was the responsibility of the NSW State Government (Murrumbidgee Irrigation Ltd., 2012b). In 1997, the irrigation area was corporatized, becoming a State-owned entity known as the Coleambally Irrigation Corporation. With the privatisation of government-owned irrigation infrastructure and assets, the ownership was transferred to the Coleambally Irrigation Co-operative Ltd (CICL) in 2000 and is now wholly owned and operated by irrigators within the CIA (Watt, 2008).

The CIA contains 79 000 ha of intensively irrigated land supplied through open earthen channels diverted from the Murrumbidgee River. A further 325 000 ha of the surrounding district area is serviced with stock, tank and opportunistic irrigation water (Jackson et al., 2010). Summer crop production (November – April) primarily consists of rice and maize with lesser plantings of soybean, sorghum, cotton, sunflowers and other horticultural/viticultural activities. The production of wheat, barley, canola and pasture constitute the major winter activities (May – October) (CICL, 2011). With a slope of close to 0°, the topography of the area is considered 'pan flat' (McVicar & Van Niel, 2012).

2.2 Water resources

2.2.1 Surface water

The CICL is responsible for the distribution of surface water within the CIA and has a bulk irrigation water license of 629 GL. The volume of surface water varies from year to year based on water allocations. For instance, the introduction of the Murray Darling Basin Cap, designed to maintain a healthy river system by regulating irrigation water diversions, lead to a decrease in water allocations in 1994/95 (see Figure 2.2).

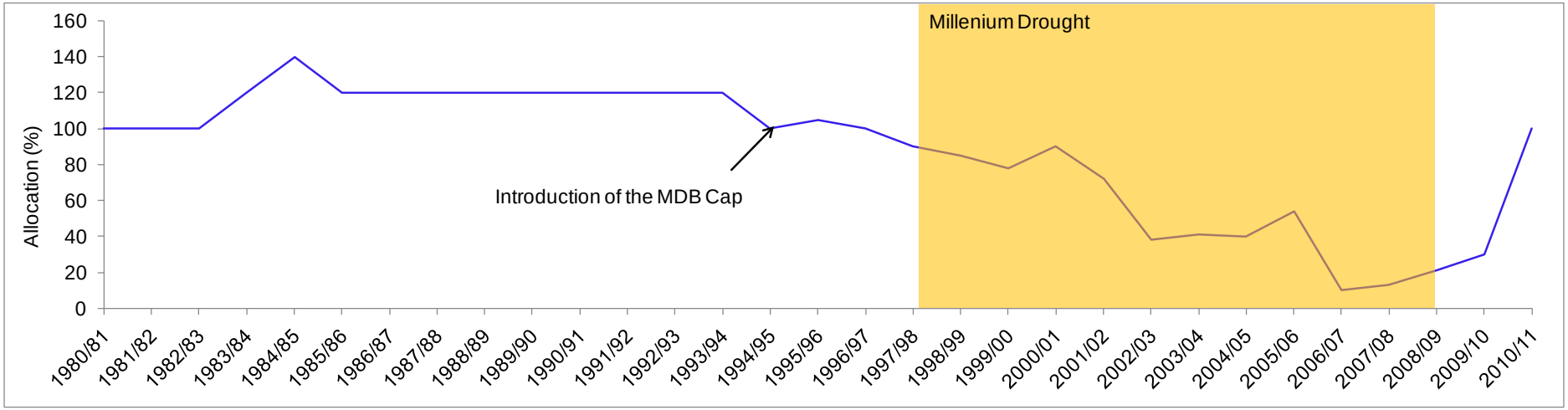

Figure 2.2 General security allocations within the Murrumbidgee catchment between 1980 and 2011 (Murrumbidgee Irrigation Ltd., 2012a).

The Millennium Drought which persisted between 1997 and 2009, inclusive, also resulted in significant decreases in water allocations; particularly for general security entitlements. Subsequently, irrigators shifted from the traditional rice farming to crops requiring less water, such as row crops, winter cereals and pastures (Smith & Nayar, 2008).

In 2002, the CICL initiated the installation of a series of water saving technologies to improve the conveyance efficiency of irrigation water within the system. As a result, the Total Channel Control® system (Rubicon Water, Vic, Australia) consisting of automatically controlled flume gates was introduced, replacing manually operated regulators and other control structures. In conjunction with an extensive radio communications network and the adoption of Supervisory Control and Data Acquisition (SCADA) software, all water orders and deliveries are now remotely controlled and have resulted in delivery efficiencies of up to 90% (Ullah, 2011).

2.2.2 Groundwater

The NSW Office of Water is responsible for the management of groundwater resources and, to date, have issued 102 groundwater extraction licences within the CIA. All monitoring and reporting for groundwater resources are conducted independently of the CICL. In 2010/11, the total metered groundwater extraction in the area was 20 341 ML; in 2011/12, this was 37 085 ML (CICL, 2011, 2012).

Compared to the 1998/99 baseline levels of total groundwater extraction of 68 940 ML, groundwater extractions over the last two irrigation seasons have been relatively low as a result of increased surface water allocation due to above-average rainfall and the return of water storages to capacity within the Murrumbidgee catchment area.

2.2.3 Surface water irrigation and associated land preparation methods

Surface water is the most common source of irrigation water in the CIA and accounts for 98.7% of water supplied (Jackson, 2009). As illustrated in Figure 2.3, gravity fed surface water application onto land prepared through laser contouring is the preferred method, followed by bed and furrow and natural contouring methods. Irrigation through pressure systems (e.g. sprinkler or drip irrigation) is minimal and accounts for approximately 2% of total surface water application (Kelly, 2013).

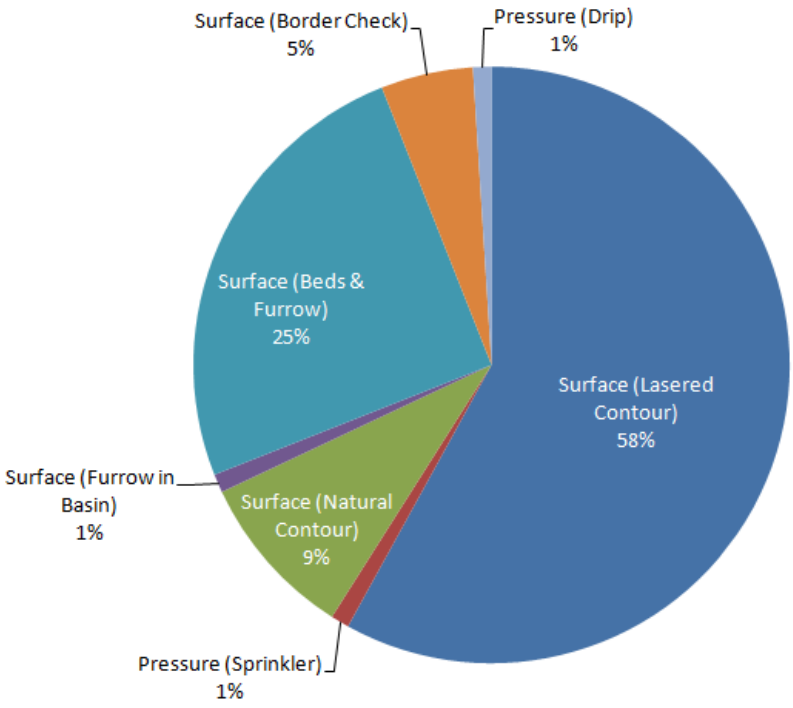

Figure 2.3 Surface water irrigation application and associated land preparation methods in the CIA (Kelly, 2013).

2.3 Climate and weather

Based on temperature and humidity, the climate experienced within the CIA is classified as having hot, dry summers and cold winters (Bureau of Meteorology, 2005). As illustrated by Figure 2.4, the

climate of the region is characterised by mean maximum January temperatures of 32.8°C and mean maximum July temperatures of 14.5°C which is consistent with temperate semi-arid conditions (Bureau of Meteorology, 2012a; Watt, 2008). The average precipitation is 406.5 mm/year with no distinct seasonal variability. Long-term average annual potential evapotranspiration rates are 1861 mm and mean annual global solar radiation is 6450 MJ/m^2 (Bureau of Meteorology, 2012b; CICL, 2010). Whilst the levels of mean global solar radiation are more than adequate to sustain the intensive agricultural cropping methods common in this region, monthly evapotranspiration exceeds precipitation throughout the year. For these reasons, supplementary irrigation water is required to meet crop water demand, particularly during the summer growing season.

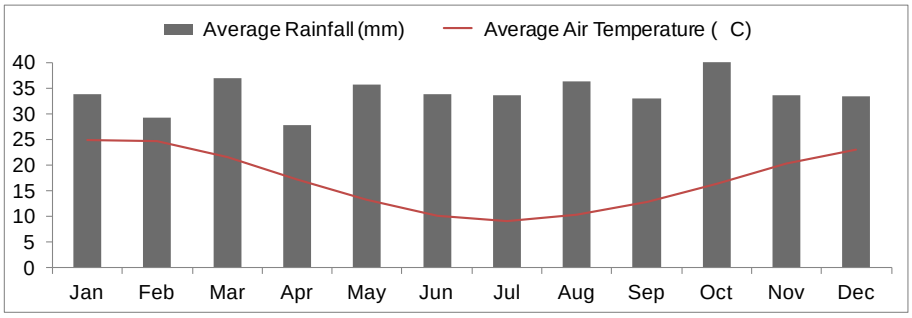

Figure 2.4 Long-term averages of rainfall and air temperature for the CIA (Bureau of Meteorology, 2012a).

2.4 Soil types

Existing on the Riverine Plain, the soils of the CIA are largely the result of alluvial deposits of sediments from ancient streams. Over time, these soils have been interspersed with wind-blown clay deposits (Hornbuckle et al., 2008). In order to meet the long-term objectives of a 30-year Land and Water Management Plan that was established in 2000, an extensive electro-magnetic survey of the CIA and surrounding areas was completed in 2007. The spatial distribution of

the five predominate soil types found in the CIA as determined by the survey is illustrated in Figure 2.5.

Listed in order of total area, the soils of the region are: transitional red-brown earths; red-brown earths; sands; self-mulching clays; and non-self mulching clays. As depicted in Figure 2.5, transitional red-brown earths are evenly distributed throughout the region. The self-mulching clays are mostly centrally located, extending into the north-eastern corner of the CIA, whilst the deposits of red-brown earth occur in the southern parts of the region. Sand deposits are found along transects of paleo-channels that run east–west through the centre of the irrigation area and along the north-western boundary of the region.

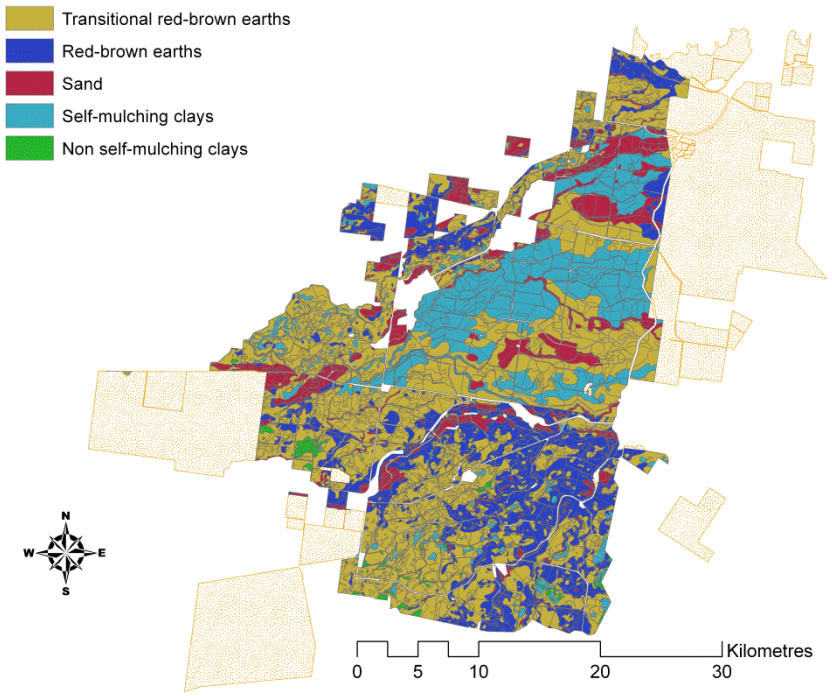

Figure 2.5 Five major soil types of the CIA.

A brief description of the characteristics of each soil type is given in Table 2.1. Please note that sands have been further defined into the sub-classes: sands and deep sands (as per Hornbuckle et al., 2008).

Table 2.1 Typical soil properties of the CIA (adapted from Hornbuckle et al., 2008).

Feature	*Self-mulching clays*	*Red-brown earths*	*Transitional red brown earths*	*Sands over Clay*	*Deep sands*
Topsoil (& depth)	Clay (0.05 - 0.15 m)	Loam to clay (< 0.05 m)	Loam to sandy loam (0.10 – 0.25 m)	Sand to loam (0.25 – 1.00 m)	Sand (> 1.00 m)
Subsoil	Heavy clay with lime	Heavy clay	Heavy clay	Cemented clayey sand above a mottled medium clay	Mottled clayey sand grading to light clay
Deep soil (1 - 2 m)	Medium clay with concretionary lime	Medium clay, often with crystalline gypsum	Sandy clay, often micaceous	Medium clay sometimes becoming more sandy with depth	Light clay

2.5 Crop production and crop water use

Table 2.2 presents the total area of plantings of the seven major summer and winter crops and the percentage of total irrigation water deliveries to each crop between 1997/98 to 2010/11. During the 1999/00 irrigation season 77.7% of water deliveries were used to produce rice, whilst only 6% was used to grow wheat. At the height of the drought in 2007/08, only 1.4% of deliveries were used for rice production compared to 20% that was used to produce wheat.

In 2010/11, the CIA received 739 mm in total rainfall which was the second highest on record, marking the end of the drought. With the widespread rainfall that occurred across the MDB, water storages returned to 100% capacity. As a result, the CIA returned to 100% of water allocations and plantings of rice returned to pre-2002/03 levels, accounting for 14 512 ha and 65.1% of irrigation water delivered (CICL, 2011).

Table 2.2 Plantings of major crops and the proportion of total irrigation water delivered per crop within the CIA for the years 1997 – 2011 (CICL, 2008, 2009, 2010, 2011).

Year	*Rice*		*Maize/Corn*		*Soybean*		*Wheat*		*Canola*		*Pasture*		*Barley*	
	Area (ha)	Water Delivery (%)	Area (ha)	Water Delivery (%)	Area (ha)	Water Delivery (%)	Area (ha)	Water Delivery (%)	Area (ha)	Water Delivery (%)	Area (ha)	Water Delivery (%)	Area (ha)	Water Delivery (%)
2010/11	14 512	65.1	4367	6.9	1240	1.5	11 334	4.8	3381	1.4	8119	4.4	9117	4.4
2009/10	3669	46	311	2	495	1	10 635	10	2523	2	6903	12	10 499	7
2008/09	2135	33.1	2472	3.4	308	1.4	4215	9.5	1471	4.9	4481	16.3	4315	6.8
2007/08	90	1.4	941	1.2	152	0.7	675	20	1584	6.1	5004	20.4	4383	11.5
2006/07	8518	54.3	1863	7.6	478	0.8	12 509	15.9	1602	1	9958	7.8	5495	4.4
2005/06	18 025	62.8	3306	7	2106	2.9	13 610	8.4	1748	0.9	15 440	8.7	6864	2.2
2004/05	8142	44	3671	7.2	1495	2.2	20 287	18.8	2681	1.3	12 865	10.8	5281	2.9
2003/04	12 597	55.8	3545	5.7	1938	3.5	21 192	14.96	1763	0.7	12 131	7.5	4768	1.82
2002/03	11 395	46	4788	9.3	1788	1	21 346	20.4	2095	1.7	10 183	7.4	4227	2.4
2001/02	27 493	67.5	3808	4.2	3297	3.4	21 103	9.2	2191	0.6	11 581	6.1	3949	1.64
2000/01	30 440	73.9	4074	5.7	4551	5.9	14 276	4.6	2153	0.4	11 998	4.7	2642	0.65
1999/00	24 138	77.7	1178	3.1	2185	3.9	12 649	6.1	2152	0.7	7485	4.4	No data	
1998/99	24 491	73.8	1059	1.3	4339	5.7	13 963	1.7	2184	1.7	13 879	8.1	No data	
1997/98	24 624	70.4	1678	2.4	4998	7.5	14 943	7.4	2053	0.4	9964	6.1	No data	

Figure 2.6 presents the total irrigated crop area of both summer and winter growing seasons in the CIA in 2010/11, and Figure 2.7 depicts the proportion of total surface irrigation water supplied to each crop in the same year.

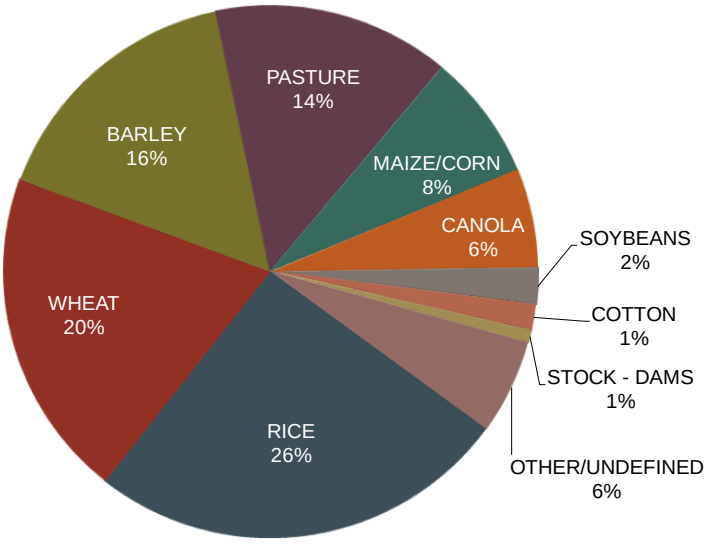

Figure 2.6 Proportions of total irrigated crop areas (ha) within the CIA in 2010/11 (CICL, 2011).

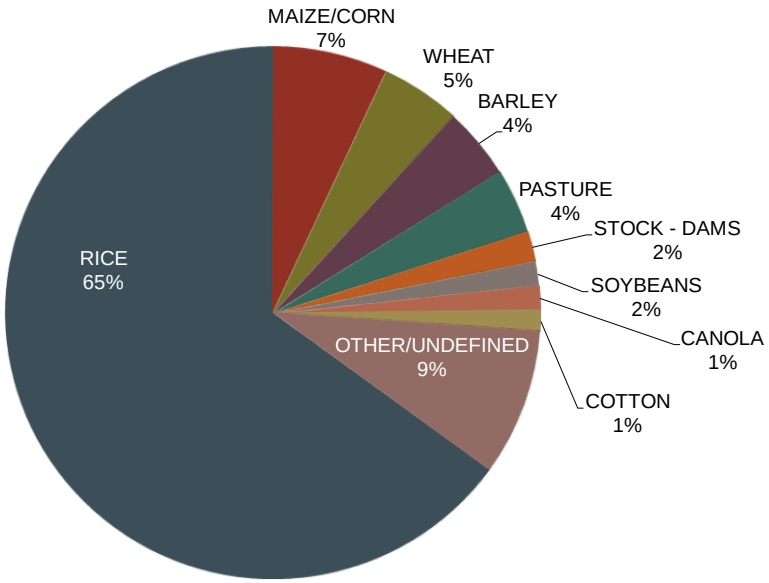

Figure 2.7 Proportion of total irrigation water delivered (ML) per crop in the CIA – 2010/11 (CICL, 2011).

In terms of area, rice was the major summer crop grown in the region, representing a total area of 14 512 ha. Rice was also the largest consumer of irrigation water, accounting for 65.1% of total irrigation water supplied in 2010/11 which was 26 5572 ML, resulting in a high level of crop water use (11.9 ML/ha). The second most abundant summer crop cultivation was maize. With a total planting of 4367 ha, the percentage of total irrigation water consumed for maize production was only 6.9% (4.2 ML/ha).

Of the winter crops, wheat represented the largest area of plantings (11 334 ha) and was also the largest consumer of irrigation water during the winter growing season and the third largest consumer overall, accounting for 4.8% of total irrigation water deliveries in 2010/11. Despite this, the water productivity of wheat cropping systems in the CIA was quite low in comparison to that of other crops grown, consuming only 2.1 ML/ha.

3 ESTIMATING MASS AND ENERGY EXCHANGE OF ATMOSPHERIC LAND-SURFACE INTERACTIONS OF AUSTRALIAN IRRIGATED AGRICULTURE

The need to understand the processes of mass and energy exchange and the functions that drive them is necessary to adapt to the impacts of a changing climate. This is particularly true for agricultural systems, where productivity is sensitive to increasing climate variability (Yu et al., 2012).

3.1 A growing population, increasing climate variability and agricultural mass and energy exchange

As the global population has increased, the area of global land use dedicated to food production has expanded. For example, during the 18th Century, it is estimated that only 5% of the Earth's ice-free surface was dedicated to food and fibre production (Spiertz, 2012); it is now estimated to be 40% (Ramankutty et al., 2008).

Land use change as a result of the population growth, subsequent urbanisation and agricultural intensification has meant that many natural ecosystems have been transformed. Already, most of the suitable, fertile land for agricultural production has been lost as a result of urbanisation (Spiertz, 2012) which has not been without cost. For instance, deforestation to enable agricultural expansion resulted in an estimated 20 – 25% increase in atmospheric carbon dioxide over the last one hundred and fifty years (Baker & Griffis, 2005). Associated land cover changes have also affected local and regional climates through shifts in the mass and energy balance and the diversion of freshwater resources has disturbed the natural order of the hydrological cycle (Foley et al., 2005).

Agricultural activities have been forced to expand into the marginal arid and semi-arid regions of the world (Spiertz, 2012); these systems account for 54% of global food production and produce 45% of the total global grain yield (Howden et al., 2007; IPCC, 2007; World Bank, 2007). With a projected population increase of nine billion people by 2050, it is expected that the pressure on our natural and agro-ecosystems is going to continue to increase. For example, it is predicted that a further one billion hectares of natural ecosystems will be lost to provide food and fibre to the future global population (Khan & Hanjra, 2009). In addition to the loss of services provided by these ecosystems, the change in land cover and land use at this scale will alter the global mass and energy balance and thus, water and carbon cycles, although the extent to which remains relatively unknown (Gilmanov et al., 2010).

In many semi-arid irrigated areas, increased climate variability and agricultural expansion and intensification have already altered the mass and energy balance. This is evidenced by decreased precipitation, reduced runoff and, thus, decreased water availability (IPCC, 2007). Although the response of the water and carbon balance of agro-ecosystems to increased climate variability is uncertain (Domingo et al., 2011; Kanniah et al., 2011), it is predicted that further increases to surface temperatures and levels of atmospheric carbon in these areas will have a negative impact on crop yields, particularly those of rice, wheat and maize (Khan & Hanjra, 2009).

Furthermore, it is widely acknowledged that the landscape function of various ecosystems of forest, wetlands and tundras are generally found to be carbon sinks (Gilmanov et al., 2010). However, the level of contribution of agricultural broad-acre cropping systems to the carbon cycle as a source or a sink of atmospheric carbon dioxide remains unknown. In order to adapt to a changing climate, it is necessary to understand the processes of mass and energy exchange and the functions that drive them. Therefore, in-depth and up-to-date information regarding the estimation of water, carbon and energy

cycles of irrigated broad-acre crops is required. This can be achieved through the implementation of eddy covariance (EC) methodologies which provide the most direct and defensible means of land-surface flux estimation (Baldocchi, 2003).

In Australia, the interaction between water and carbon dioxide fluxes of irrigated broad-acre crops as measured by EC systems are yet to be reported. Therefore, the results of this study will, for the first time, provide accurate and up-to-date information regarding energy, water vapour and carbon dioxide fluxes of the most commonly irrigated broad-acre crops grown in semi-arid irrigated areas of Australia.

In order to evaluate the interactions between water, carbon dioxide and energy fluxes of agro-ecosystems, it is necessary to understand the general concepts of micrometeorology. Therefore, this chapter presents the theory behind eddy covariance technologies for the direct measurement of atmospheric land-surface fluxes. Methodologies to further partition carbon dioxide flux into its metabolic components (total ecosystem respiration, gross primary production and net ecosystem exchange) are also explored. It is also important to understand flux behaviour in response to various environmental variables assessed through the application of geostatistical methods presented in this chapter.

3.2 Micrometeorology and the atmospheric boundary layer

Micrometeorology is a branch of meteorology that focuses on the processes that occur in the atmospheric layers closest to the surface of the Earth (Lee et al., 2004b). Specifically, these layers refer to the components of the atmospheric boundary layer (i.e. the surface layer and the mixed or transition layer; ABL) between the Earth's surface and the free troposphere (Kaimal & Finnigan, 1994; Malhi et al., 2004). Typically, the depth of the ABL is 1 – 2 km during the day and up to a few hundred metres at night-time (Isaac et al., 2004).

It is within the atmospheric boundary layer that most mass and energy exchange processes occur as a result of surface heating driven by the energy from the Sun (Isaac et al., 2004) and wind field modification according to the characteristics and aerodynamic properties of the land cover (Davin & de Noblet-Ducoudre, 2010b). For example, the aerodynamic effect of a forest canopy structure, determined by the roughness length, generally has a cooling effect on the Earth's surface through increased turbulence in the ABL. For grasslands, the surface roughness length is smaller, reducing the turbulent transfer of heat and water vapour and thus, increasing temperatures at the surface Grass also has a smaller root zone, thereby decreasing the efficiency of soil moisture extraction, also increasing the temperature at the surface (Davin & de Noblet-Ducoudre, 2010a).

The length and time scale of micrometeorological studies of atmospheric processes that occur within the ABL generally occur from seconds to decades and can be measured from the leaf and canopy scale to the regional scale.

Over time a number of methods have been developed to determine various components of the air-surface exchange, both directly and indirectly (Watson & IPCC, 2000). Indirect methods to determine the mass and energy exchange include techniques such as upwind-downwind measurements (Denmead et al., 1998) and flux gradient methods (Baldocchi et al., 1988). The upwind-downwind measurement is a mass balance method that requires the measurement of gas concentrations at different heights along each of the experimental boundaries. The gas concentrations are then multiplied by their corresponding wind vectors to give the horizontal flux at each sample height. The difference between these fluxes integrated between the upwind and downwind boundaries will yield the production value (Denmead et al., 1998). Flux-gradient methods provide an alternative to the mass balance approach and assume that turbulent transfer is equal of the molecular diffusion of a given substance (Baldocchi & Meyers, 1998).

These approaches, whilst useful, are limited because they infer, rather than directly measure, fluxes (Watson & IPCC, 2000). Therefore, methods based on eddy covariance theories have been developed to directly measure interactions between the land-surface and the atmosphere. In addition to the direct measurement of land-surface fluxes, the benefit of using eddy covariance technologies is that they are able to provide information regarding processes in the ABL at the ecosystem scale. When trying to determine and subsequently predict how whole ecosystems will respond to environmental perturbations, information of these processes at these scales becomes very important (Baldocchi, 2003).

3.3 Eddy covariance

Whilst the theoretical framework of eddy covariance methodologies was first recognised in 1895 (Reynolds, 1895), mainstream adoption of these methods has grown with more recent improvements in micrometeorological theory (e.g. Moore, 1986; Webb et al., 1980) and the development of fast-response digital and sensor technologies (Baldocchi, 2003).

Due to the technical and temporal limitations of early EC technologies, most studies focused on the energy exchange (i.e. transfer of sensible and latent heat and momentum fluxes only) of short vegetation, e.g. grasslands and agricultural crops and pastures. The timescale of these studies was generally determined by the length of the growing season and were in the order of weeks to months, rather than years (Baldocchi, 2008; Baldocchi, 2003; Garratt, 1984).

Prior to the 1970s, fluxes of carbon dioxide (CO_2) were predominantly determined via indirect methods of measurement, which proved to be difficult where the canopy structure was non-uniform, as is the case with tall forests (Baldocchi, 2003). As technologies improved, CO_2 flux could be estimated using EC technologies and like the first studies of heat and momentum fluxes, early studies of CO_2 exchange focused mainly on agricultural crops including sorghum in the U.S.A.

(Anderson & Verma, 1986); corn in Canada (Desjardins et al., 1984); and rice in Japan (Ohtaki, 1980).

With the advent of fast-response anemometers and infrared gas analysers and improvement of data acquisition systems, research into ecosystem exchange of trace gases, including carbon dioxide, in conjunction with energy exchange began to develop and naturally progressed to the long-term monitoring of other landscapes. These include forest systems (e.g. Barr et al., 2006; Cabral et al., 2010; Kominami et al., 2008; Van Dijk & Dolman, 2004; Von Randow et al., 2008), tropical savannas (e.g. Beringer et al., 2011; Giambelluca et al., 2009; Hutley et al., 2005; Miranda et al., 1997; Vourlitis et al., 2001) and wetlands (e.g. Jacobs et al., 2002; Sulman et al., 2012).

Given the concerns of rising atmospheric CO_2 concentrations and the uncertainties regarding the carbon sequestration in the terrestrial biosphere (Isaac, 2004), EC technologies have become the standard tool to monitor the exchange of trace gases between the atmosphere and the Earth's surface, and, to date, there has been an extensive amount of research conducted on various terrestrial ecosystems. For example, a global network of regional flux communities, FLUXNET, was formed and has enabled the integration of data across the globe. It has also driven the relative standardisation of EC instrumentation and data processing methods, and although opportunistic (i.e., field site selection based on funding and research priorities rather than geostatistical design), the network configuration includes a diverse range of biomes and climates (Baldocchi et al., 2001).

3.3.1 The theoretical framework of eddy covariance flux measurement

The eddy covariance (EC) technique is the most widely used and most defensible method to directly measure interactions between the land-surface (fluxes) and the Earth's atmosphere. The EC method is based largely on the fundamental laws of fluid dynamics and flux

measurement (Baldocchi, 2003). In its simplest terms, flux is a measure of how a fluid moves through a given area within a given timeframe (Burba & Anderson, 2010). In the context of micrometeorology, flux (F) refers to the turbulent movement of air that transports a given entity, s (e.g., heat, moisture or CO_2). The general equation is given by:

$$\boldsymbol{F = \overline{\rho_a w' s'}} \quad (1)$$

where ρ_a is the air density and w is the instantaneous vertical wind speed (Burba & Anderson, 2010; Rosenberg, 1974).

More specifically, when measuring trace gases such as carbon dioxide, flux is the covariance between the instantaneous vertical fluctuations (w) and the mixing ratio of the trace gas (c), given by the equation:

$$\boldsymbol{F_c = \overline{w' \rho_c'}} \quad (2)$$

where ρ_c is the density of the trace gas (Baldocchi, 2003; Burba & Anderson, 2010).

As a well as monitoring the mass balance of trace gases, the EC technique is also able to measure energy and water vapour exchange (i.e. sensible and latent heat fluxes) between vegetation and the free atmosphere (Baldocchi, 2008).

Sensible heat flux (H_s) is the term used to describe the exchange of energy between the Earth's surface and the ABL (Isaac, 2004). It is determined by multiplying mean air density (ρ_a) by the covariance between deviations in instantaneous vertical wind speed (w) and air temperature (T) and is given by the equation:

$$\boldsymbol{H_s = \rho_a C_p \overline{w' T'}} \quad (3)$$

where Cp is the specific heat capacity of the air (Baldocchi et al., 1988; Burba & Anderson, 2010).

Latent heat flux (*LE*) is the flux of heat from the Earth's surface through evaporation or plant transpiration that is subsequently condensed in the troposphere. It is given by the equation:

$$\boldsymbol{LE = \lambda \rho_a \overline{w'q'}} \quad (4)$$

where $\overline{w'q'}$ is the covariance between fluctuations of vertical wind speed *w'* (m/s) and humidity *q'* (kg water/kg air) and λ is the latent heat of vaporisation of water (Baldocchi, 2003; Li et al., 2008).

These measurements of net carbon, water and energy exchange between the land-surface and the atmosphere are obtained through the implementation of fast response (10 – 20 Hz) EC instrumentation, which is generally averaged into 30 or 60 minute intervals (Hutley et al., 2005). For a full review of the EC methodology, instrumentation and application as well as theoretical and technical advancements see Baldocchi et al. (1998), Baldocchi (2003), Burba & Anderson (2010) and Lee et al. (2004).

3.3.2 Surface energy balance and energy balance closure

As well as ascertaining turbulent fluxes of mass and energy, EC instrumentation in conjunction with ancillary instrumentation (e.g. net radiometers and soil heat flux plates) can be used to determine various surface energy components used to solve the energy balance (Wilson et al., 2002a). The energy balance can be represented by the simplified equation of the first law of thermodynamics:

$$\boldsymbol{R_n - G = H + LE} \quad (5)$$

where R_n represents the net radiation and *G* represents the ground heat flux (modified from Brutsaert, 1982).

The energy balance (or budget) is one of the main processes that drives the circulation of the atmosphere forced by global heating patterns (Brutsaert, 1982). In relation to EC methodologies, the level of energy balance is a good measure of how well a system is

performing and provides an independent assessment of scalar flux estimates, because theoretical assumptions in the conservation equations and Reynolds decomposition are similar. As such, it is an important test of EC data that influences the interpretation of flux measurement and how these should be compared with modelled flux simulations (Wilson et al., 2002a).

In the past, there have been numerous studies regarding energy balance closure of EC sites (e.g. Barr et al., 2006; Barr et al., 2011; Foken et al., 2010; Foken et al., 2006; Franssen et al., 2010; Kidston et al., 2010; Mauder et al., 2007). In general, surface energy fluxes ($H + LE$) are underestimated by 10 – 30% relative to available energy ($R_n - G$) (Wilson et al., 2002a). According to the literature (e.g. Foken et al., 2010; Foken et al., 2006; Kidston et al., 2010; Liu et al., 2011; Wilson et al., 2002a), there are several reasons as to why this could be the case, including but not limited to:

1. Systematic bias (due to instrumentation error, correction methods and quality control procedures),
2. Different reference levels and sampling scales of various instruments used to determine turbulent fluxes, net radiation and soil heat flux (e.g. 10 Hz vs. 10 min interval),
3. Loss of low and/or high frequency contributions to the turbulent flux,
4. Other energy sinks not included in the energy balance assessment (e.g. canopy heat storage) and
5. Heterogeneity of the land surface.

The principal method used to evaluate energy balance closure is to perform an ordinary least squares regression (OLS) analysis to determine the relationship between the averaged estimates (e.g. 30 or 60 min intervals) of the dependent flux variables against the independently derived available energy; if the intercept is zero and the slope is equal to one, then the energy balance is said to be closed (Wilson et al., 2002a). It is important to note that this method is only

technically valid if there are no random errors in measurements of the independent variables, R_n and G. To overcome this, an alternative method to evaluate the energy balance is to average over the random errors in the data at longer timescales was developed (Tsai et al., 2007; Wilson et al., 2002a). Known as the Energy Balance Ratio (*EBR*), this is determined by the equation:

$$\boldsymbol{EBR} = \frac{\sum(\boldsymbol{H}+\boldsymbol{LE})}{\sum(\boldsymbol{R_n}-\boldsymbol{G})} \quad (6)$$

The disadvantage of this method is the potential to neglect possible biases in the data including the tendency to overestimate positive daytime fluxes while underestimating negative night-time fluxes (Wilson et al., 2002a).

3.3.3 Analytical techniques to assess the successful application of eddy covariance methodologies

Baldocchi (2008) lists some principles of eddy covariance as a direct tool to successfully measure mass and energy balance. The experimental design must meet a number of criteria (Baldocchi, 2008). The data collection requires:

1. Flat terrain and homogenous land-cover,
2. Adequate fetch of uniform vegetation up wind of sensor location,
3. Steady atmospheric conditions, and
4. Sensor and data-logging equipment sophisticated enough to capture the smallest and fastest eddies.

With these criteria met, the constant flux layer and logarithmic profile are well established (Burba & Anderson, 2010); any deviations from these ideal circumstances (e.g. heterogeneous terrain or land cover) will promote advection leading to a divergence in fluxes where vertical fluctuations vary with height, complicating flux measurement

(Aubinet et al., 2003; Baldocchi, 2003; Baldocchi et al., 1988; Lee, 1998; Lee & Hu, 2002).

Another limiting factor, particularly when modelling water and carbon fluxes, is the continuous time series data that are required to compute daily and annual sums. These datasets are often fragmented by various standard operating procedures, such as routine calibration and maintenance, sensor or system malfunction, unfavourable atmospheric conditions (including stable conditions and, in the case of open path infrared gas analysers, precipitation) and other land management practices specific to the site (e.g. farming operations such as prescribed burning) (Baldocchi et al., 2001; Moffat et al., 2007). Data may also be rejected according to quality control measures based on various theoretical requirements; these may include ogive tests and stationarity or fiction velocity tests (Baldocchi et al., 2001; Foken et al., 2004; Foken & Wichura, 1996; Foken et al., 2006; Oncley & Friehe, 1996).

The ogive test is used to ensure that all significant low frequency eddies are accounted for. Cospectra is a distribution of the covariance of *w'* and a scalar by frequency (Burba & Anderson, 2010). The ogive function is the cumulative integral of the co-spectra between two variables as summed from high-frequency to low-frequency contributions (Barnhart et al., 2012; Foken et al., 2006; Oncley & Friehe, 1996). It is given by the equation:

$$\boldsymbol{og}_{\boldsymbol{w,x}}(\boldsymbol{f}) = \int_{\boldsymbol{fNyquist}}^{\boldsymbol{f_0}} \boldsymbol{Co}_{\boldsymbol{w,x}}(\boldsymbol{f})\boldsymbol{df} \qquad (7)$$

where $Co_{w,x}$ is the covariance of a turbulent flux, w is the vertical wind component and x is the horizontal wind component or scalar. The highest frequency, $f_{Nyquist}$, is determined by the sampling rate, and the lowest frequency, f_0, is determined by the sampling duration (Barnhart et al., 2012). The frequency at which the ogive converges to a constant value can then be converted to an optimal integration

period (e.g. 30 min or 1 hour averaging period) for the EC measurement (Foken & Wichura, 1996).

Stationarity, or steady-state, refers to periods of time where, statistically, the rate of change is zero (Foken et al., 2004; Foken & Wichura, 1996). Changes in meteorological variables over the course of a day, as well as changing weather patterns and mesoscale variability can lead to conditions of non-stationarity (Foken et al., 2004). There are currently two methods to determine steady-state conditions, the details of which can be found in Vickers & Mahrt (1997) and Foken & Wichura (1996). Regardless of the method implemented, both agree that the time series is steady-state if the relative non-stationarity (RN_{cov}) is less than 30% (Foken et al., 2004). The RN_{cov} is the difference between the covariance of the vertical wind component (w) and the horizontal wind component or scalar (x) determined for the whole averaging period $(\overline{x'w'}_0)$ and a specified interval $(\overline{x'w'})$ (Foken et al., 2005). It is given by the equation:

$$\mathbf{RN_{cov}} = \left|\frac{(\overline{x'w'}) - (\overline{x'w'})_o}{(\overline{x'w'})_o}\right| \quad (8)$$

The stationarity test is particularly useful for the filtration of night-time data where there is a greater occurrence of stable stratification periods with little to no turbulence (Burba & Anderson, 2010).

Similarly, tests based on a friction velocity threshold can be used to ensure well-mixed conditions (Goulden et al., 1996). Friction velocity (u*) is a scaling velocity related to momentum transfer that increases with surface roughness. The u* threshold is an indicator that is often used to filter EC data for periods of low turbulence which would affect the flux measured by EC systems (Gu et al., 2005). Data falling below this threshold is considered unreliable and is therefore removed from the time series. The u* threshold is an alternative method used to correct night-time time CO_2 fluxes that may be underestimated and can also be used to determine ecosystem components of carbon

metabolism (Saito et al., 2005). The partitioning of CO_2 fluxes is discussed further in Section 3.4.1.

Data may also be rejected if the flux footprint (or effective fetch) is outside the area of interest; this can be influenced by sensor height, surface roughness and canopy structure as well as local meteorological conditions, including wind speed and direction and intensity of turbulence (Göckede, 2004; Schmid, 2002; Vesala et al., 2008). As the complexity and heterogeneity of the study site increases, the flux footprint becomes increasingly more important; in which case it is essential to know which part of the surrounding area has the greatest contribution to the flux measurements (Rebmann et al., 2005).

According to Schmid (2002), 'the footprint of a measurement is the transfer function between the measured value and the set of forcings on the surface–atmosphere interface'. Early footprint methodologies based on internal boundary layer growth were initially developed by Pasquill (1972) and presented by Pasquill & Smith (1983) as:

$$\boldsymbol{\eta(r)} = \int_{\Re} \boldsymbol{Q_\eta}\,\boldsymbol{(r + r')f(r, r')dr'} \qquad (9)$$

where η is the measured value at the location, r; $Q_\eta(r + r')$ is the distribution of source or sink strength in the surface–vegetation volume; and $f(r, r')$ is the footprint or transfer function, depending on *r*, and on the separation between measurement and forcing, *r'*. Footprint methodology was further developed by Gash (1986), who presented the cumulative fetch as an integral of the sources contributing to the measured flux within a restricted area (Göckede et al., 2004).

Since then a number of footprint models have evolved based on different mathematical concepts; these include Eulerian analytical footprint models (e.g. Horst & Weil, 1992; Kormann & Meixner, 2001), Lagrangian stochastic footprint models (e.g. Kurbanmuradov & Sabelfeld, 2000; Leclerc & Thurtell, 1990) and Large Eddy Simulation models (e.g. Leclerc et al., 1997; Saiki et al., 2000). For a

comprehensive review of the different approaches to calculating the flux footprint, including advantages and disadvantages, see Kljun et al. (2003), Foken & LeClerc (2004) and Vesala et al. (2008).

When combined, system failure, routine operating procedures, post-processing and quality control of time series data can often result in a temporal average of 65 – 75% annual coverage of fluxes (Falge et al., 2001a; Falge et al., 2001b). Gaps in the time series may be further compounded if conditions of low turbulence are often experienced and a filter based on friction velocity is imposed; under these particular conditions, typical gaps in an annual dataset can range from 20 – 60% with most gaps occurring at night (Moffat et al., 2007).

These gaps can be problematic for a number of reasons:

1. Seasonal or annual estimation of mass and energy exchange may be difficult to obtain;
2. Missing data can lead to biased relationships between water, carbon and energy fluxes and climatic variables; and
3. Large gaps could lead to a low-quality dataset (Hui et al., 2004).

Therefore, it is necessary to implement defensible gap-filling strategies to form complete datasets of acceptable quality in order to provide a more accurate estimation of the mass and energy balance. These can then be used to validate or inform various land-surface models with greater confidence. Furthermore, comparability between datasets of unique sites is improved by adopting standardised methodologies by all regional and global flux communities (Falge et al., 2001a; Falge et al., 2001b; Hui et al., 2004).

Many and varied gap-filling strategies for long-term EC dataset have been developed over time, including, but not limited to, methods such as simple interpolation (mean daily variation, or MDV), look-up tables, linear and non-linear regression, Kalman filters, light response curves and the use of artificial neural networks. In the interest of

developing a standardised procedure for the flux community, Falge et al. (2001a; 2001b) and, more recently, Moffat et al. (2007) present a comprehensive review of current gap-filling techniques. The results of all three studies showed that all methods considered in the analysis performed equally well over the ten benchmark datasets of six European forested sites, although further work to assess model performance for different vegetation types and climatic conditions is required.

3.4 Understanding the environmental controls of water and carbon fluxes

3.4.1 Partitioning of carbon dioxide fluxes to assess gross primary productivity and total ecosystem respiration

Whilst eddy covariance methodologies provide a direct measure of carbon dioxide flux (F_c) between the land surface and the atmosphere, further modelling of EC data is required to partition F_c into its constituent fluxes that are associated with distinct biophysical processes (Scanlon & Kustas, 2010). By partitioning F_c into its assimilatory (gross primary productivity; *GPP*) and respiratory (total ecosystem respiration; *Re*) components, a greater understanding of the processes that drive carbon cycling within the irrigated agricultural environment can be achieved.

F_c, (or net ecosystem exchange; *NEE*) is the balance between *GPP*, which is the photosynthetic assimilatory process of carbon uptake by the plant, and *Re*, which is the carbon released to the atmosphere through plant respiratory processes, microbial activity and organic decomposition of soils. Net ecosystem exchange is given by (Falge et al., 2001a):

$$\boldsymbol{NEE = Re - GPP} \tag{10}$$

There are a number of flux partitioning methods that have been developed over time (Lasslop et al., 2010). Firstly, there are those

methods that rely on night-time data to determine the components of carbon metabolism. Based on the assumption that *GPP* is equal to zero at night (as there is no photosynthetic activity), *Re* is equal to F_c. Therefore, the difference between daytime *NEE* and night-time *NEE* can then be used to calculate *GPP* using an empirical model to extrapolate night-time respiration (Goulden et al., 2011; Rocha & Goulden, 2009; Wohlfahrt et al., 2005). However, this method relies on flux data obtained during periods of turbulence to ensure adequate mixing in the surface layer so that the data used to determine the empirical model is truly representative of ecosystem function. For this reason, this method may be biased, because of the suppression of fluxes due to frequent periods of relatively stable air stratification at night (Lasslop et al., 2010; Zhu et al., 2006), which leads to less availability of reliable data used to fit the empirical model.

The second approach is to extrapolate *Re* from light-response curves fitted to daytime *NEE* data (Lasslop et al., 2010). Whilst avoiding the use of questionable night-time data, this method is also not without its limitations as it usually does not account for the variation of *NEE* as a function of temperature and vapour pressure deficit (Lasslop et al., 2010).

3.4.2 Geostatistical regression analysis of water and carbon flux response to micrometeorological drivers using Bayes Information Criterion

In order to investigate the key physiological parameters that drive ecohydrological processes, modelling of observations of water, carbon dioxide and energy fluxes is often required (Richardson & Hollinger, 2005). Micrometeorological data is non-stationary due to changes in phenology and physiological characteristics over time (Hollinger & Richardson, 2005; Stoy et al., 2005). In addition, it does not conform to the least squares assumptions of normality and constant variance (Loescher et al., 2006); therefore, traditional methods of simple and

multiple linear regression techniques are not suitable when evaluating the relationship between flux data and independent climatic variables. For example, Richardson & Hollinger (2005) showed that eddy covariance data fitted with an ordinary least squares model led to an over estimation of night-time respiration and thus, an underestimation of net ecosystem exchange (represented by observed carbon dioxide flux). Furthermore, there are a number of complex interactions that occur between flux components depending on light, nutrient and water availability that also influence ecohydrological behaviour and individually regressing one variable could mask the effect of another (Mueller et al., 2010). For instance, GPP is dependent on both temperature and light. Therefore, omitting temperature from the regression analysis will obscure the influence of the light (or vice versa), rendering it statistically insignificant when perhaps it is not (Mueller et al., 2010). Additionally, many micrometeorological variables follow seasonality similar to carbon dioxide fluxes. By regressing one variable against carbon dioxide flux, the relationship may actually be a result of a correlation between seasonal cycles rather than an indication of the true relationship (Huntzinger et al., 2011). For these reasons, it is necessary to employ statistical methods that incorporate numerous variables and can account for the temporal correlation (i.e. autocorrelation) between carbon dioxide flux components and its climatic controls (Huntzinger et al., 2011; Stoy et al., 2005). To overcome the limitations of traditional regression methods, more sophisticated statistical approaches including orthogonal wavelet transformation (e.g. Delpierre et al., 2012; Stoy et al., 2009) and model selection in conjunction with geostatistical regression (e.g. Huntzinger et al., 2011; Mueller et al., 2010; Yadav et al., 2010) have been applied to determine the relationship between climatic drivers and flux components. With respect to the latter approach, model selection is most commonly achieved through the application of the Bayes Information Criterion (BIC; Schwarz, 1978) where the aim is to select the most probable combination of covariates that best explains the variability of fluxes (Forster, 2000; Huntzinger

et al., 2011). The benefit of using this approach as opposed to more traditional hypothesis-based model selection is that it can be used to compare non-nested models that may otherwise overlook those covariates that, when combined, are significant in explaining the variability in carbon flux components (i.e. net ecosystem exchange, gross primary productivity or respiration) but individually they may not (Mueller et al., 2010; Yadav et al., 2010).

Based on a maximum-likelihood estimator, BIC, as given by Yadav et al. (2010), is:

$$\boldsymbol{BIC = -2L^{*}\left(\sigma_N^2, \sigma_S^2, l; z\right) + k\, ln(n)} \tag{11}$$

where n is the number of observations, k is the number of covariates, σ_N^2 is the variance of the variability that is temporally uncorrelated, σ_S^2 is the variance of the variability that is correlated in time, l is the correlation range parameter, z is the parameter of interest, and $L^{*}(\sigma_N^2, \sigma_S^2, l; z)$ is the log-likelihood of the model being considered. The model that produces the lowest BIC value is then considered the best model to use for the geostatistical regression. It is important to note, however, that given that some covariates are dependent on others (e.g. temperature and vapour pressure deficit), a number of models could similarly account for the variability in fluxes (Yadav et al., 2010).

Once the 'best' model has been selected, the second step in the process is to apply geostatistical regression (i.e. universal kriging), which is a parametric approach often used to model environmental phenomena in studies of geology, ecology and hydrology (Huntzinger et al., 2011; Yadav et al., 2010). In geostatistical regression, the dependent variable, y, (e.g. ET_a or GPP) is expressed as the sum of a deterministic component ($\mathbf{X\beta}$) and a stochastic term (ε):

$$\boldsymbol{y = X\beta + \varepsilon} \tag{12}$$

where the deterministic component represents the portion of the signal that can be explained by a set of covariates and the stochastic

component describes the autocorrelation that cannot be explained by the deterministic component (Huntzinger et al., 2011; Mueller et al., 2010; Yadav et al., 2010). The deterministic component, **Xß**, is further decomposed into **X**, which is an *n* x *p* matrix containing rows of *p* environmental variables (e.g. air temperature, net radiation, wind speed) scaled by a *p* x *1* vector of unknown coefficients, **ß** (Huntzinger et al., 2011). This coupling of BIC model selection with geostatistical regression methods will enable the identification of an optimal set of micrometeorological variables that can be incorporated into **X** that are best able to explain observed variability in water and carbon dioxide fluxes, represented by the regression (or drift) coefficient ($\widehat{\boldsymbol{\beta}}$).

The application of rigorous quality control and gap-filling procedures detailed in this section strengthens the integrity of the EC flux dataset used for this study.

4 METHODOLOGY

4.1 Estimating the mass and energy exchange of broad-acre cropping systems in the CIA

The mass and energy exchanges of the selected cropping systems were measured by employing eddy covariance technologies. Through the implementation of fast response sensors, direct measurement of carbon dioxide, water vapour and energy fluxes between the land-surface and the atmosphere was achieved.

4.1.1 Eddy covariance measurements

The EC instrumentation for the four installations (hereby referred to as flux towers) was almost identical. Two flux towers were placed in-situ over the growing season in 2010/11 to monitor the mass and energy exchange of the two major summer crops cultivated in the area, maize and rice. Both flux towers consisted of a three-dimensional sonic anemometer (CSAT3, Campbell Scientific Inc., USA), which measured fluctuations in longitudinal, lateral and horizontal wind speed and direction (u, v, w; m/s), and an open-path infrared gas analyser (LI-7500, LI-COR Inc., USA) designed to measure CO_2, water vapour and momentum fluxes. Both the sonic anemometer and gas analyser were positioned to face into the expected prevailing wind direction on a boom that extended 1 m horizontally from the tower. As the main interest of this study was to investigate water and carbon dioxide flux response to micrometeorological drivers instantaneous measurements of flux variables were required (Burba, 2013), therefore the sampling rate of each system was set at 10 Hz and recorded with a data logger (CR3000, Campbell Scientific, Inc. USA). The fluxes (as a measure of the covariance between the scalar (e.g. CO_2 or H_2O) and the vertical wind component) were then computed as an average of the 10 Hz data over 30 minute intervals. Both the 10 Hz data and the 30 minute averaged data were recorded on a 2 GB Compact Flash card which was downloaded on a monthly basis.

4.1.2 Micrometeorological measurements

Micrometeorological instruments were also stationed at each site to complement the EC flux measurements. Ancillary observations of wind speed and direction were made with a standard wind vane and anemometer (RM Young Wind Sentry 3001, Campbell Scientific, Inc. USA). Air temperature and relative humidity were measured with an aspirated and shielded thermistor and capacitance sensor (HMP45C, Campbell Scientific, Inc. USA), and a tipping bucket rain gauge (TB3, Hydrological Services Pty. Ltd. Australia) was used to measure rainfall. Net radiation (R_n) was measured using a four-component net radiometer (CNR1, Kipp & Zonen B.V.) on a boom fixed 2 m above the ground surface and oriented to the north. Ground heat flux (G) was measured using two self-calibrating soil heat flux plates (HFP01SC, Hukseflux Thermal Sensors B.V.) at distances of 10 m to the north and 25 m to the west of each flux tower. These were buried at depths of 80 mm in conjunction with two thermocouple configurations buried 1 m apart at depths of 60 mm and 20 mm (114 TCAV-L, Campbell Scientific Inc., USA). Volumetric soil moisture content was not measured. In the absence of suitable time series data, a default value based on soil samples taken at each site was used to calculate the heat storage in the soil layer above the heat flux plates. Solar radiation values were taken from a nearby weather station operated and maintained by CICL.

4.2 Data processing, quality control and gap-filling strategies

4.2.1 Cospectral analysis

The application of eddy covariance technologies to determine mass and energy balances has not yet been reported within an Australian irrigated agricultural environment. It was necessary, therefore, to perform a comprehensive cospectral analysis to determine an averaging period to ensure all significant low-frequency eddies would

be accounted for. This can be achieved through an ogive test, represented by the cumulative integral of the cospectrum, beginning with the highest frequency (Foken et al., 2006; Oncley & Friehe, 1996; for further details of this test please see Section 3.2.3). The point at which the ogive curve has reached its asymptote is the point at which one can be sure that the sample period is long enough to capture all low frequency eddies (Moncrieff et al., 2004). Note that as cospectra describe how much of the flux is transported at each frequency, the area under the curve represents the flux (Burba & Anderson, 2010).To perform the ogive test, the raw, non-gapfilled 10 Hz data were processed using open-source software, EdiRe© (an open-source software package specifically designed to assist in eddy covariance data processing; Clement, 1999). Daytime data were integrated over 120 minute averaging periods between the hours of 07:00 and 19:00 Australian Eastern Standard Time (AEST) for both summer and winter crops to avoid the influence of the daily cycle of fluxes and non-steady state conditions, as per Foken et al. (2006). Longer periods are generally not scrutinised due to the daily cycle of fluxes and high non-steady state conditions (Foken et al., 2006). Because the ogive test fails if missing values occur within the time series, only intervals devoid of gaps were included in the analysis, avoiding the bias of abnormal cospectra. In this study, ogives were constructed based on sensible heat flux co-spectra only ($w'T_{sonic}'$). The main reason for doing so was because the sonic temperature (T_{sonic}) and vertical wind speed (w) were instantaneously derived from the sonic anemometer, negating the need to account for sensor separation or time delays between two signals (i.e. if temperature and wind speed were measured by two different instruments). As such, $w'T_{sonic}'$ was considered close to ideal, and the actual scalar flux (water vapour or CO_2) would lie somewhere below this curve (Burba & Anderson, 2010).

4.2.2 Spike detection, corrections and gap-filling

The flux data that were averaged over each 30 minute interval was post-processed using standard eddy covariance protocols and in-house software developed through the OzFlux community (Isaac & Cleverly, 2011), further modified to suit the needs of this study. For instance, additional calculations were incorporated into the program to account for the heat storage in the water column to calculate *G* for the rice crop. The quality control, flux calculation and correction process is illustrated in Figure 4.1. As depicted, the raw data (Level 1; L1) was ingested into the program and preliminary quality control checks of the raw data were performed. These were based on artificial spike detection (where values of a given variable are greater than 5 – 7 standard deviations from the mean), sensor diagnostics and known maintenance periods to produce a Level 2 (L2) dataset with quality control flags. Corrections, flux calculations, further range checks, u* filtration and removal of unwanted data (e.g. removal of contaminated turbulent flux data originating in the quadrant directly behind the sensor) were performed on the L2 dataset to produce a clean, non-gapfilled Level 3 (L3) dataset. Detailed information regarding the specific corrections is presented in Table 4.1. Once all data had been processed, a gap-filling procedure was implemented whereby data gaps of less than 60 minutes were filled using simple linear interpolation techniques and larger gaps were filled using daily climatologies calculated for the same observation period; this produced a Level 4 (L4) clean, gap-filled dataset.

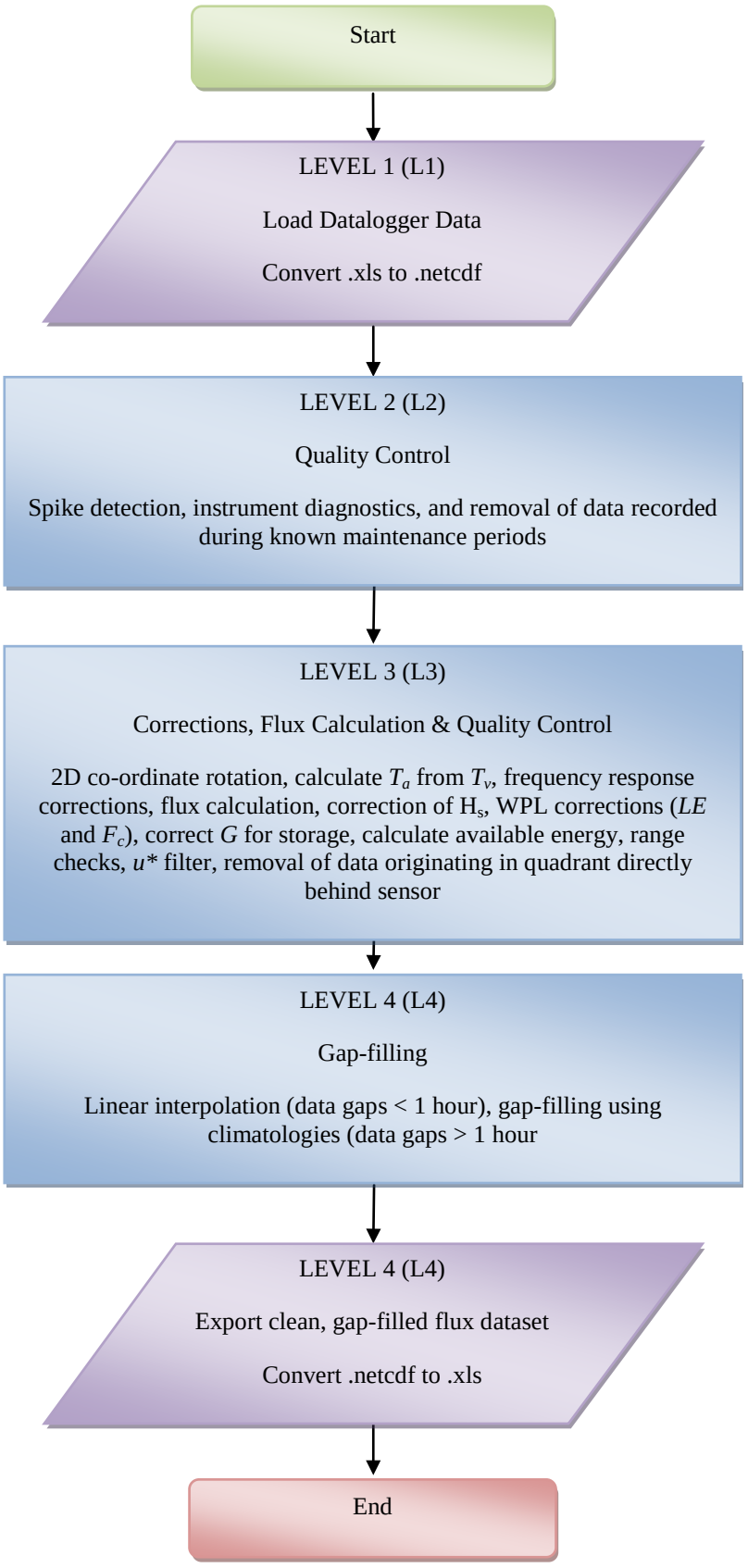

Figure 4.1 Quality control, flux calculation and correction process

Table 4.1 Corrections and calculations applied to flux data to produce a Level 3 (L3), non-gap-filled dataset

Correction/calculation	*Purpose*	*Primary references*
Two dimensional co-ordinate rotation	To align the mean lateral and vertical velocities to zero i.e. $\overline{u}$ = $\overline{w}$ = 0	(Lee et al., 2004b)
Calculate air temperature (T_a) from virtual temperature (T_v), absolute humidity and pressure	To provide a more robust measurement of air temperature based on sonic thermometry measurements (i.e. as measured by the CSAT3)	(Loescher et al., 2005)
Frequency response corrections	This includes a suite of corrections to compensate for flux losses as a result of spectral attenuation (invoked by sensor design and time response, sensor separation, electronic filters etc.)	(Massman, 2000, 2001; Massman & Clement, 2004)
Flux calculation	Calculate fluxes from covariances; this is detailed in Section 3.3.1	(Lee et al., 2004b)
Webb Pearman Leuning (WPL) corrections	To compensate for fluctuation effects of temperature and water vapour on *LE* and F_c fluxes	(Leuning, 2004; Webb et al., 1980)
Correct *G* for storage	To calculate the heat stored in the soil layer above the soil heat flux plate and incorporate this into estimates of *G*	(Campbell Scientific Inc., 2007)
Friction velocity (*u**) threshold	To correct for the underestimation of night-time F_c fluxes (see Section 4.3.1)	
Removal of contaminated fluxes from quadrant opposite orientation of EC sensors	Turbulent flux data was also removed to prevent the influence of flow distortion as a result of air passing through the tower and solar powered battery array behind the sensors	(Zhang et al., 2013)

4.2.3 Flux footprint analysis

Due to limited water supplies, crops grown in the CIA are limited in their extent and are often grown alongside non-irrigated fallow lands and remnant vegetation. Given the heterogeneous nature of irrigated farmland in the CIA, it is necessary to ensure that the source emissions are representative of the areas of interest. For these reasons, a comprehensive review of the effective fetch (or flux footprint) was undertaken using the Microsoft® Excel based ART (Agroscope Reckenholz-Tänikon) Footprint Tool designed by Neftel et al. (2008) based on the analytical model developed by Korman & Meixner (2001). The EC inputs required to run this tool can be seen in see Table 4.2. In this instance, the time step used was 30 minute-averaged data. Model outputs include a number of different parameters and can be seen in Table 4.3.

A simple two dimensional description of the footprint is illustrated in Figure 4.2. *KM_p01a* is the intersection of 1%-ellipse nearest to sensor, *KM_p01b* is the intersection of 1%-ellipse farthest from the sensor and *KM_p01c* is half the width of the 1%-ellipse of the crosswind component (Spirig & Neftel, 2007).

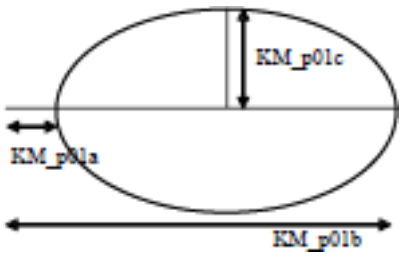

Figure 4.2 Two-dimensional schematic view of the footprint model (Spirig & Neftel, 2007).

Once complete, the model outputs were post-processed using bespoke scripts developed in the MATLAB® environment (The MathWorks Inc, 2010). Based on our data, daytime and night-time data were sorted according to the value of net radiation whereby night-time was

defined as the period where net radiation was less than 0.5 MJ/m^2. Values where 90% of the integral fell within the footprint function were identified, and the mean length of the ellipse was calculated for both daytime and night-time periods.

Table 4.2 Input parameters required to determine the flux footprint using the ART footprint tool (Spirig & Neftel, 2007).

Parameter	*Description*	*Units*	*Admissible range*
Time	Measurement time	days after1.1.1900	>1.0
x_{sensor}	x coordinate of receptor (E-W coordinate)	m	-5000 – 5000
y_{sensor}	y coordinate of receptor (S-N coordinate)	m	-5000 – 5000
u*	Friction velocity	m/s	0.01 – 5
L	Obukhov length	m	-99 999 – 99 999
σ_v	standard deviation of cross wind speed	m/s	0 – 20
wdir	Wind direction	Degrees	0 – 360
z_m	Measurement height (*z-d*)	m	0 – 1000
U	horizontal wind speed	m/s	0 – 30

Table 4.3 Outputs of the ART footprint tool and corresponding units or dimensions where L = length and T = time (Spirig & Neftel, 2007).

Output	*Description*	*Units/dimensions*
Zo	Zero displacement height	m
Phitot	Integral of footprint function over considered domain	%
Field_x	Footprint contribution of field x	%
Umaj	U, Constant in power-law profile of the wind velocity	$L^{1-m} T^{-1}$
Kmaj	K, Constant in power-law profile of the eddy diffusivity	$L^{1-m} T^{-1}$
M	Exponent of the wind velocity power law	-
N	Exponent of the eddy diffusivity power law	-
A,B,C,D,E	A-E parameters defining footprint function	-
KM_p01a	Intersection point of 1%- ellipse nearest to sensor	m
KM_p01b	Intersection point of 1%- ellipse farthest from sensor	m
KM_p01c	Half width of 1%-ellipse	m

4.2.4 Surface energy balance

4.2.4.1 Determination of surface energy balance components

For the rice crop, additional components of G (see Section 3.3.2) were incorporated to account for the heat storage in the floodwater (W) as well as the soil heat storage (S), adapted from Tsai et al. (2007), i.e.

$$\boldsymbol{G = S + W} \tag{13}$$

therefore

$$\boldsymbol{R_n - (S + W) = H + LE} \tag{14}$$

where

$$\boldsymbol{S = \rho_g\, c_g\, z_g\, \frac{\partial T_g}{\partial t}} \tag{15}$$

and

$$\boldsymbol{W = \rho_w\, c_w\, z_w\, \frac{\partial T_w}{\partial t}} \tag{16}$$

where ρ_g and ρ_w represent the density of wet soil and water respectively; c_g and c_w represent the heat capacity of wet soil and water respectively; z_g and z_w are the depth of the soil heat flux plates in relation the soil surface and the depth of the floodwater respectively; and dT_g/dt and dT_w/dt represent the rates of change in soil temperature and water temperature respectively. In the absence of water temperature data, the average air temperature as measured by the EC system was used to estimate W based on the assumption that mean water temperature is similar to mean air temperatures, after De Datta (1987).

4.2.4.2 Determination of surface energy balance closure

When using eddy covariance systems, the sum of sensible and latent heat ($H_s + LE$) is generally less than the available energy ($R_n - G$) (Leuning et al., 2005). Research has shown that annual temporal

coverage of surface energy fluxes can be underestimated by 25 – 35% (Falge et al., 2001a; Falge et al., 2001b) with an average underestimation of 20% based on the findings of Wilson et al. (2002a), who investigated 22 FLUXNET sites varying in topography and land cover (including agriculture, grasslands and coniferous forests). Therefore, it is considered necessary to conduct an audit of the energy balance to assess the overall performance of the instruments and to obtain an independent assessment of the scalar flux estimates under these particular conditions. In this study, an evaluation of the energy balance closure was determined specifically by using the Energy Balance Ratio (*EBR*; see Section 3.3.2) to average over random errors in the measurement of the independent variables over longer timescales (Tsai et al., 2007; Wilson et al., 2002b). The *EBR* was calculated for all 30 min fluxes over the entire observation period.

4.3 Flux partitioning to determine ecosystem respiration and gross primary productivity

4.3.1 Determination of friction velocity threshold

The friction velocity (or u^*) threshold (see Section 3.4.2) is used to determine stable atmospheric conditions and can be used to correct for the underestimation of night-time CO_2 fluxes and determine ecosystem components of carbon metabolism (*GPP*, *NEE* and *Re*). The u^* threshold can be found by plotting night-time values of u^* against corresponding CO_2 fluxes; the u^* threshold is located at the point where the fluxes begin to decrease as u^* decreases (Jans et al., 2010). To determine the u^* threshold, rank-ordered night-time u^* values and corresponding CO_2 fluxes were divided into 25 groups. The average values of each group were then calculated and plotted to evaluate the relationship between u^* and CO_2 flux (Long, 2008).

4.3.2 Determination of an empirical model to partition carbon dioxide fluxes

Eddy covariance systems, whilst providing estimates of net ecosystem exchange (*NEE*, measured as CO_2 fluxes), cannot directly measure ecosystem respiration (*Re*) or gross primary productivity (*GPP*). Instead, models are required to partition *NEE* into *Re* and *GPP* (see Section 3.3.1; Baldocchi et al., 2001; Stoy et al., 2006).

At night, *GPP* is equal to zero, hence *NEE* is equal to total *Re*. Therefore, the difference between daytime *NEE* and night-time *NEE* can be used to calculate *GPP* using an empirical model to extrapolate night-time respiration (Rocha & Goulden, 2009; Wohlfahrt et al., 2005). To determine the components of carbon metabolism (i.e. *NEE*, *Re* and *GPP*), the approach used by Leuning et al. (2005) and Saito et al. (2005) was adopted for this study. At night, it was assumed that photosynthetic activity, and therefore *GPP*, was zero. Based on this assumption, *Re* at night was considered to be equal to night-time *NEE* (F_c). As *Re* is sensitive to temperature (Lloyd & Taylor, 1994), night-time CO_2 fluxes are plotted against corresponding soil or air temperatures, and a simple exponential function is fitted to the data. This equation is given by:

$$\boldsymbol{Re} = \boldsymbol{A}\mathbf{exp}(\boldsymbol{BT}) \qquad (17)$$

where *A* and *B* are empirical constants determined by regression and *T* represents temperature. This exponential function can then be used to deduce daytime estimates of *Re* and thus, *GPP*, where the sign convention is such that positive *NEE* is a flux of CO_2 into the atmosphere and both *Re* and *GPP* are positive (Davis et al., 2003).

The application of this methodology also enables the correction of night-time carbon dioxide fluxes that may be underestimated due to periods of atmospheric stability (as indentified by the u^* threshold) by adjusting fluxes according to the same exponential function (as night-time F_c (*NEE*) is equal to night-time *Re*.

4.4 Examining the relationship between water and carbon dioxide fluxes

4.4.1 Water and carbon dioxide flux response to environmental drivers

Gross primary productivity (*GPP*) is the key indicator of ecosystem functions such as respiration and biomass accumulation (Suyker & Verma, 2012), which is primarily affected by local hydrology (Alberto et al., 2009). It is, therefore, important to understand the extent to which certain environmental factors influence ET_a and *GPP* rates, particularly in the CIA where in-depth studies using EC methods are yet to be reported.

ET_a, and thus *GPP*, are controlled by a number of climatic factors, including net radiation (R_n), air temperature (T_a), vapour pressure deficit (*VPD*), wind speed (*U*), rainfall (*P*) and soil moisture (Zha et al., 2010). The degree to which ET_a and *GPP* are influenced by these factors is highly dependent upon the general climatic conditions of a given region (Matsoukas et al., 2011). For example, ET_a in tropical regions is controlled primarily by monsoonal winds during the monsoon season (Rao, 2008). Other studies have shown that in semi-arid climates the magnitude and distribution of precipitation control energy partitioning and thus, ET_a (Krishnan et al., 2012).

The relationships between ET_a, *GPP* and the aforementioned environmental variables (excluding soil moisture) were investigated through the application of geostatistical regression based on model selection methods (specifically, Bayes Information Criterion; BIC). For more information, see Section 3.4.2.

4.4.2 Water and carbon dioxide flux response to biophysical crop characteristics

As well as being governed by climatic variables, ET_a and thus, *GPP*, are also controlled by a number of biophysical crop characteristics (Allen, 1988) which is best represented by measurements of leaf area index (LAI). LAI is leaf area per unit ground area. Moreover, it amalgamates the key structural and architectural (e.g. gap-size and light-interception) elements of a plant canopy that regulate many of the biophysical processes of atmospheric land-surface interactions, including photosynthesis, respiration, and ET_a (Chen et al., 1997). As LAI changes over time according to different phenological stages of the plant, it is a useful variable to investigate the response of ET_a.

4.4.3 Biophysical water productivity

Water productivity (WP) is the ratio of net benefits to the amount of water used to produce goods and services (Cai et al., 2011). From a hydrological perspective, WP is often expressed as either the grain yield per unit of water lost through ET_a or the grain yield per unit of irrigation water supplied (Alberto et al., 2011; Zwart et al., 2010). In terms of this study, the benefits are measured by the amount of total biomass accumulation (represented by *GPP*, or above-ground biomass) per unit of water lost through ET_a over the growing season (Suyker & Verma, 2010), given by the equation:

$$\boldsymbol{WP_{ET_o}} = \frac{\sum \boldsymbol{GPP}}{\sum \boldsymbol{ET_a/ET_o}} \tag{18}$$

This will then provide an indication of the relationship between water and carbon dioxide fluxes of these cropping systems. To better compare values of WP for different cropping systems, daily ET_a values are normalised by daily reference evapotranspiration values (ET_o) (Suyker & Verma, 2010).

4.5 Regional estimation of fluxes

4.5.1 Land cover/land use classification

A land cover and land use (LCLU) classification was performed to determine the locations and total area of maize, rice, wheat and other various crops throughout the CIA for both the summer and winter growing seasons. To do this, cloud-free satellite imagery (specifically, LANDSAT 5 TM) was downloaded from the USGS website (http://glovis.usgs.gov/) and processed by employing a supervised classification procedure using standard ENVI 5.0® and ArcGIS 10.1® software. The accuracy of each classification was assessed through a confusion (or error) matrix whereby the classified image was compared to ground-truthing information gathered each field visit during the campaign and seasonal water orders provided by CICL. The seasonal water orders provide information regarding the amount of water requested per farm and per crop and the actual amount of water delivered to the property.

4.5.2 Regional upscaling of water and carbon fluxes

Without conducting an extensive field campaign, the most cost-effective method to estimate water vapour and carbon dioxide at a regional scale is to use remote sensing/geographic information system technologies in conjunction with ground-based information. In this case, LCLU classification maps (see Section 4.6.1) were used to identify areas within the CIA where similar crops were grown. Soil maps derived from an electromagnetic survey were used to identify areas of similar soil type; the survey was originally commissioned by the CICL to determine areas within the region where crop production may be inefficient due to insufficient quantities of clay in the soil profile, particularly for rice production. Both maps were analysed using standard geoprocessing methods in ArcGIS® to ascertain where agricultural fields of a single cultivar were being grown on similar

soils, based on the assumption that each individual cultivar (i.e. maize, rice or wheat) grown on similar soils will have a similar response to micrometeorological drivers of mass and energy exchange. Once these areas had been identified, the point-based estimates of water and carbon fluxes derived from the flux towers were directly extrapolated across the region. Extrapolation was a simple multiplication of total area by total cumulative fluxes for maize, rice and wheat, with the acknowledgement that this approach does not provide an accurate or detailed assessment of water and carbon fluxes at this scale.

4.6 Ancillary data and additional calculations

4.6.1 Leaf area index and determination of phenological growth stages

Leaf area index (LAI) is a key structural characteristic of an ecosystem given that the associated green leaf matter plays a major role in controlling many of the biological and physical processes between atmospheric and land-surface interactions (Chen et al., 1997). Estimates of LAI can provide useful information with respect to the photosynthetic and transpiration potential of a canopy as well as providing a remote sensing measure of surface reflectance within the canopy. In this study, LAI was measured indirectly through the use of a commercially-available optical instrument, LAI-2000 (LI-COR, Inc. USA), which operates on the premise that the amount of foliage within a canopy can be deduced from how much radiation passes through it (LI-COR, 1992). LAI measurements were taken throughout the growing season for maize and rice (summer 2010/11) every 7 – 28 days, weather permitting. LAI measurements for the growing season of winter 2011 were not made due to budgetary restrictions.

The phenological stages for each crop were determined through observations made during each site visit in conjunction with information relayed by the landholder. These data were augmented

with analogous phenological data from the NSW Department of Primary Industries (Yanco) for the same period.

4.6.2 Soil sampling and analysis

Two soil samples, one 25 m directly west of the flux tower and the other directly 10 m south of the flux tower, were taken from the top profile (0 – 0.3 m) at each site at the time of the flux tower installation. Each sample was tested for moisture content (%), total organic carbon (mg/kg) and bulk density (mg/m^3). These values were then incorporated into the data processing program as default values or variables required to calculate ground heat fluxes. It is acknowledged that this methodology is flawed as the default values, particularly soil moisture content, are not representative of real-time conditions; therefore estimates of *G* are a loose approximation at best.

4.6.3 Harvest index and yield data

The harvest index (HI) is the ratio of the yield of grain to the biological yield (Donald & Hamblin, 1976), or, put simply, the ratio of seed mass to the total above-ground plant biomass (Lecoeur & Sinclair, 2001). It is commonly expressed as:

$$\boldsymbol{HI} = \frac{\boldsymbol{total\ grain\ yield}}{\boldsymbol{total\ dry\ weight}} \tag{19}$$

Just prior to harvest, samples of each crop were taken from 1 m^2 sites to determine the harvest index; the total number of samples was proportional to the total area planted to each variety at each site, and each sample was selected at random. These samples were oven-dried at 80°C over 3 – 4 days. The dried material was then thrashed to separate the grain from the remaining organic matter and both components were weighed individually to determine the harvest index. Overall yield data were obtained directly from the landholder post-harvest.

4.6.4 Calculation of zero-plane displacement and surface roughness length

The zero-plane displacement height (d_0) and aerodynamic (or surface) roughness length (z_0) of a given canopy are two of the key parameters, based on canopy height and structure, that influence land-surface interactions (Yang & Friedl, 2003). Zero-plane displacement is the mean height at where momentum is absorbed by the canopy (Thom, 1975). The surface roughness length is the height above the surface at which the mean logarithmic profile is zero (Zhou et al., 2006).

At each scheduled maintenance or site visit, crop heights of 20 randomly located individual plants were measured. These values provided an average canopy height (h) which was then used to determine the zero-plane displacement, commonly defined as:

$$\boldsymbol{d_0 = 2/3\ h} \tag{20}$$

The average canopy height was also used to calculate the surface roughness length throughout the growing season, based on Brutsaert (1982):

$$\boldsymbol{(h/z_0) = 3e} \tag{21}$$

where e is a constant number which is often referred to as Euler's number and is equal to approximately 2.72.This information was then used to set parameters within the data processing program to estimate the fluxes over a given crop.

4.6.5 Calculation of reference and potential crop evapotranspiration

Reference crop evapotranspiration (ET_o) is the evapotranspiration of a hypothetical grass reference crop 0.12 m tall, with a fixed surface resistance of 70 s/m and an albedo of 0.23. It was developed as a means of investigating the atmospheric evaporative demand regardless

of crop type, crop development or agricultural management practices and was calculated by the equation (Allen, 1988):

$$\boldsymbol{ET_o = \frac{0.408\Delta(Rn-G)+\gamma\left(\frac{900}{T+273}\right)u_2(e_s-e_a)}{\Delta+\gamma(1+0.34u_2)}} \quad (22)$$

Where R_n is the net radiation (MJ/m^2/day); G is the soil heat flux (MJ/m^2/day); T is the mean air temperature measured at 2 m height from the soil surface (°C); e_s is the saturation vapour pressure (kPa); e_a is the actual vapour pressure (kPa); Δ is the slope vapour pressure curve (kPa/°C); γ is the psychrometric constant (kPa/°C); u_2 is the wind speed at 2 m height (m/s); and ($e_s - e_a$) is the vapour pressure deficit (Kpa).

Because ground cover, canopy properties and thus, aerodynamic resistances, differ from crop to crop, a method of calculating potential crop evapotranspiration (ET_c) was developed. ET_c is the amount of water lost through evapotranspiration of different crops grown under standard conditions and is calculated by multiplying the ET_o with a specific crop coefficient (K_c) and is given by the formula (Allen, 1988):

$$\boldsymbol{ET_c = K_c \times ET_o} \quad (23)$$

The MIA experiences similar climatic conditions to the CIA, therefore the crop coefficients used to determine ET_c in the former region were used to estimate ET_c in the CIA. The K_c values are presented in Table 4.4.

In addition to calculating ET_c, ET_o was also used to calculate biophysical water productivity (see Section 4.4.3).

.

Table 4.4 Crop coefficients (K_c) used to determine potential crop evapotranspiration (ET_c) in the CIA (adapted from Meyer et al., 1999; Wu et al., 2000).

Crop	*Jan*	*Feb*	*Mar*	*Apr*	*May*	*Jun*	*Jul*	*Aug*	*Sep*	*Oct*	*Nov*	*Dec*
Rice	1.1	1.1	1	0.4	–	–	–	–	–	1	1.1	1.1
Maize	0.85	0.85	0.6	0.3	–	–	–	–	–	0.35	0.5	0.7
Wheat	–	–	–	–	0.4	0.6	0.9	1.05	1.05	0.8	0.5	–

4.6.6 Irrigation and crop specific data

Land preparation, sowing dates, seeding rates, fertilisation and pest/disease/weed management strategies and irrigation schedules were collated through information received directly from the landholders for each particular site and crop. Any irrigation information that was incomplete was supplemented with water delivery statements to each farm (per crop) obtained from CICL records for each season.

4.6.7 Instrument maintenance and calibration

EC systems are often deployed in remote locations and are exposed to the natural elements (e.g. electrical storms, strong winds) and animals. Exposure to these elements may damage the sensors to varying degrees, thus affecting their performance and potentially resulting in large data gaps. Data sets requiring a large amount of gap-filling will reduce the integrity of the time series (Burba & Anderson, 2010). Regular calibration of the sensors is also necessary to maintain measurement accuracy. This is particularly important for the successful operation of the open-path gas analyser where the signal response can be significantly affected by temperatures greater than 30°C as well as periods when the temperature difference is greater than 10 °C or when a large pressure change occurs (> 40 kPa), especially when measuring H_2O concentrations (LI-COR, 2001). For the duration of this study routine maintenance was carried out every 4 – 6 weeks; this involved cleaning of the gas analyser optical windows to ensure the automatic gain control values were less than 55 – 65% as per recommendations (LI-COR, 2001); cleaning of sonic anemometer to remove any foreign objects (e.g. spider webs and bird droppings) that may distort airflow); and cleaning of solar panel to ensure optimal performance of battery array/power supply. Individual calibration of the LI-COR 7500 sensors occurred every 2 – 5 months during the flux tower installations. Calibration was performed according to the

recommendations of the manufacturer (see LI-COR, 2001). The EC sensors were not cross-calibrated during this study; the implications of this are discussed in Section 7.3.

5 ASSESSMENT OF QUALITY CONTROL PARAMETERS AND MICROMETEOROLOGICAL DRIVERS

5.1 Specific crop and site selection

Crop selection was based on the three major broad-acre crops produced in the area: rice and maize grown over the summer months and wheat, the predominant winter crop. Adequate fetch (or footprint) upwind of sensors was the primary consideration to ensure that mostly all observed fluxes were representative of the single cultivar of interest. The willingness of the landowner to participate in the experiment was also an important consideration.

With the benefit of having two complete EC systems, two cropping systems were monitored over the summer and winter growing seasons of 2010/11. The locations of the flux tower in relation to one another are depicted in Figure 5.1.

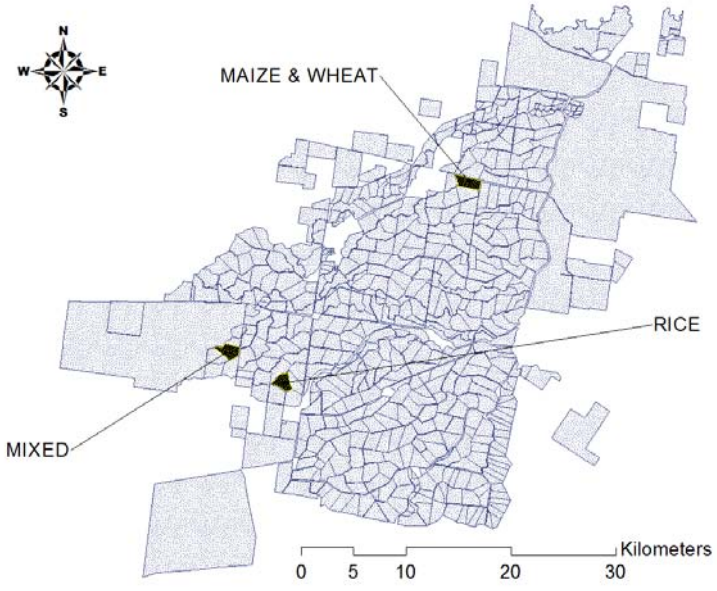

Figure 5.1 Location and crop varieties of experimental flux tower sites within the CIA – 2010/11.

5.1.1 Summer 2010/11 - Maize

A flux tower situated in the north-east of the CIA (Lat. -34.760, Long. 146.015, Elevation 120 m; see Figure 5.1) was erected to monitor carbon, water vapour and energy fluxes over a maize crop. This site is largely rectangular in shape (~ 900 x 700 m) and approximately 60 ha in area. The soil type is classified as transitional red-brown earth. These soils have an average bulk density of 1369 kg/m^3 at a depth of 0.1 m (for more information, see Hornbuckle et al., 2008).

Landform preparations for the maize crop included a pass with a chisel plough, a bed maker ripper and a bed shaper. The crop was sown at a rate of 80 000 seeds/ha (Pioneer 32P55) on October 7, 2010 and harvested on April 4, 2011, yielding ~12 t/ha and a harvest index of 0.52. Nitrogen fertiliser (urea) was aerially top-dressed on November 18, 2010 at a rate of 100 kg/ha. Surface irrigation water totalling 5.6 ML/ha was applied to the crop via a furrow system over the course of the growing season.

The flux tower was placed in the field on October 27, 2010 and remained in-situ until May 17, 2011, 42 days post harvest. At the time of the initial installation the crop had emerged and was nearing the end of the early stages of juvenile growth (i.e. 4 leaves present, as defined by Jans et al., 2010), as illustrated by Figure 5.2.

The sonic anemometer, gas analyser and temperature/relative humidity probe were placed at a height of 3.1 m above the ground surface. The rain gauge, wind vane/cup anemometer and net radiometer were located 1.0 m, 5.1 m and 2.0 m above the ground surface, respectively. As pollen shed began, when the crops were averaging a height of 2.5 m, the sensor masts were extended so that the sonic anemometer, gas analyser and temperature/relative humidity probe were 5.05 m above the ground surface whilst the rain gauge, wind vane/cup anemometer and net radiometer were placed at 4.4 m, 7.1 m and 4.0 m above the ground surface, respectively. The initial flux tower installation is depicted in Figure 5.3.

Figure 5.2 Leaf emergence of the maize crop at the time of the flux tower installation.

Figure 5.3 Initial flux tower installation over the maize crop.

5.1.2 Summer 2010/11 - Rice

A second flux tower was erected in the south-west of the CIA (Lat. -34.925, Long. 145.821, Elevation 120 m; see Figure 5.1). This site is an irregular polygon in shape. It is approximately 100 ha in area with soil properties similar to those listed for the maize crop.

Prior to planting, the earth was cultivated with a chisel plough. Phosphorus and nitrogen were also applied at rates of 14 kg/ha and 150 kg/ha, respectively, to improve potential biomass and yield. The crop was aerial sown at a rate of 188 kg/ha (Quest) on November 12, 2010 and harvested the week beginning April 20, 2011 with a yield of 10.1 t/ha (dry weight) and a harvest index of 0.50. Surface irrigation water was applied from November 6 – 12, 2010 at an average rate of 7.6 ML/ha. Water levels of 0.05 m were maintained prior to panicle initiation and 0.30 m thereafter; the water was drained on March 28, 2011.

The flux tower was installed in approximately the middle of the field prior to planting on November 3, 2010 and remained in place until May 16, 2011. The sonic anemometer, gas analyser and temperature/relative humidity probe were placed at a height of 2.6 m above the ground surface. The rain gauge, wind vane/cup anemometer and net radiometer were placed at 1.0 m, 3.2 m and 1.9 m above the ground surface, respectively. The flux tower installation is depicted in Figure 5.4.

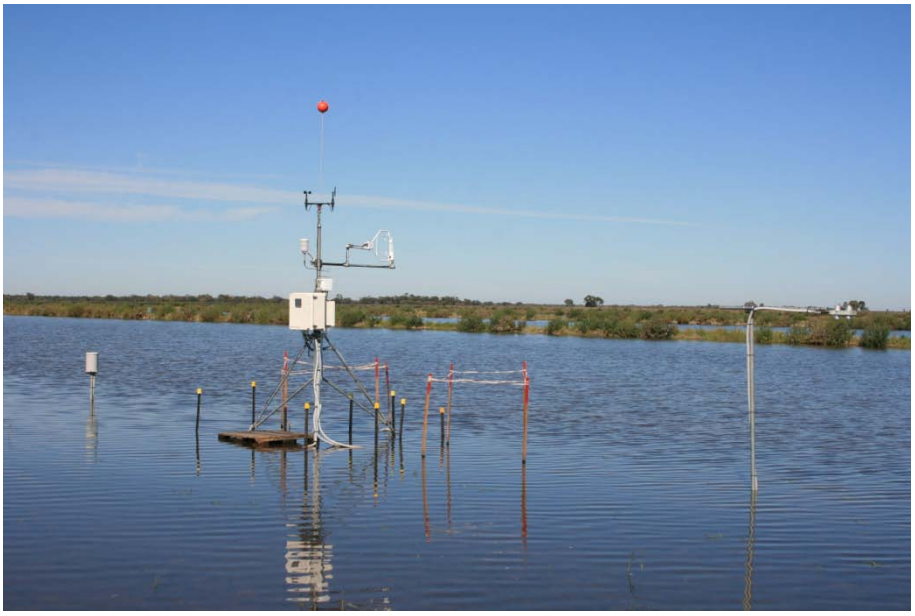

Figure 5.4 Flux tower installation over the rice crop.

5.1.3 Winter 2011 - Wheat

The flux tower that was used to monitor the carbon, water and energy fluxes of the maize crop was used to monitor wheat that was sown into the same field the following season (Lat. -34.760, Long. 146.015, Elevation 120 m; see Figure 5.1). The crop was planted on May 6, 2011 and harvested on December 3, 2011 with a yield of 5.0 t/ha and a harvest index of 0.61. Yield data and fertiliser application details of this particular crop were not made available by the landowner. Total surface irrigation water supplied through the furrow system over the growing season was applied at a rate of 2.6 ML/ha.

Based on anecdotal evidence of the region, the predominate winter winds in the CIA generally originate in the south-west; therefore the flux tower was repositioned on May 17, 2011 to improve fetch for winds approaching from this direction. The flux tower remained in place until it was decommissioned on December 13, 10 days after harvest. The sonic anemometer, gas analyser and temperature/relative humidity probe were placed at a height of 3.6 m above the ground surface. The rain gauge, wind vane/cup anemometer and net radiometer were placed at 1.9 m, 5.0 m and 2.0 m above the ground surface, respectively. The flux tower installation is depicted in Figure 5.5.

Figure 5.5 Flux tower installation over the wheat crop.

5.1.4 Winter 2011 - Mixed Cropping System (Wheat, Canola and Faba Beans)

In the south-west of the CIA, the second flux tower was relocated (Lat. -34.903, Long. 145.762, Elevation 120m; see Figure 5.1) to monitor a mixed cropping system comprised of wheat, canola and faba beans. This site is an irregular polygon in shape and is approximately 118 ha in area. The soil types are almost equal distributions of red brown earths and transitional red brown earths.

Land preparations prior to harvest included a burn to remove the stubble of the previous maize crop. The field was then sprayed with herbicide. The wheat was sown via direct drilling methods on May 17, 2011 at a seed application rate of 80 kg/ha (Merinda) and harvested on December 7, 2011 with a yield of 5.5 t/ha. The harvest index was 0.68. Two applications of fertiliser were made; 250 kg/ha was incorporated with the seed at sowing and a further 90 kg/ha broadcast on July 17, 2011. A total of 2.3 ML/ha of surface irrigation water was delivered to the wheat crop through a furrow system over the growing season, whilst the canola crop and faba bean crop received a total of 0.5 ML/ha and 2.0 ML/ha, respectively.

The flux tower was installed on May 18, 2011 and remained in-situ until it was decommissioned on December 13, 2011, 5 days after harvest. The sonic anemometer, gas analyser and temperature/relative humidity probe were placed at a height of 3.8 m above the ground surface. The rain gauge, wind vane/cup anemometer and net radiometer were placed at 1.0 m, 5.3 m and 2.0 m above the ground surface, respectively. The flux tower installation is depicted in Figure 5.6.

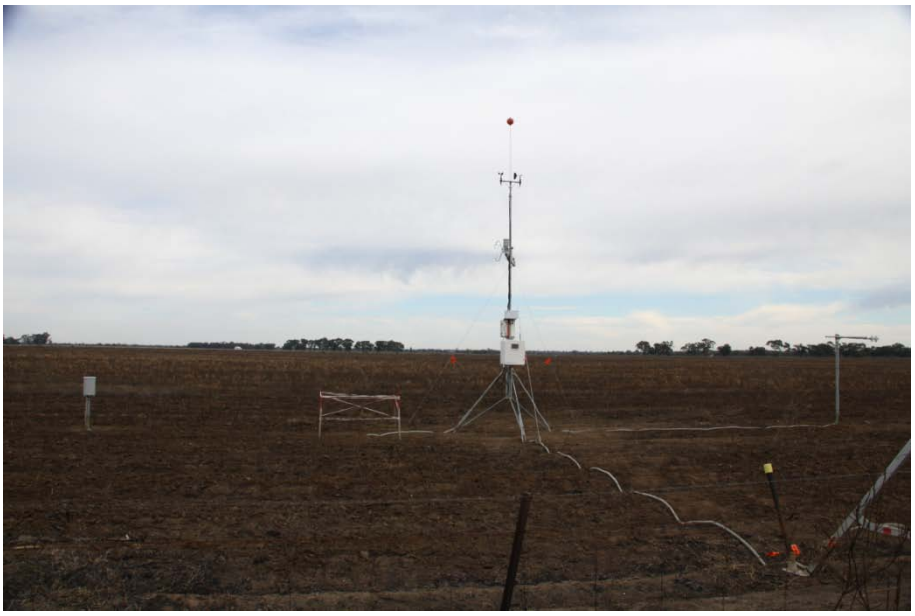

Figure 5.6 Flux tower installation over the mixed cropping system.

5.2 Micrometeorology

5.2.1 Wind speed and direction

A wind rose illustrating wind speed and direction was produced for each flux tower location using a Matlab© function (fcnwindrose; Schultz, 2011) requiring inputs of wind direction and intensity for each 30 min period.

Figure 5.7 illustrates the distribution of 24 hr daily wind speed and direction of the maize crop throughout the observation period. As indicated, the prevailing winds originated mostly from the south-west (180°– 215°) at speeds of 0 – 7 m/s.

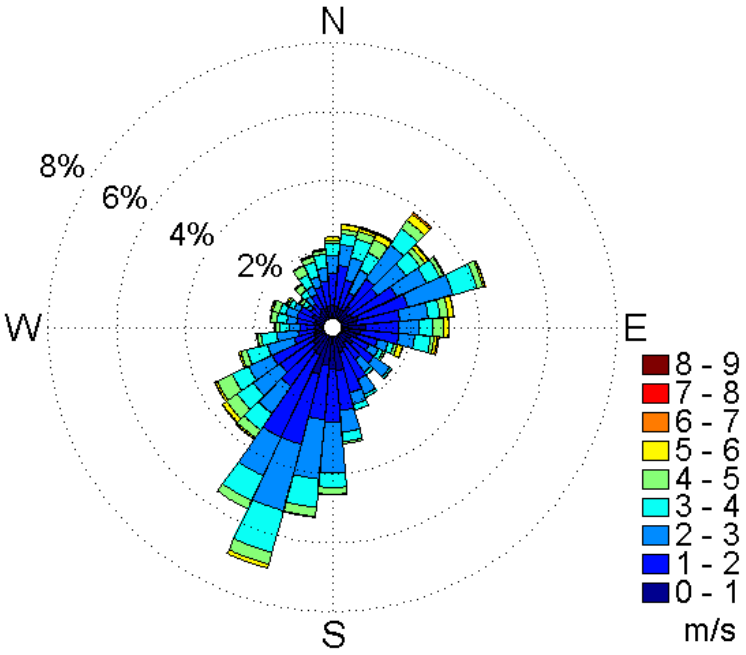

Figure 5.7 Maize – Daily wind vector distribution.

The wind rose indicates that there was a significant secondary wind run from the north-east. It was also from the north-east that winds of the greatest intensity originated. For example, the maximum wind speed reached was 8.3 m/s on October 31, 2010 at 00:30 AEST from a bearing of 8°. This coincided with a low pressure trough and a cold

front that passed through the region during the period (see Figure 5.8 for the synoptic pressure map showing approximate location of the CIA).

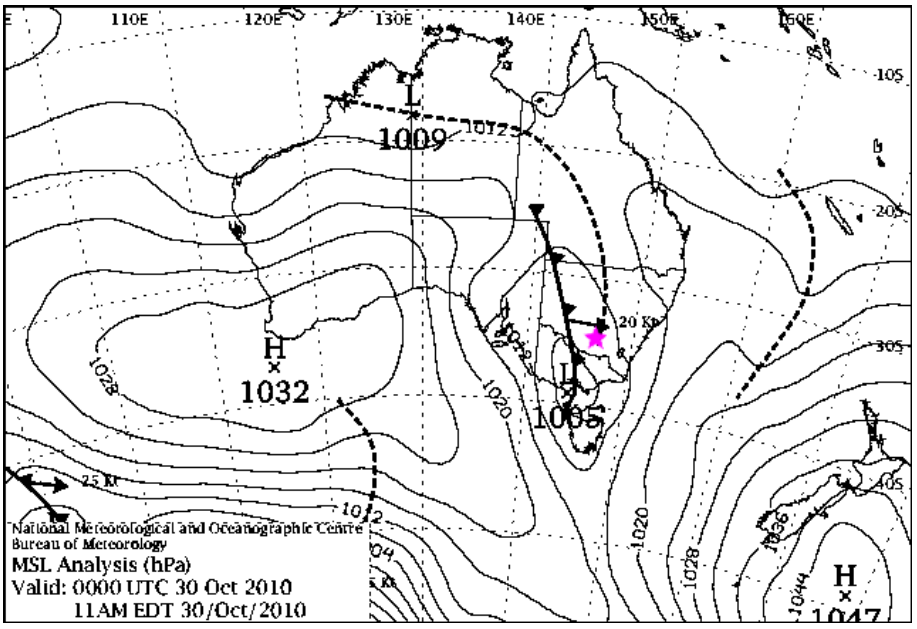

Figure 5.8 Mean sea level pressure analysis for the Australian region valid at 0000 UTC October 30, 2010 (Bureau of Meteorology, 2010a). The coloured star indicates the location of the CIA.

Figure 5.9 and Figure 5.10 illustrate the daytime and night-time wind profiles experienced at the maize site, respectively. Daily wind profiles were similar to the daily distributions except for greater instances of winds at speeds of 2 – 4 m/s. Generally, the night-time wind distribution followed the daily trend although the night-time wind speeds were much less and ranged mostly between 0 – 2 m/s. This is to be expected given that more stable atmospheric conditions generally occur at night. Another point of difference for night-time conditions is the stronger influence of winds originating in the east-north-east, reaching speeds of 4 – 5 m/s.

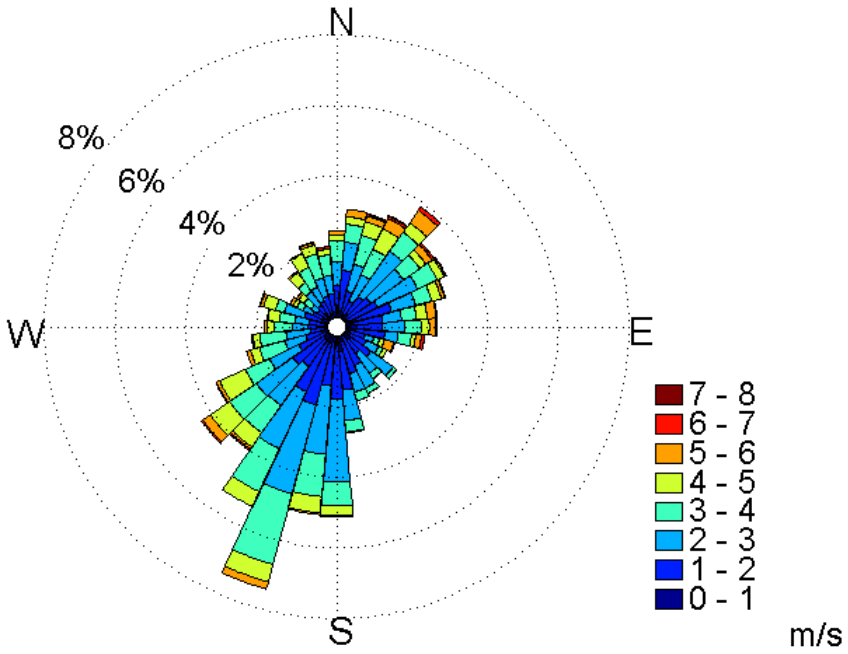

Figure 5.9 Maize – Daytime wind vector distribution.

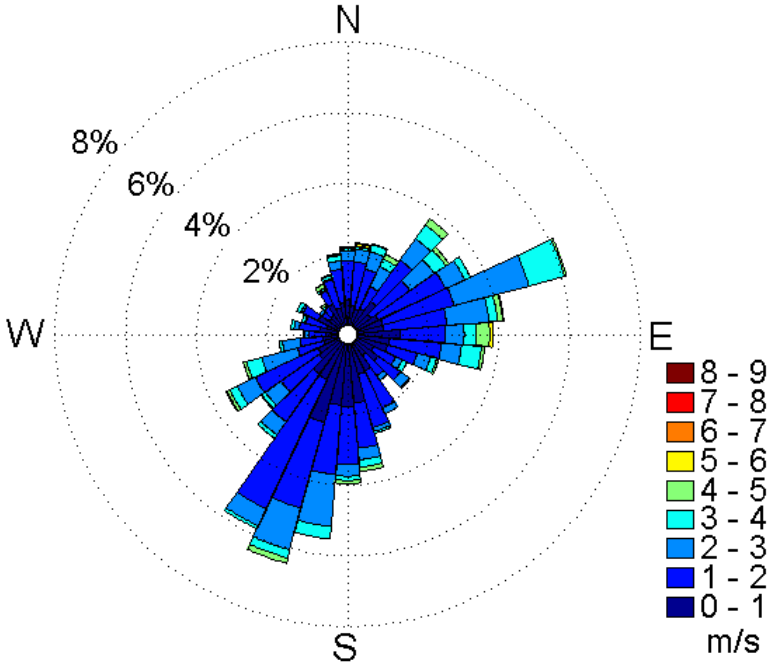

Figure 5.10 Maize –Night-time wind vector distribution.

The distribution of the 24 hr daily wind directions over the rice crop is presented in Figure 5.11. As illustrated, the prevailing winds originated from a south-south-easterly direction (145° – 175°) at speeds of 0 – 8 m/s.

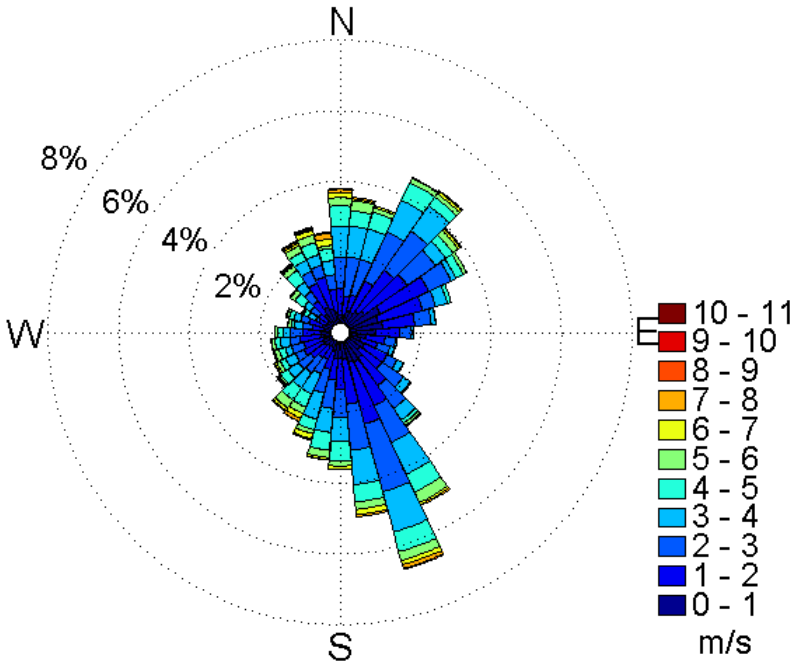

Figure 5.11 Rice - Daily wind vector distribution.

Like the maize crop, there was also a strong influence of winds originating from the north-east. Again, winds of greatest intensity originated from the north (bearing 324°) and reached a maximum speed of 10.8 m/s. This occurred on December 8, 2010 at 10:30 AEST and coincided with a low pressure trough that had moved over the region (see Figure 5.12).

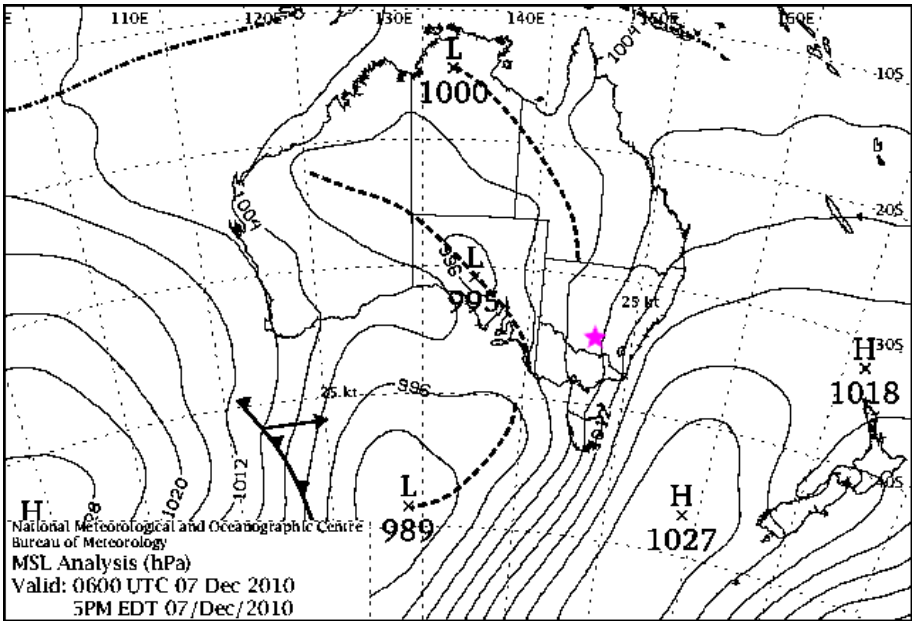

Figure 5.12 Mean sea level pressure analysis for the Australian region valid at 0600 UTC December 7, 2010 (Bureau of Meteorology, 2010b). The coloured star indicates the location of the CIA.

Figure 5.13 and Figure 5.14 illustrate the daytime and night-time wind profiles experienced at the rice site, respectively. During the day, the wind directions were more evenly distributed. At night, more than 20% of the wind originated from the south-south-east. At this particular site, night-time atmospheric conditions were less stable than what was experienced at the site of the maize crop. For example, winds greater than or equal to 4.0 m/s accounted for 7.4% of the night-time dataset over the rice crop; for the maize crop, this figure was only 2.4%.

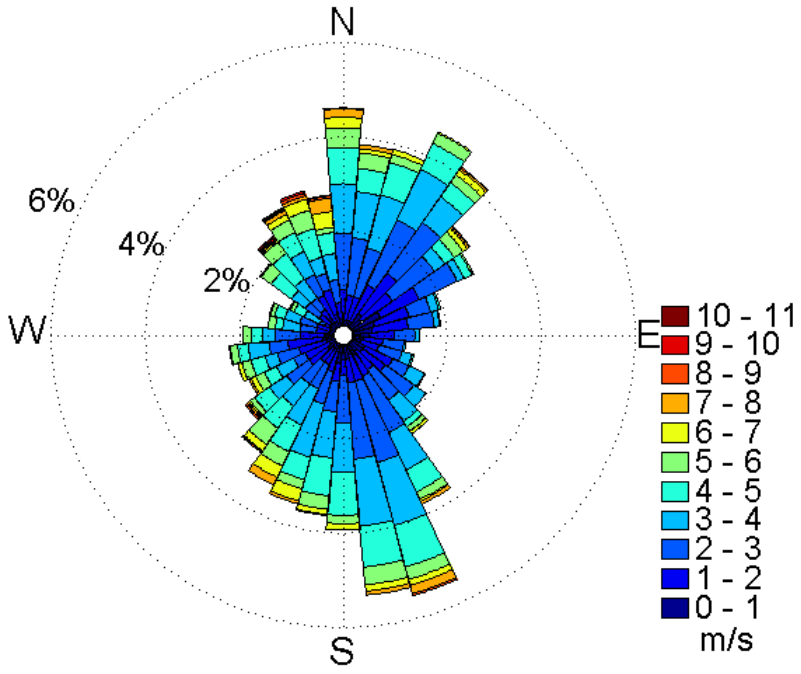

Figure 5.13 Rice – Daytime wind vector distribution.

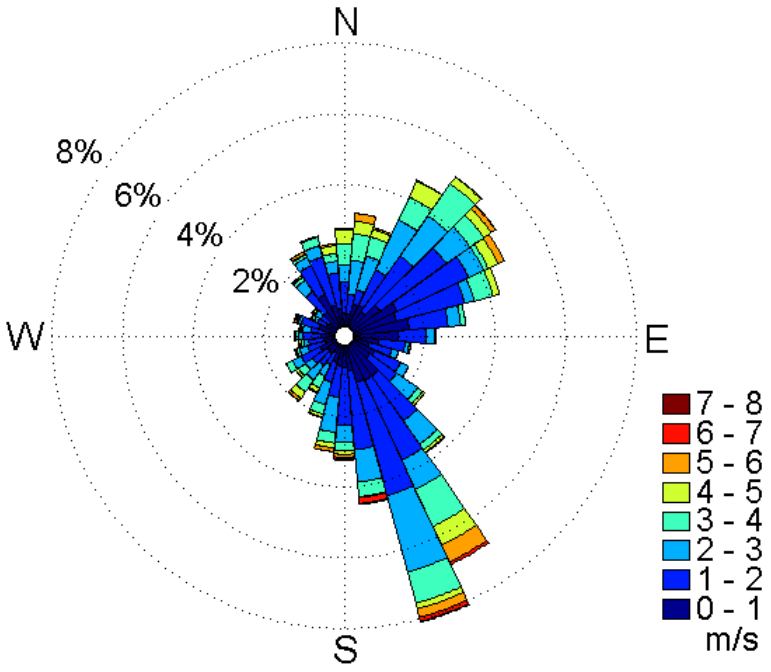

Figure 5.14 Rice – Night-time wind vector distribution.

Considering both summer flux tower locations, it is apparent that the dominate winds were different. For example, the majority of winds swung from the north-east to the south-west over the maize crop; for the rice, the winds swung from north to south-east. This may be attributable to differences in topography and/or physical barriers that may affect wind flow between the sites. For instance, Figure 5.15 and Figure 5.16 present the rate of change of elevation (slope) calculated from a digital elevation model (spatial resolution = 1'') produced by Geoscience Australia (2011), further modified using ArcGIS 10.1® for this analysis. These figures illustrate the slope of the terrain immediately surrounding the maize and rice crops, respectively.

Figure 5.15 Slope of area immediately surrounding the maize crop. The location of the flux tower is marked with an 'x'.

Figure 5.16 Slope of area immediately surrounding the rice crop. The location of the flux tower is marked with an 'x'.

As illustrated, there was no significant topographic variation immediately surrounding the maize and rice crops, therefore the difference in airflow is most likely attributable to the presence of tall, dense vegetation located directly to the north and east of the flux tower (see Figure 5.17 and Figure 5.18). The nature and breadth of these tree plantings may have forced the airflow through a north-east and south east corridor.

Figure 5.17 Tall, dense vegetation (highlighted by white ellipse) located to the north of the flux tower.

Figure 5.18 Tall, dense vegetation (highlighted by white ellipse) located to the east of the flux tower.

Figure 5.19 presents the daily wind vector distribution over the winter wheat cropping system. As illustrated, the daily wind distribution over the winter growing season was similar to that of the maize crop over the summer growing season, with the prevailing winds originating in the south-west (bearing 180° – 245°), however, winter wind speeds were greater. For instance, winds speeds of 6.0 m/s or greater accounted for 3.3% of the total data set during the winter period. For the summer crop, winds 6.0 m/s or greater represented only 0.5% of the total dataset.

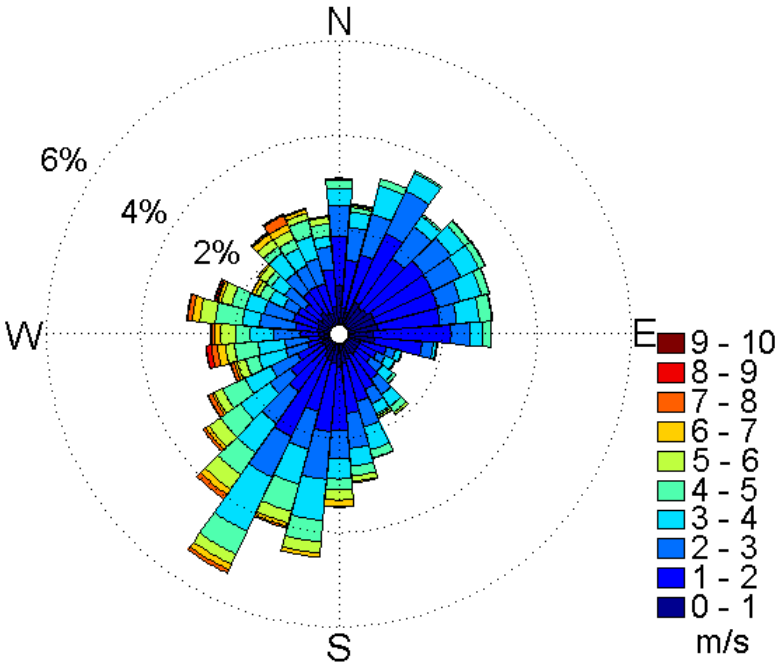

Figure 5.19 Wheat – Daily wind vector distribution.

The maximum wind speed reached was 9.6 m/s and occurred on July 4, 2011 at 14:30 AEST. This originated from a westerly direction (bearing 291°) and coincided with the presence of a complex trough over the region (see Figure 5.20).

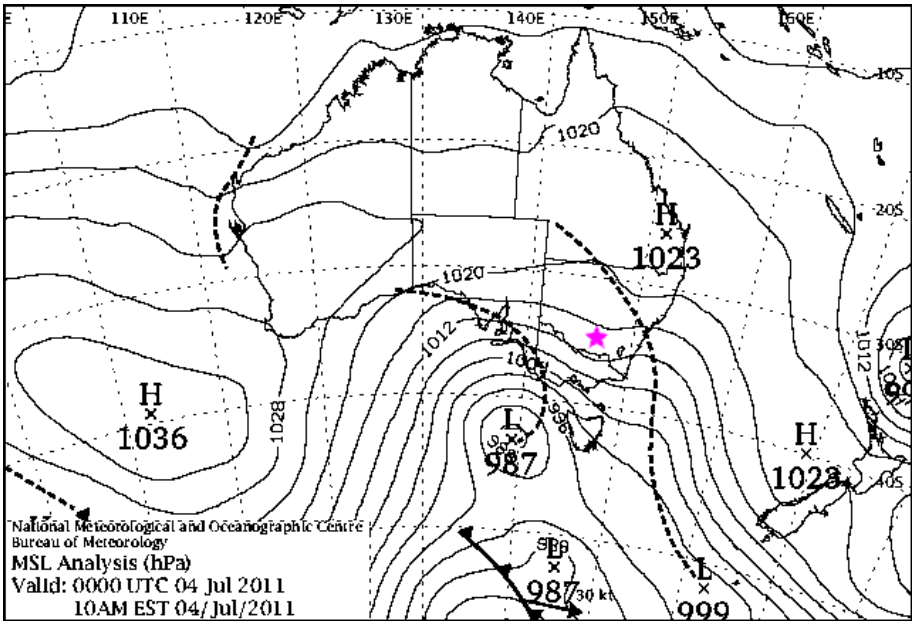

Figure 5.20 Mean sea level pressure analysis for the Australian region valid at 0000 UTC July 4, 2011 (Bureau of Meteorology, 2011). The coloured star indicates the location of the CIA.

Daytime and night-time wind profiles of the wheat crop are presented in Figure 5.21 and Figure 5.22. The daytime wind run was similar to that observed over the 24 hr period whilst night-time wind runs were different. For example, 32.0% of daily winds originated in the south-west and 28.2% originated in the north-east. At night, the reverse was true, with 27.4% originating in the south-west and 33.4% originating in the north-east.

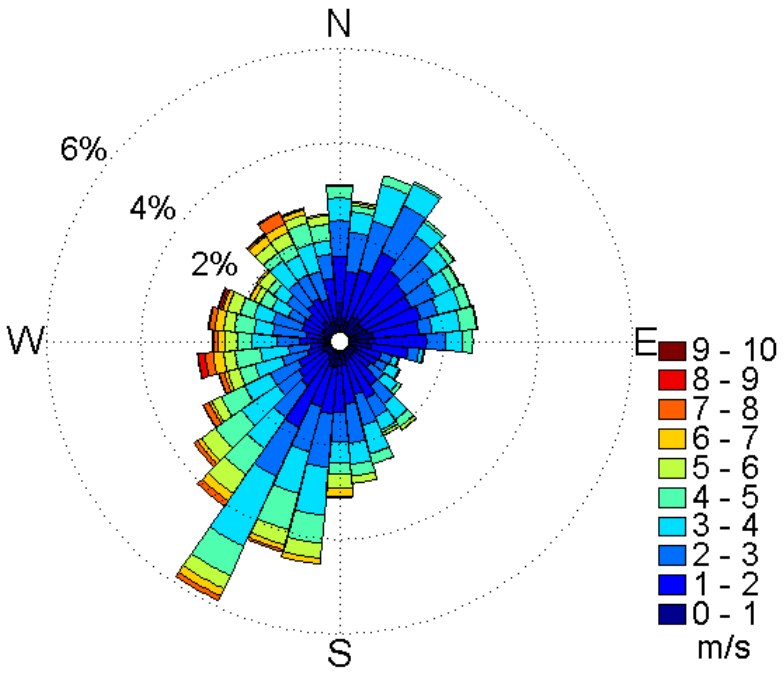

Figure 5.21 Wheat – Daytime wind vector distribution.

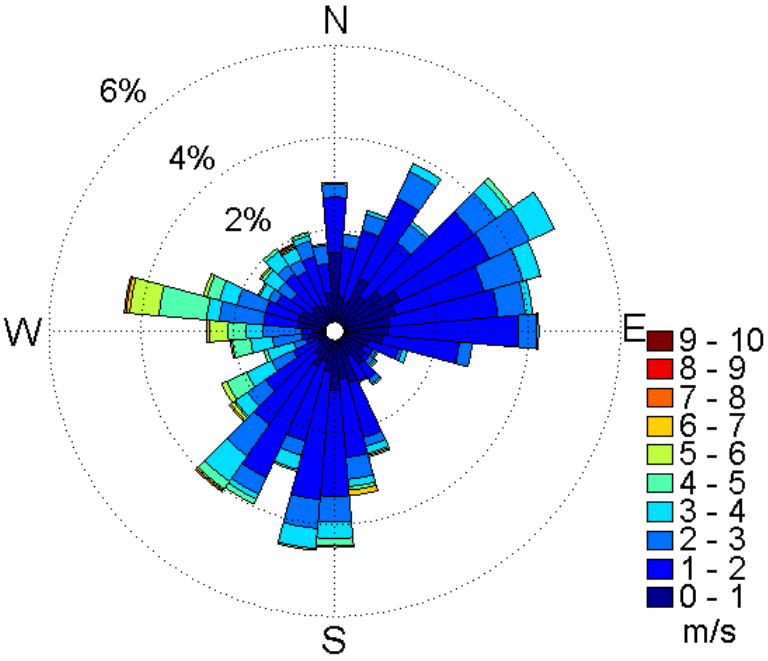

Figure 5.22 Wheat – Night-time wind vector distribution.

Figure 5.23 illustrates the daily wind vector distribution over the winter mixed cropping system. At this location, the daily wind speed and direction were more evenly distributed, although the prevailing wind direction followed the general trend seen at the three other sites. At this site, winds blew predominately from the south-west (31.7%) with a strong influence from the east-north-east (15.8%). Most wind speeds occurred between 1 – 4 m/s. The maximum wind speed reached was 9.8 m/s on July 5, 2011 at 12:00 AEST with airflow from a westerly direction (bearing 278°). This was influenced by the same pressure systems depicted in Figure 5.20.

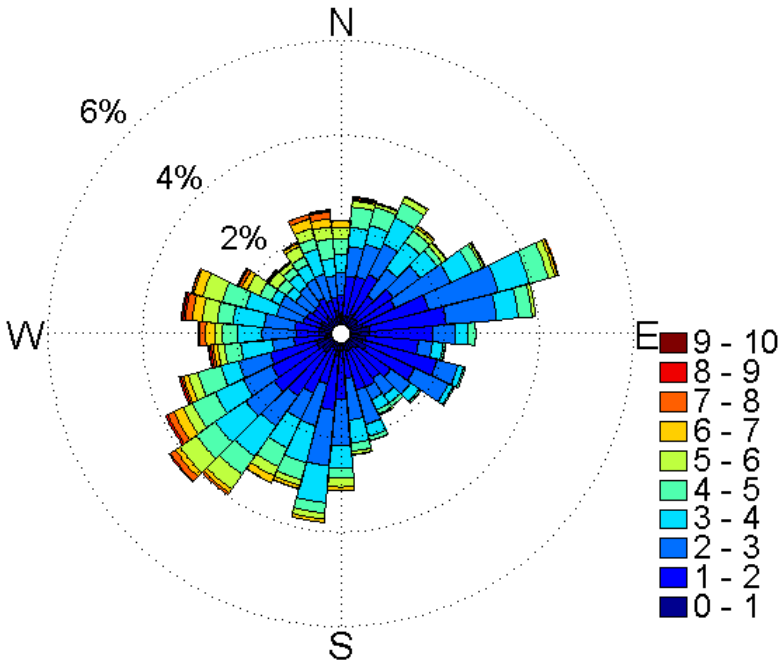

Figure 5.23 Mixed cropping system – Daily wind vector distribution.

The daytime and night-time wind profile over the mixed cropping system is depicted in Figure 5.24 and Figure 5.25, respectively. As shown, the daytime and night-time wind directions were similar. During the day, the majority of the wind (82.9%) occurred at speeds equal to or less than 5.0 m/s. At night, there was a stronger influence of winds originating in the east-south-east (12.6%) which was not

seen during the day (7.1%). The majority of night-time wind speeds (80.6%) occurred at speeds equal to or less than 3.0 m/s.

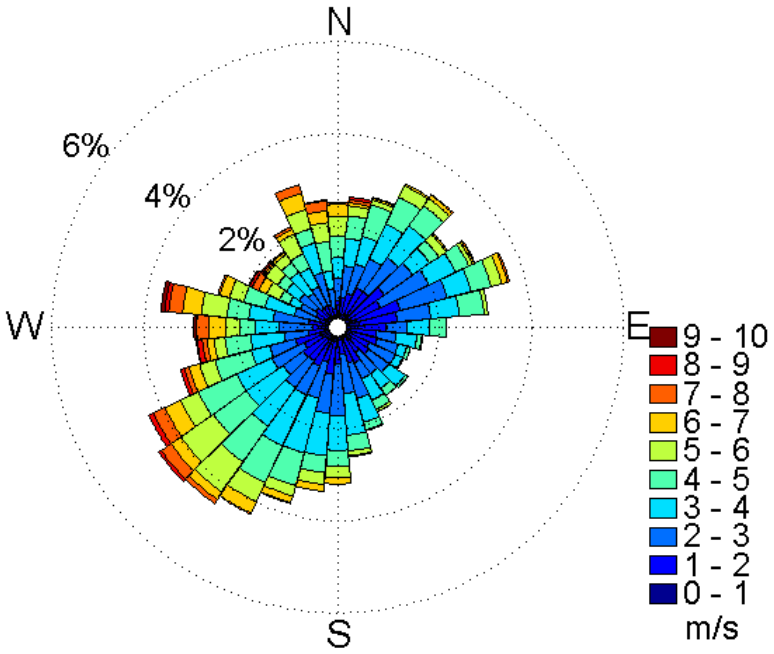

Figure 5.24 Mixed cropping system – Daytime wind vector distribution.

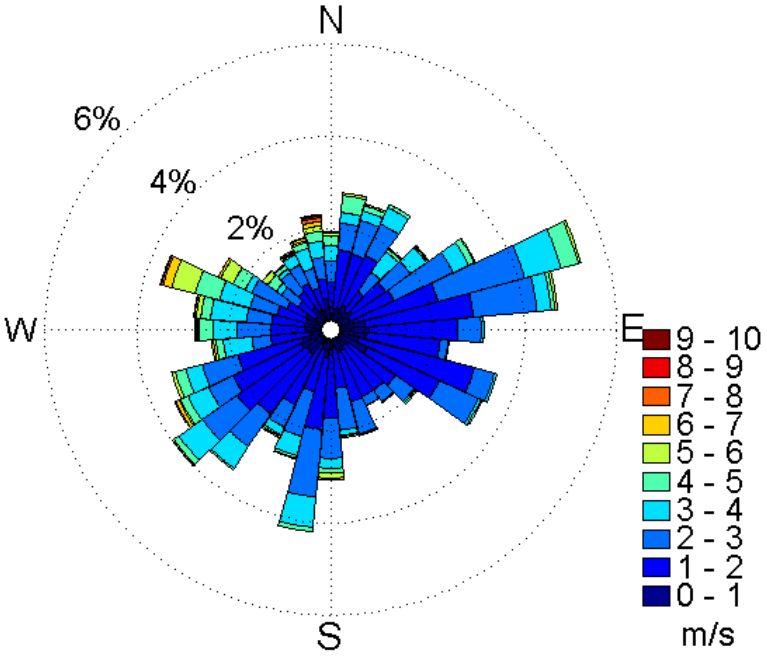

Figure 5.25 Mixed cropping system – Night-time wind vector distribution.

5.2.2 Air and soil temperature

The mean daily air temperature (at an elevation of approximately 120 m), mean soil temperature (at depth 0.02 – 0.06 m) and maximum/minimum air temperature bounds for the flux tower sites for both summer and winter are presented in Figure 5.26 and Figure 5.27, respectively.

(a)

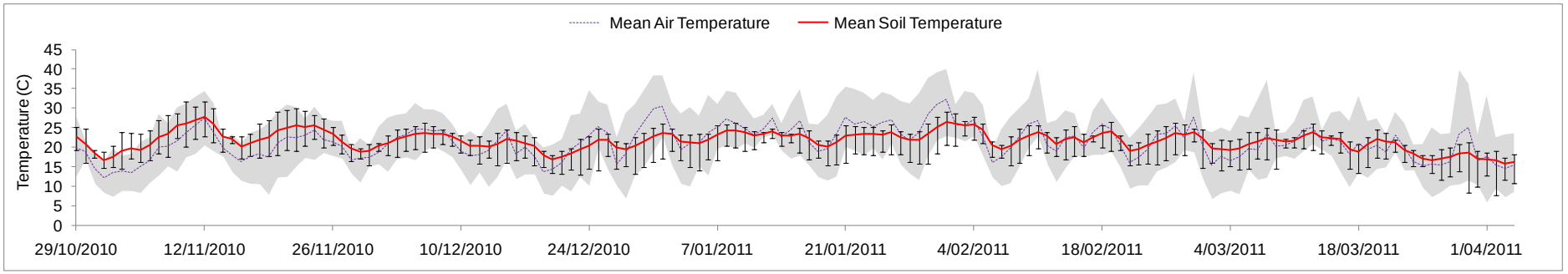

(b)

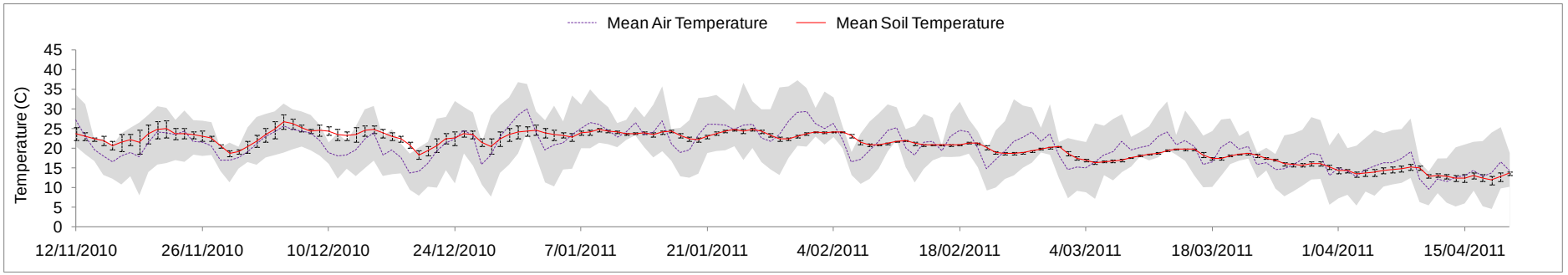

Figure 5.26 Mean daily air and soil temperatures observed during the summer for (a) maize and (b) rice. The grey shaded area depicts the maximum/minimum air temperature bounds. The error bars represent the standard deviation in soil temperatures.

(a)

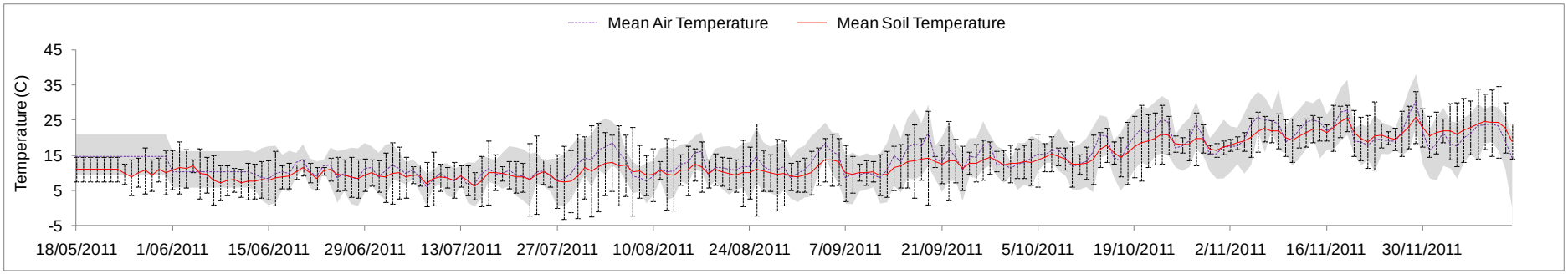

(b)

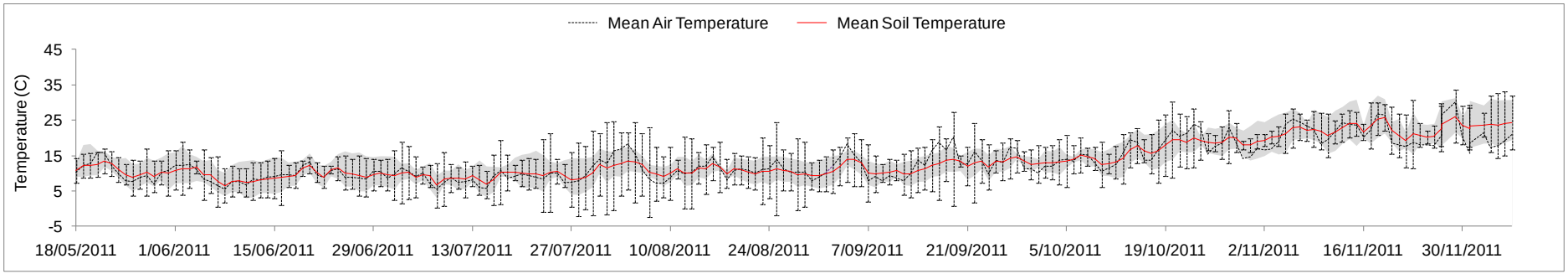

Figure 5.27 Mean daily air and soil temperatures observed during the winter for (a) wheat and (b) the mixed system. The grey shaded area depicts the maximum/minimum air temperature bounds. The error bars represent the standard deviation in soil temperatures.

Over the observation period, the mean air temperature for maize was 21.3°C and the mean soil temperature was 21.7°C. The standard deviations, represented by the error bars, illustrate the daily variability in soil temperatures. Generally, soil temperatures followed the daily fluctuations of daily air temperatures throughout the growing season. Soil temperature variability was greatest during the early stages of vegetative growth (October 29 – November 24, 2010), prior to canopy closure. After closure, the canopy intercepted most of the sunlight (> 90%, see Figure 5.28) with minimal penetration to the soil surface, resulting in decreased variability in soil temperatures (from 22.8 ± 3.6°C on November 9, 2010 to 20.9 ± 0.1°C on February 16, 2011).

Figure 5.28 Sunlight interception after canopy closure.

The mean air temperature over the rice crop was 20.3°C, more than 1°C less than that experienced over the maize crop. Soil temperature variability for the rice crop was also different to that of the maize crop, where the mean daily soil temperature was 20.5°C. As Figure 5.26 illustrates, daily soil temperature fluctuations did not occur under the rice crop and soil temperatures exhibited very little variability

between January 5, 2011 and April 2, 2011. This coincided with the closing of the canopy and thus near full shading of the soil surface at panicle initiation, which occurred on January 7, 2011.

For the wheat crop, the mean air temperature experienced over the observation period was 14.6°C. The minimum air temperature observed was 5.9°C and occurred on July 8, 2011. The maximum temperature was 30.2°C and occurred on November 29, 2011. Like the maize crop, soil temperatures generally followed the daily fluctuation of air temperatures over the growing season, whilst soil temperature variability, with a daily average of 13.4 ± 5.0°C, was greater than that of maize. This was likely the result of less sunlight interception by the canopy cover, thus allowing greater penetration of sunlight to the soil surface. The minimum soil temperature was 6.2°C and occurred on July 15, 2011. The maximum soil temperature occurred on November 29, 2011 and reached 25.8°C.

The mean daily temperature observed over the growing season for the mixed cropping system was 13.3°C. The minimum air temperature was 5.4°C and occurred on June 8, 2011. The maximum air temperature was 30.0°C, which occurred on November 29, 2011. Like the maize and wheat crops, mean soil temperatures followed the daily fluctuations of mean air temperatures. Variability in soil temperatures was very similar to that reported for the wheat crop with a mean of 13.5 ± 5.0°C. The minimum soil temperature was 6.6°C and the maximum soil temperature was 26.0°C, which corresponded with the dates where maximum and minimum air temperatures were recorded.

5.2.3 Precipitation and solar radiation

Total precipitation, total incoming solar radiation and mean daily incoming solar radiation values observed at each flux tower location are given in Table 5.1

Table 5.1 Total rainfall, total incoming solar radiation (SR) and mean daily incoming solar radiation over the observation period.

Crop	*No. days of observation*	*Rainfall (mm)*	*Total SR (MJ/m^2)*	*Mean daily SR (MJ/m^2/day)*
Maize	158	480	5598	35.4
Rice	160	471	5504	34.4
Wheat	211	204	2159	10.2
Mixed	204	238	2540	12.5

According to the Bureau of Meteorology (2012b), the CIA experienced the highest total rainfall on record during the observation period. Over the summer growing season (October – March), the maize crop received 480 mm of rainfall, well above the long-term average (1957 – 2012) of 185 mm for the same period. The total rainfall observed by sensors located in the rice crop was similar to that of the maize crop and received 471 mm over the observation period. During the winter months, total rainfall received was 204 mm for the wheat crop and 238 mm the mixed system. Whilst this was much less than that observed during the summer months, total rainfall at both sites was also greater than the long-term average, which is 136 mm for the same period.

Total incoming solar radiation over the summer growing season was similar at both flux tower locations. Likewise, the total incoming radiation observed at the two sites over the winter growing season was also similar. In the summer, as expected, incoming solar radiation values were much greater than those observed during the winter months. For the maize crop, the total incoming solar radiation was 5598 MJ/m^2 with an average of 35.4 MJ/m^2/day. For the rice, total incoming solar radiation was 5504 MJ/m^2 with an average of 35.6 MJ/m^2/day. For the winter crops, total incoming solar radiation was much less. For the wheat crop, total incoming solar radiation was 2159 MJ/m^2 and 2540 MJ/m^2 for mixed cropping system. The mean daily incoming solar radiation values were also very similar for both

winter sites which were 10.2 MJ/m^2/day and 12.5 MJ/m^2/day, for the wheat crop and the mixed crop, respectively.

Figure 5.29 and Figure 5.30 present daily precipitation and the amount of incoming solar radiation observed at each site during the summer and winter growing seasons, respectively. Despite experiencing similar climatic conditions at each flux tower location for each growing season, the rainfall varied greatly between the sites. For example, on November 13, 2010, total rainfall received at the maize site was 53.9 mm whilst the rice crop received only 15.0 mm. For the winter crops, the wheat crop received a total of 11.4 mm of rain on the November 9, 2011 whereas total rainfall observed at the mixed cropping site on the same day was almost twice as much (26.4 mm).

Spatio-temporal variation in rainfall impact levels of plant water availability and volumetric soil water content. Ultimately, this impacts on the way the radiative energy budget is partitioned, particularly in semi-arid regions, thus affecting the distribution of turbulent fluxes of sensible heat, latent heat and carbon dioxide (Krishnan et al., 2012; Liu et al., 2010). Water and carbon dioxide flux response to various environmental variables is discussed in detail in Section 6.3.

(a)

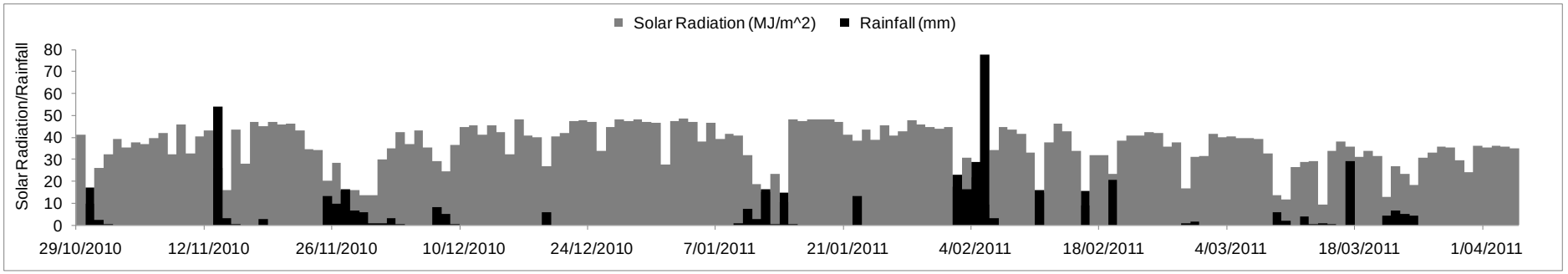

(b)

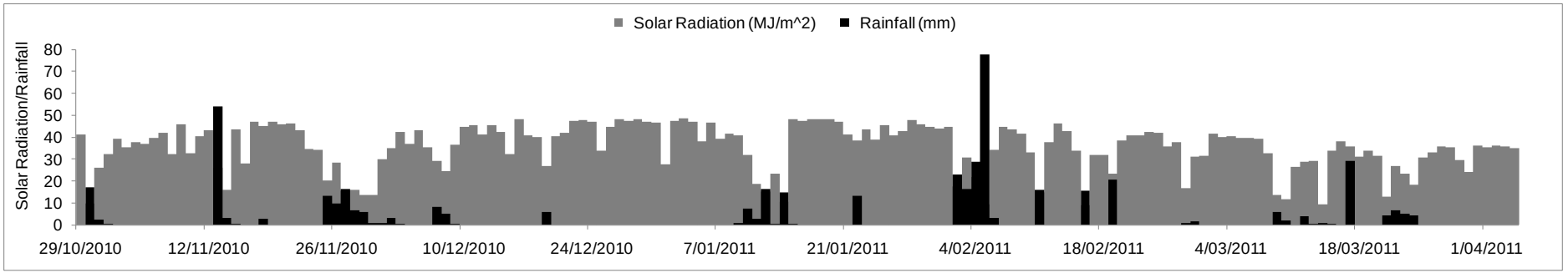

Figure 5.29 Daily precipitation and incoming solar radiation observed for (a) maize and (b) rice during the summer growing season.

(a)

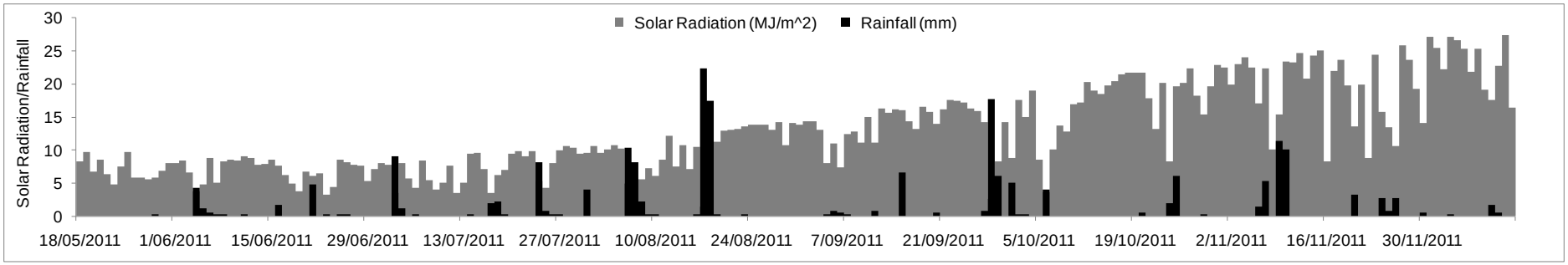

(b)

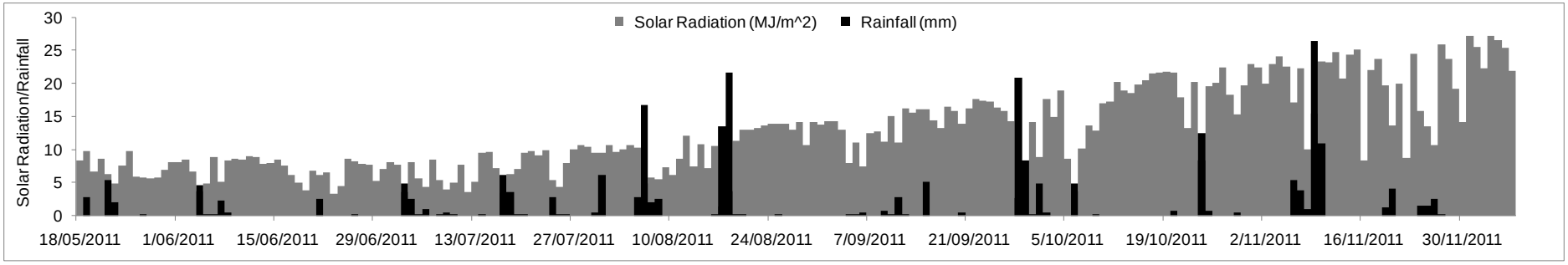

Figure 5.30 Daily precipitation and incoming solar radiation observed for (a) wheat and (b) the mixed system during the winter growing season.

5.3 Data processing and analysis

5.3.1 Zero-plane displacement and surface roughness length

Knowledge of the zero-plane displacement height (d_0) and aerodynamic (or surface) roughness length (z_0) was required to set parameters within the flux data processing program to estimate fluxes. Based on data recorded over the growing seasons, whereby the canopy height of 20 randomly located plants was measured, both d_0 and z_0 were calculated according to the equations listed in the Section 4.6.4. The calculated values of d_0 and z_0 for both summer and winter crops are presented in Table 5.2 and Table 5.3, respectively. Where crop height measurements were unavailable, d_0 and z_0 could not be calculated (N/A).

Table 5.2 Zero-plane displacement (d_0) and surface roughness lengths (z_0) of summer crops; all measurements are in metres.

Date	*Maize*		*Rice*	
	d_0	z_0	d_0	z_0
29/10/2010	0.12	0.02	N/A	
18/11/2010	0.29	0.05	0.00	0.005
22/11/2010	0.45	0.08	N/A	
25/11/2011	0.52	0.09	N/A	
16/12/2011	1.67	0.31	0.27	0.05
18/01/2011	1.96	0.36	0.46	0.09
22/02/2011	N/A		0.70	0.13
13/03/2011	N/A		0.70	0.13
04/04/2011	N/A		0.65	0.12

Table 5.3 Zero-plane displacement (d_0) and surface roughness lengths (z_0) of winter crops; all measurements are in metres.

Date	*Wheat*		*Mixed*	
	d_0	z_0	d_0	z_0
30/05/2011	0.06	0.01	N/A	
16/06/2011	0.11	0.02	0.06	0.01
06/07/2011	0.15	0.03	N/A	
10/08/2011	0.22	0.04	0.21	0.04
15/09/2011	0.38	0.07	0.44	0.08
20/10/2011	0.52	0.10	0.62	0.11

5.3.2 Cospectral analysis

Within the flux community, it is often standard practice to use a 30 minute averaging period when processing and analysing eddy covariance data (Leuning et al., 2005). However, research has shown that significant contributions of flux can occur at lower frequencies, particularly over complex or inhomogeneous terrain and tall canopies (Finnigan et al., 2003). Therefore a comprehensive cospectral analysis was performed to determine the optimal averaging period for irrigated broad acre crops within the CIA. This was achieved by conducting an ogive test (for details of this test, see Burba & Anderson, 2010; Foken et al., 2006; Oncley & Friehe, 1996) whereby the raw 10 Hz data was processed using EdiRe© (an open-source software package specifically designed to assist in eddy covariance data processing; Clement, 1999) over a 120 minute averaging period to provide cospectra of the sensible heat flux ($w'T_{sonic}'$; where w is vertical wind speed and T_{sonic} is sonic temperature) for each dataset. To avoid bias, only days with complete records, where possible, were included in the analysis. The ogives constructed for each crop during the vegetative growth stage are presented in Figure 5.31. The ogives produced for the remaining phenological stages are not presented as they conveyed the same information, regardless of crop type, growing season or phenological stage.

It was found that all significant low-frequency eddies were captured within a 10 – 30 minute period for all four cropping systems as illustrated by the ogive curves reaching an asymptote within this timeframe (Moncrieff et al., 2004). However, for standard processing methods consistent with the wider flux community, a 30 minute averaging period was selected for further processing and analysis in this study.

(a)

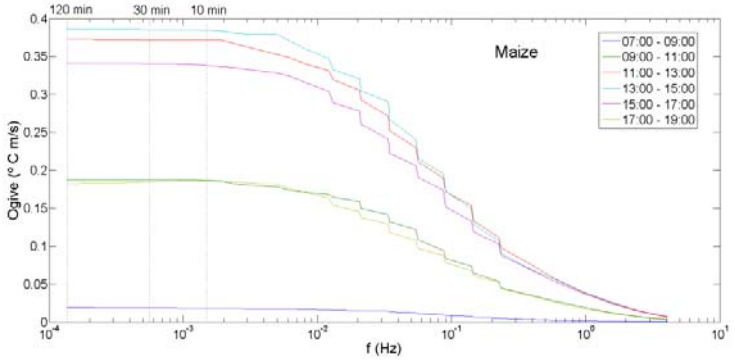

(b)

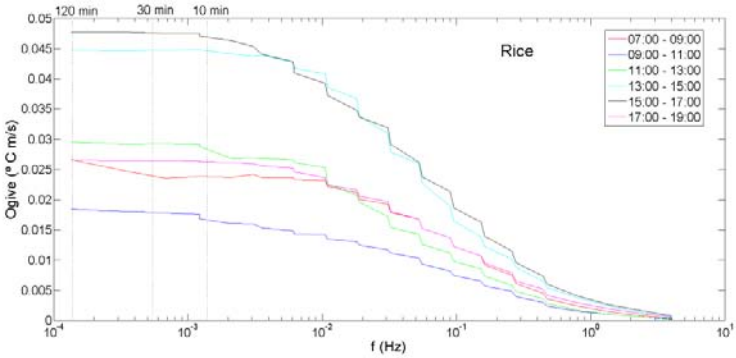

(c)

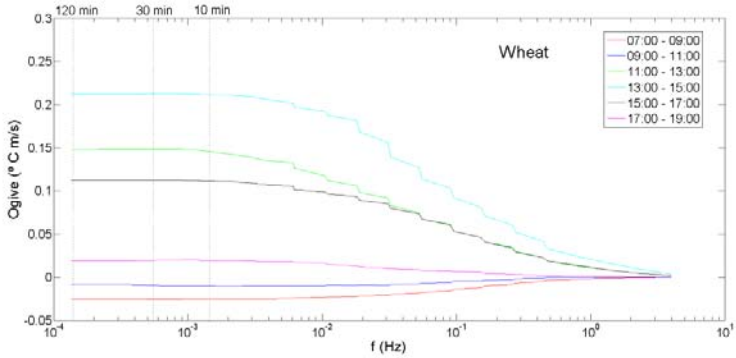

(d)

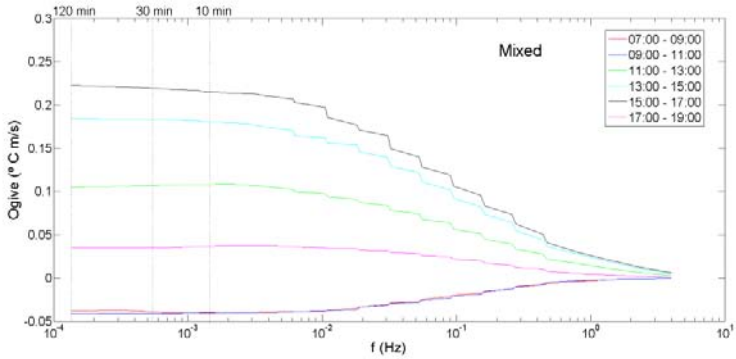

Figure 5.31 Ogives (°C m/s) for each crop during the vegetative stage. (a) maize, (b) rice, (c) wheat and (d) the mixed system.

5.3.3 Spike detection, corrections and gap-filling

The 30 minute averaged time series for each dataset was processed according to the criteria stipulated in Section 4.2.2. Once gap-filled, the quality control flags were examined to determine the amount of data that was either missing from the original dataset, or removed according to the parameters set in the post-processing program. Table 5.4 illustrates the percentage of flux data removed and subsequently gap-filled for each experimental site in this study.

Table 5.4 Percentage (%) of flux data that required gap-filling.

Crop	F_c	*LE*	H_s	R_n	*G*
Maize	46.9	32.7	4.0	0.4	0.1
Rice	50.7	37.1	3.9	4.9	25.5
Wheat	45.7	39.9	19.1	4.2	4.7
Mixed	47.7	41.9	6.2	1.2	5.6

The average percentage of F_c data that removed from all four time-series datasets was 47.8% with a range of 45.7% – 50.7%. The average amount of *LE* data removed was 37.9% and the range was 32.7% – 41.9%. During the day, the quality control flags indicated that the majority of the data was removed as a result of gas analyser and sonic anemometer failure. These gaps generally coincided with rainfall events, which are known to affect the operation and accuracy of EC sensors (Burba & Anderson, 2010). The incidence of rainfall often resulted in sensor diagnostic flags and spikes in the time series that were subsequently removed during the QC process. Given the atypical amount of rainfall received in the CIA in 2010/11, a larger amount of F_c and *LE* data than was originally anticipated required gap-filling. As presented in Table 5.4, gaps in F_c were greatest in all four datasets as a result of a large number of night-time CO_2 fluxes that registered below the $\boldsymbol{u^*}$ threshold (see Section 4.3.2).

The percentage of sensible heat flux (H_s) gap-filled data was similar for all flux tower sites (4.0%, 3.9% and 6.2%) with the exception of the wheat crop (19.1%). This can partially be attributed to instrument failure during the first week of the observation period at the wheat site. Whilst the amount of gap-filling required for each dataset was typical of EC studies where gaps are generally found to account for 20 – 60% of an annual dataset (Moffat et al., 2007), their existence is a cause for concern. A significant proportion of the turbulent flux data has been interpolated; therefore the results reported in this study may be heavily influenced by random and systematic bias error.

5.3.4 Flux Footprint

Table 5.5 presents the distance from which approximately 90% of the flux contributions originated upwind of the sensors for both day time and night-time conditions. Sensor height, maximum canopy height, maximum zero-plane displacement and the minimum distance to the boundary are also presented here.

Table 5.5 Effective fetch (Daytime and Night-time), maximum crop heights, sensor heights, maximum zero-plane displacement (d_0) and the minimum distance to the boundary for each crop; all measurements are in metres (m).

Crop	*Daytime Fetch*	*Night-time fetch*	*Max. Crop Ht*	*Sensor Ht*	d_0	*Min. Distance*
Maize	112	210	2.94	5.05	1.96	217
Rice	153	235	1.05	2.55	0.65	325
Wheat	175	432	0.78	3.55	0.52	187
Mixed	320	334	0.92	3.75	0.62	385

There are a number of factors that influence the size of the flux footprint (or effective fetch). As a general rule, the instrument height should be twice the height of the canopy (2:1) to ensure that the sensors are located above the roughness sub layer and within the

boundary layer (Burba & Anderson, 2010). In each instance, this rule was satisfied, with the exception of the maize crop. To ensure the sensors were well within the boundary layer, the ideal sensor height would have been 5.8 m, given that the maximum crop height was 2.9 m.

Measurement height will also have an effect on the length of the flux footprint and sensor height should ideally be 100 times less than the desired fetch (i.e. 1:100) to ensure all fluxes transported by very small eddies occurring at very high frequencies are registered by the sensors (Burba, 2013; Burba & Anderson, 2010). Strictly speaking, the measurement height should be referenced from the height of zero-plane displacement, rather than the soil surface (Burba, 2013). The desired fetch in this instance is the minimum distance to the boundary (from the flux tower). For both the rice crop and mixed cropping system, this rule is satisfied (i.e. the ratio of sensor height to minimum distance is < 0.01). For the maize and wheat crop, the ratio was only marginally worse (0.014 and 0.016, respectively).

Figure 5.32 – Figure 5.35 depict the location of the flux tower and the 90% cumulative probability of the source emissions in relation to the boundaries of the experimental sites. As demonstrated, the effective fetch during the night at each experimental site was greater than what it was during the day. This can be attributed to the greater proportion of low wind speeds and more stable atmospheric conditions that generally occur at night (Burba & Anderson, 2010).

For both summer crops, the effective fetch was representative of the field of interest (i.e. within the boundaries of the paddock) for day time and night-time conditions. During the winter, the day time and night-time flux footprints of the mixed cropping system were also within the field of interest. This was not the case for the winter wheat crop, where the night-time flux footprint extended beyond the field boundaries. In this instance, fluxes may have been influenced by the presence of Eucalypt trees that lined the north-eastern boundary as

well as the adjacent block of fallow land, directly east of the crop. However, at night, the majority of the winds (approximately 73%) originated between compass bearings of 90° – 360°. Additionally, all fluxes originating from a bearing of 45° – 135° were filtered from the time series as part of the quality control process (see Section 4.2). Therefore the cumulative flux contribution that originated from the north east to south east at distances greater than 187 m (the shortest distance to the boundary) was considered negligible.

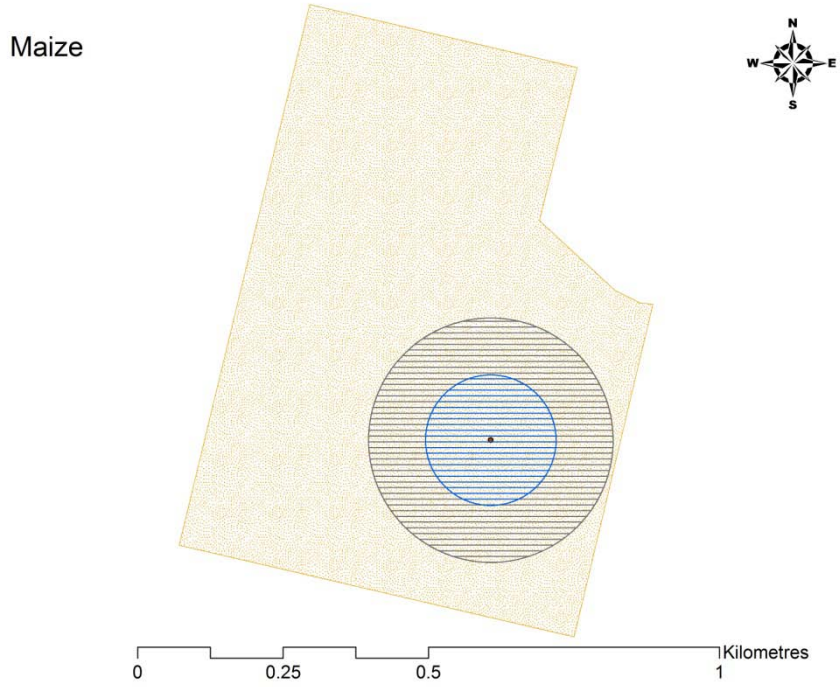

Figure 5.32 Flux footprint of the maize crop. Note that the blue circle represents the effective fetch during the day; the grey circle represents the effective fetch at night.

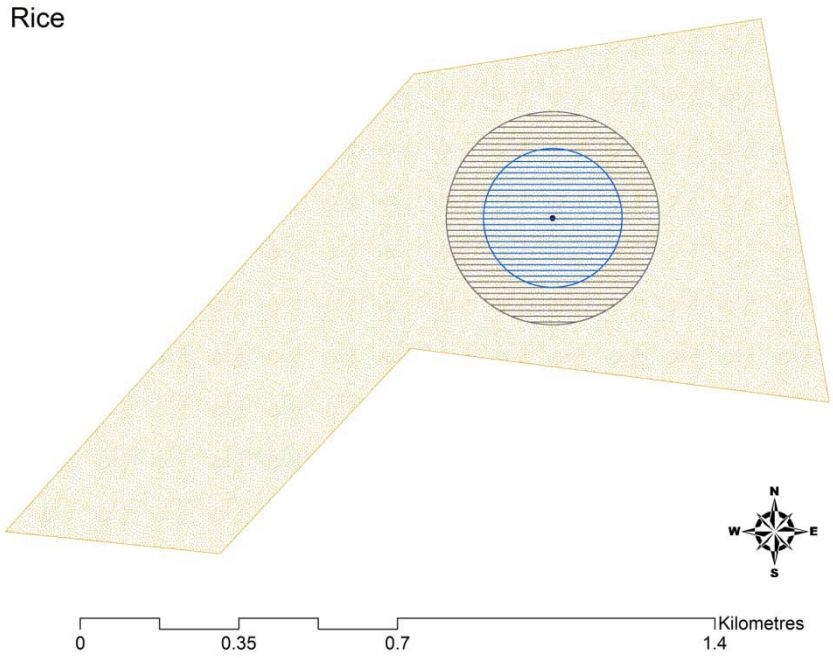

Figure 5.33 Flux footprint of the rice crop. Note that the blue circle represents the effective fetch during the day; the grey circle represents the effective fetch at night.

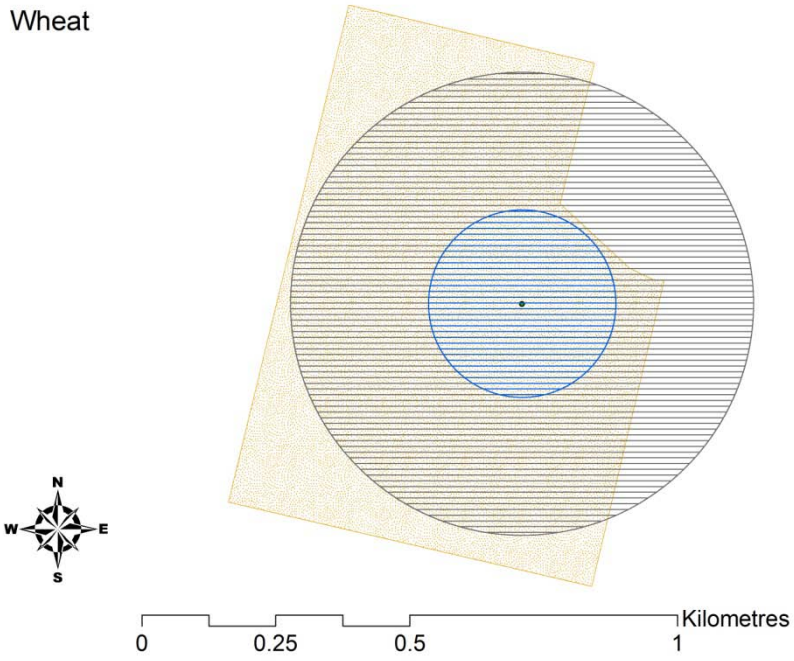

Figure 5.34 Flux footprint of the wheat crop. Note that the blue circle represents the effective fetch during the day; the grey circle represents the effective fetch at night.

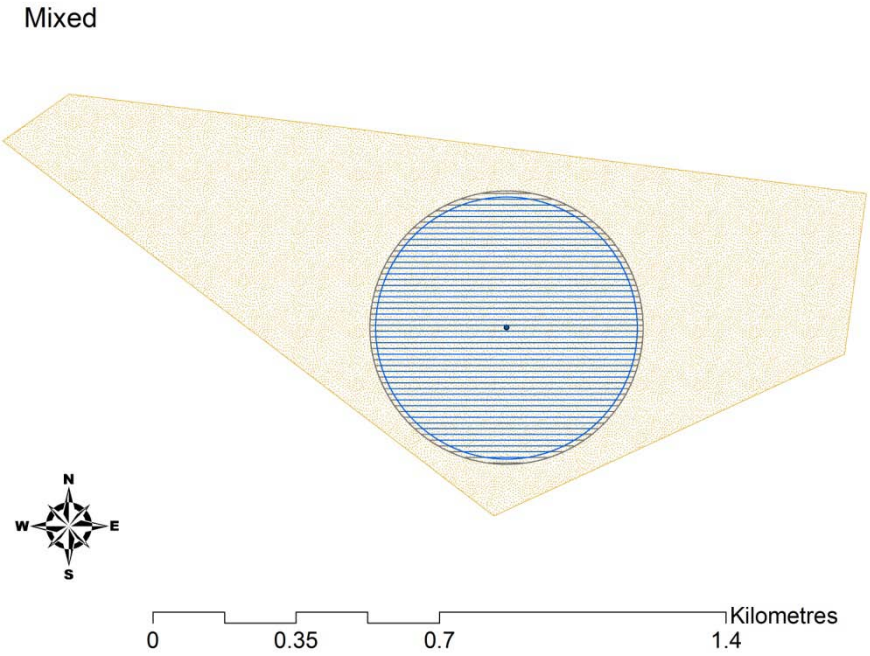

Figure 5.35 Flux footprint of the mixed cropping system. Note that the blue circle represents the effective fetch during the day; the grey circle represents the effective fetch at night.

5.3.5 Determination of energy balance closure

The degree of energy balance closure at each site was determined by calculating the energy balance ratio (*EBR*), which is the ratio of the sum of sensible and latent heat (H_s + LE) to the amount of available energy (R_n - G). The *EBR* was calculated for each 30 minute interval over the observation period for each flux tower location, the results of which are presented in Table 5.6.

Table 5.6 *EBR* values calculated from the 30 minute averaged time series data at all flux tower locations.

Crop	*EBR*
Maize	0.80
Rice	0.71
Wheat	0.65
Mixed	0.48

As demonstrated, the *EBR* ranged between 0.48 – 0.80. The greatest amount of energy balance closure was achieved at the site of the maize crop. The closure of the energy balance was least successful over the mixed cropping system. In each case, the lack of energy balance closure could be partially attributed to the underestimation of the turbulent heat fluxes. This generally occurs as a result of the failure to include one or more of the storage flux components in the air column beneath the EC instrumentation (Kilinc et al., 2012). This includes not only soil heat storage, but also heat storage within the plant biomass, heat storage within the canopy air mass and biochemical photosynthetic energy consumption (Kilinc et al., 2012; Oncley et al., 2007). To incorporate these components would require the observation of additional meteorological and biometric parameters, which, due to resource limitations, were unable to be measured during this study.

Further underestimation of storage heat flux (*G*) may also be attributed to the failure to measure volumetric soil water content at each flux tower location, which is required to calculate the specific heat capacity of soil to accurately determine soil heat storage (Oncley et al., 2007). In this study, a default value based on soil samples taken at each site was used to calculate *G*. Therefore, the variation in soil moisture and thus *G*, as a result of precipitation and irrigation events was unaccounted for.

In addition to the omission of the aforementioned storage components, the energy balance observed over the rice crop was further impacted by the need to account for an additional component of *G*, i.e. the energy stored in the water column (*W*) required for rice production in the CIA (see Section 4.2.4). This also requires additional observations of temperatures in the water column, which were not measured during the course of this study. Instead, the average air temperature measured by the EC system was used to calculate *W* based on the assumption that daytime water temperature fluctuation is minimal and that mean water temperature is similar to mean air temperatures, after De Datta

(1987). This approximation of temperatures in the water column may have led to an overestimation of *G*, increasing the energy imbalance at this site.

The energy balance can also be affected by air flow distortion as a result of edges or obstacles and heterogeneities (e.g. albedo and surface roughness length) between the land cover (Kidston et al., 2010). It is for these reasons that the *EBR* value at the flux tower located within the mixed cropping system was the lowest. Figure 5.36 illustrates the location of the flux tower in relation to its proximity to the different crops, as well as the proximity of the EC sensors in relation to other structures including a wire fence that lines the internal boundary (note that the sonic anemometer is facing due west, away from the canola crop). Here, the presence of the fence between the wheat and canola plantings may have exacerbated the degree of flow distortion, and thus the degree of energy imbalance compared to that of the other three sites. Additionally, dynamic and thermal heterogeneities between land surfaces can modify the air flow in the ABL (Inagaki et al., 2006). Thermal heterogeneities, in particular, have a strong impact on the flow structure that can lead to in-homogenous surface heating, creating a horizontal pressure gradient that can then lead to generate eddies at greater timescales (mesoscale circulations) that are not measured by the EC system (Foken et al., 2010; Foken et al., 2006; Inagaki et al., 2006). Therefore the difference between the surface roughness and spectral properties between the two crops pictured here would have almost certainly distorted air flow in the ABL, further impacting on the energy balance.

Figure 5.36 Location of wire fence dividing the wheat and canola plantings. The presence of the wire fence is highlighted by the annotated white ellipse.

Regardless of the degree to which the energy balance could not be closed, the mean *EBR* of all for sites (0.66 with a range of 0.48 – 0.80) were within the bounds of typical EC studies. For example, Stoy et al. (2013) conducted a synthesis of 173 FLUXNET sites of various plant functional types (including forests, wetlands, savannas and agricultural crops) which showed that the mean energy balance closure was 0.84 with a range of 0.28 – 1.67. With respect to the energy balance closure of agriculture, Stoy et al. (2013) also showed that cropping systems were among the worst performers (mean *EBR* = 0.78), alongside wetlands and mixed forests. At flux tower sites of uniform vegetation types, greater energy balance closure was achieved (e.g. the mean *EBR* of evergreen broadleaf forests was 0.94). These results re-emphasise the influence that landscape heterogeneity had on the degree of energy balance closure in this study.

It is important to note that the level of energy balance closure will also add to the uncertainty of the results reported; i.e. the greater the energy balance imbalance, the less certainty in the flux measurement. Some researchers choose to adjust CO_2 fluxes proportionally to the

loss of other turbulent fluxes and others do not (Foken et al., 2004), which will have an implication on how flux measurements are interpreted (Wilson et al., 2002a). For instance, if known measurement errors are modest and *EBR* is between 0.7 – 1.0, then the energy balance should be forced to close and the CO_2 fluxes adjusted according to the proportion of original turbulent flux loss (H_s and *LE*) (Foken et al., 2004; Twine et al., 2000). Generally, these datasets are considered reliable and are often used for model calibration and simulation of atmospheric-land surface interactions. If $EBR < 0.7$, forcing the energy balance closure greatly reduces the reliability of flux datasets; this data should be used with caution if modelling studies are intended (Twine et al., 2000; Wilson et al., 2002a). Moreover, failure to close the energy balance could have significant impacts at an operational level. For instance, an under estimation of ET_a may be a cause for concern for irrigation managers who are required to schedule adequate water applications to ensure optimal plant growth and maximise yield (Twine et al., 2000).

Whilst there are a number of methods to force energy balance closure e.g. Bowen Ratio closure (see Twine et al., 2000) and the energy-closure fraction (Barr et al., 2006), there is no general solution or approach within the scientific community of addressing the energy balance problem (Wohlfahrt & Widmoser, 2013). As this study does not include a modelling component, the energy balance has not been forced to close; therefore, no adjustments to CO_2 fluxes were made.

6 ESTIMATION OF ENERGY, WATER VAPOUR AND CARBON DIOXIDE FLUXES

6.1 Seasonal distribution of energy balance components

The cumulative totals of the energy balance components observed at each flux tower location are presented in Table 6.1.

Table 6.1 Seasonal distribution of energy balance components (MJ/m^2).

Crop	*No. Days of Observation*	R_n	G	H_s	LE
Maize	158	2556	21	504	1530
Rice	160	2931	259	-19	1920
Wheat	211	2035	-34	388	954
Mixed	204	2350	-46	384	1016

As illustrated, there is a distinct seasonal distribution of energy balance components between the summer and winter crops. The magnitude of latent heat exchange observed during the summer growing season was almost twice that of the latent heat exchange observed during winter. For example, the cumulative total of *LE* for the summer rice crop was 1920 MJ/m^2 and for the winter wheat crop it was only 954 MJ/m^2.

The nature of ground heat flux contributions (*G*) were also very different between the summer and winter growing seasons. During the summer months, the cumulative total of *G* was positive indicating that heat was being absorbed by the surface. During winter, the cumulative total of *G* was negative; an indication that heat was being lost from the surface. The contribution of *G* to the total available energy was small and ranged between ~ 0.8 – 2.0% for both summer and winter crops with the exception of the rice crop where *G* accounted for 8.8% of the

available energy. Maximum daily average values of ground heat storage observed at the maize, wheat and mixed cropping systems did not exceed 2.6 MJ/m^2. This indicated that there was significant shading beneath the canopy that did not allow for direct heating of the soil (Kilinc et al., 2012). For the rice crop, the maximum rate of G observed was 12.6 MJ/m^2. This is directly related to the additional components of G that must be incorporated to account for the heat storage in the permanent irrigation water application (W) as well as the soil heat storage (S) (see Section 4.2.4.1)

The partitioning of available energy ($R_n - G$) into sensible (H_s) and latent heat (LE) fluxes was also very similar at each flux tower location, except for the rice crop location. For all but rice, H_s accounted for 13.2% – 19.9% of the total heat fluxes ($H_s + LE$), regardless of season or crop.

The rice crop displayed very different behaviour, where H_s accounted for less than 1% of total heat flux, indicating that the energy balance was predominately driven by latent heat exchange. The difference in energy partitioning is most likely the direct result of the different water management strategies adopted for each crop. For example, for the maize crop, a total of 5.6 ML/ha of irrigation water was supplied intermittently throughout the growing season; for the rice crop, a permanent application of water (7.6 ML/ha) was required to maintain levels of 0.05 – 0.3 m above the soil surface throughout the majority of the growing season. The presence of the permanent water led to greater rates of evaporation from the surface and hence, latent heat exchange. This is particularly relevant during the early vegetative growth stages when the water surface was directly exposed to atmosphere (see Figure 6.1).

H_s is further suppressed by the dense rice plant canopy during the warmest period of the growing season (Hatala et al., 2012b). Figure 6.2 illustrates the density of the canopy during the reproductive stage of growth when leaf area index is generally at its greatest (Alberto et

al., 2011). Figure 6.3 also presents H_s in relation to mean air temperature and phenological growth stage of the rice crop. As illustrated, H_s was least during the reproductive stage of growth, especially between December 23, 2010 and January 29, 2011. During this particular interval, the average air temperature was 29.4°C. The average sensible heat flux was -1.6 MJ/m^2/day with a range of -5.0 – 1.4 MJ/m^2/day. In contrast, the average air temperature during the entire vegetative stage was 27.0°C and the average sensible heat flux was 0.4 MJ/m^2/day with a range of -5.0 – 3.5 MJ/m^2/day.

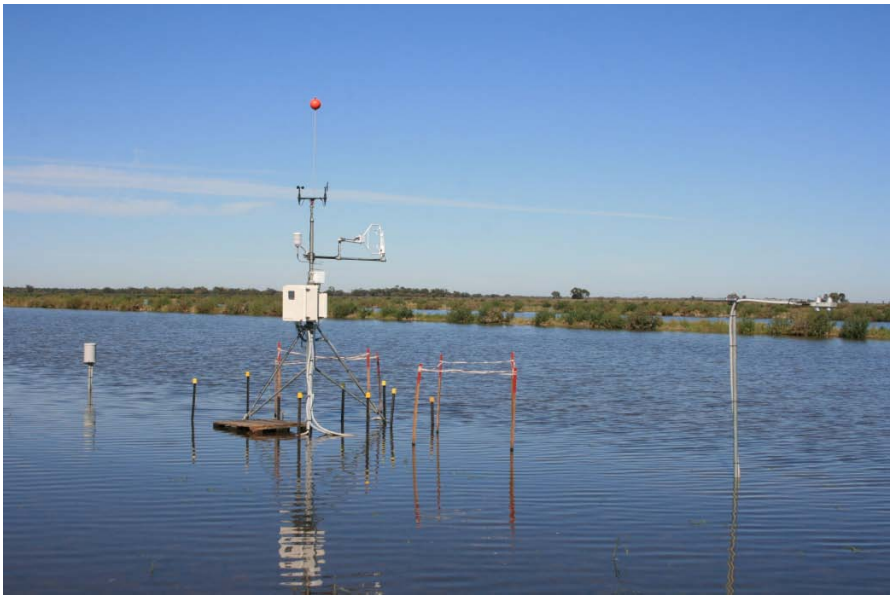

Figure 6.1 The flux tower installation over the rice crop during the early vegetative stages of growth.

Figure 6.2 Image of the dense plant canopy during the reproductive growth stage of rice.

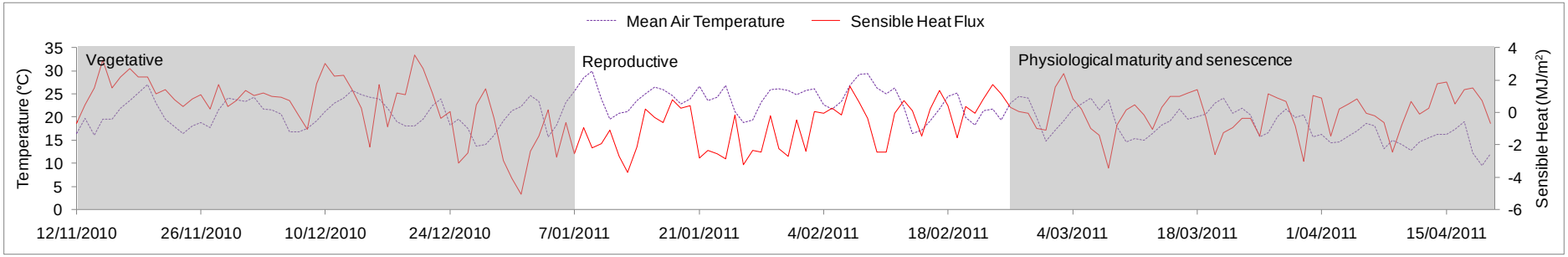

Figure 6.3 Daily fluxes of sensible heat in relation to mean air temperatures and phenology of the rice crop.

6.2 Evapotranspiration

6.2.1 Seasonal distribution of evapotranspiration

Table 6.2 presents the cumulative totals of reference evapotranspiration (ET_o) calculated from meteorological data by the Penman-Monteith equation, potential evapotranspiration (ET_c) as a function of crop coefficients and ET_o and the actual evapotranspiration (ET_a) observed at each of the flux tower locations during the observation period.

Table 6.2 Cumulative totals of reference evapotranspiration (ET_o), potential crop evapotranspiration (ET_c) and actual evapotranspiration (ET_a) observed at each site (mm).

Crop	*No. Days of Observation*	ET_o	ET_c	ET_a
Maize	158	716	490	624
Rice	160	808	834	783
Wheat	211	771	575	389
Mixed	204	837	605	414

As mentioned in the previous section, the cumulative totals of ET_a (i.e. latent heat flux) during the summer growing season were almost double those of the winter growing season. As illustrated in Figure 6.4 and Figure 6.5, increased evapotranspiration rates were generally driven by higher levels of incoming solar radiation during the summer months, which led to an increase in evaporation from soil surfaces and transpiration from plant material (Hatala et al., 2012b).

(a)

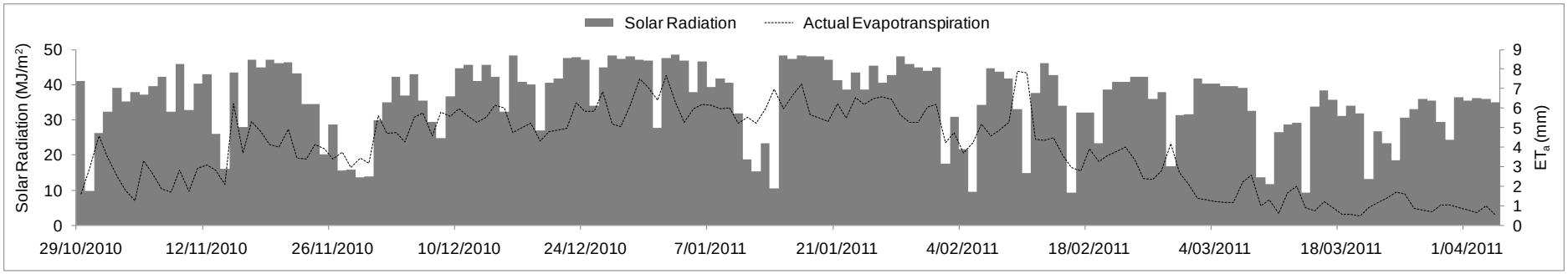

(b)

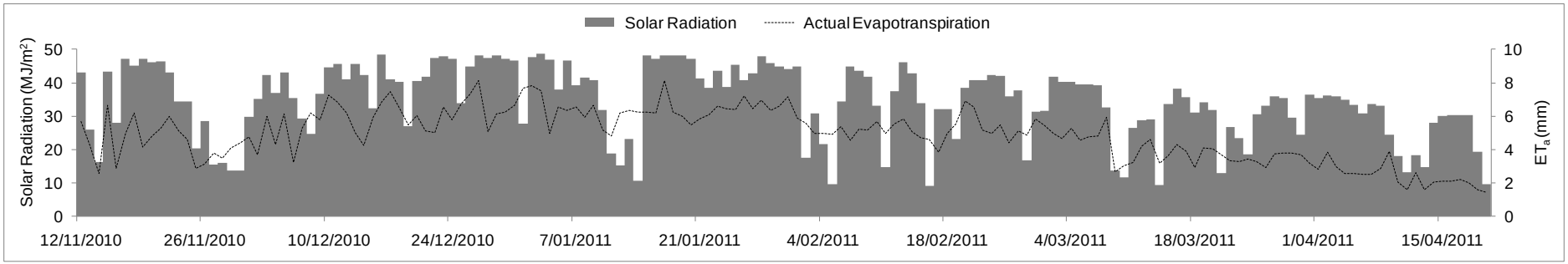

Figure 6.4 Average daily actual evapotranspiration rates and levels of incoming solar radiation observed at the flux tower locations of the summer (a) maize and (b) rice crops.

(a)

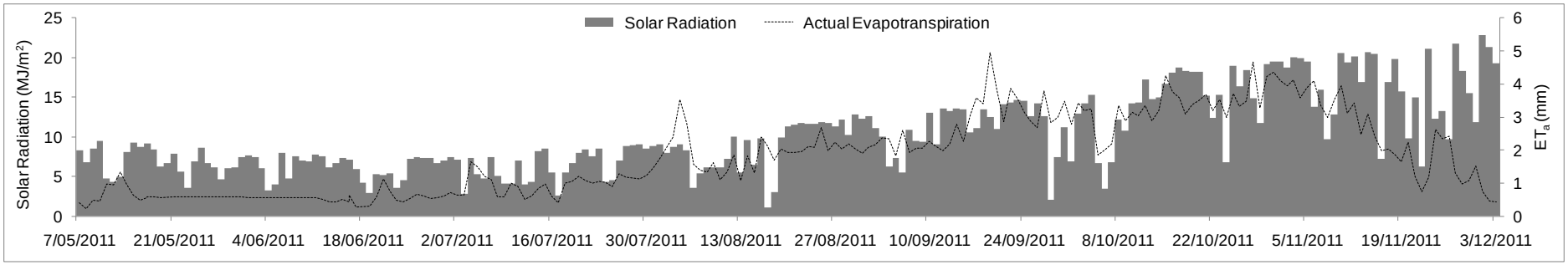

(b)

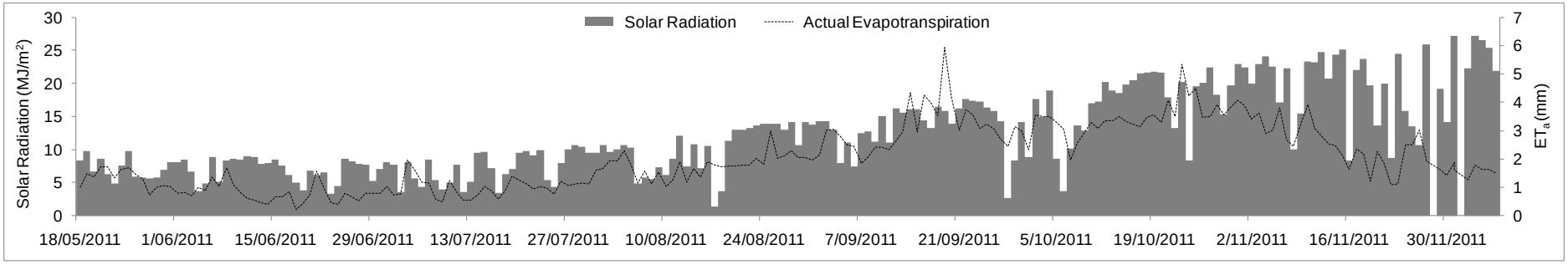

Figure 6.5 Average daily evapotranspiration rates and levels of incoming solar radiation observed at the flux tower locations of the winter (a) and (b) mixed cropping systems.

Furthermore, the cumulative ET_a totals for the two summer crops were quite different (624 mm and 783 mm for the maize and rice crop, respectively), despite having experienced similar climatic conditions over the growing season. For example, the average incoming solar radiation observed over the maize crop was 35.4 MJ/m^2/day and ranged between 9.2 and 48.7 MJ/m^2/day. These observations were comparable to those observed over the rice crop where the average incoming solar radiation was 34.6 MJ/m^2/day with the same range.

Additionally, the range of average daily ET_a rates over the observation period was also similar for both summer crops (~ 0.5 – 8 mm/day). Despite this, the seasonal evapotranspiration budget of the rice crop exceeded that of maize by 25%. This can be attributed to the difference in the average ET_a rates at both sites, e.g. the average daily ET_a rate observed over the rice crop was 4.9 mm/day, whereas the average daily ET_a rate of maize was 3.9 mm/day. As discussed in Section 6.1, this is primarily related to the exposure of the permanent water surface to the atmosphere, resulting in increased evaporation from the surface and thus, increased ET_a rates.

The average daily rates and cumulative season totals of ET_a of the two winter cropping systems were similar (1.8 mm/day and 389 mm; and 2.0 mm/day and 414 mm for the wheat and mixed cropping system, respectively). The similarities can be partially attributed to the large proportion of fluxes originating upwind of the sensor, representative of the wheat planted within the mixed cropping system.

Cumulative potential crop evapotranspiration rates (ET_c) of the summer maize crop underestimated ET_a by ~ 11%. This could be an indication that either the latent heat fluxes were being overestimated, or that the hypothetical calculation of ET_o by the Penman-Monteith method, which is required to determine ET_c, was underestimated. Conversely, the ratio of cumulative ET_c/ET_a of the winter crops was ~ 1.5. This indicated that ET_c determined as a function of crop coefficients and reference evapotranspiration were overestimated. In

addition, the K_c values used to estimate ET_c were originally developed through the measurement of ET_a using a weighing lysimeter. As ET_a was estimated using EC systems which are able to provide a direct measure of latent heat fluxes, the K_c used here may not be suitable for this analysis.

It is important to note that evapotranspiration rates for the two summer crops were atypical of those usually observed in the CIA. For example, Evans (1971) found that average daily rates of evapotranspiration of rice grown in the region ranged between 1.8 – 14 mm/day. Humphreys et al. (1994) also found that rice water use (i.e. irrigation + rainfall - deep percolation - surface drainage) varied between 9.0 – 15.4 ML/ha, depending on the climatic conditions experienced during the growing season. Figure 6.6 also illustrates the annual average rice water use in the Murrumbidgee Irrigation Area, which experiences a similar climate to the CIA. As depicted, total rice water use was lowest in 2010/11 (approximately 10.7 ML/ha) and greatest in 2006/07 (approximately 17.8 ML/ha).

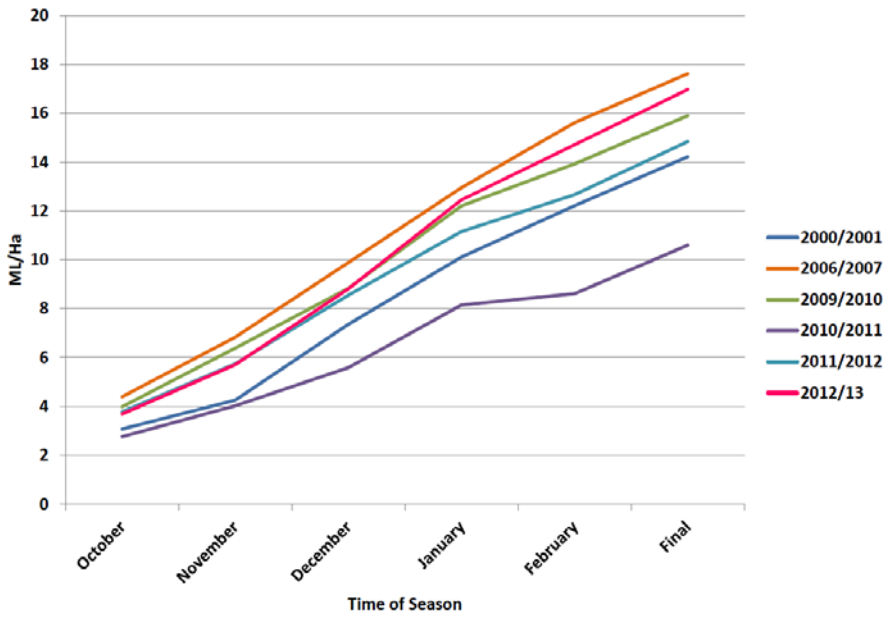

Figure 6.6 Seasonal comparison of rice water use (ML/ha) in the Murrumbidgee Irrigation Area (Murrumbidgee Irrigation Ltd, 2013).

Generally, for rice production in the CIA, 2 ML/ha of irrigation water is required to fill the soil profile; surface drainage accounts for an additional 2 ML/ha (Smith, 2013). In this particular study, total input was 7.6 ML/ha (irrigation) + 4.7 ML/ha (rainfall) = 12.3 ML/ha. Subtracting deep percolation and drainage losses, total rice water use was 8.3 ML/ha. The results of the study showed that the cumulative total of ET_a for the rice crop was 783 mm (or ~ 7.8 ML/ha). According to these figures, there is a remaining 0.5 ML/ha unaccounted for (8.3 – 7.8 = 0.5 ML/ha). Given that this 2010/11 marked the end of a ten year drought in the region, this additional water was most probably lost through deep percolation required to fill very dry soil profiles (Smith, 2013).

Previously published values of monthly ET_o and ET_c of maize were also greater than those estimated in the CIA in 2010/11(see Table 6.3). In both cases, ET_o was calculated using the Penman-Monteith method (Allen, 1988) and ET_c was calculated using crop factors (K_c) developed by Meyer et al. (1999). Except for November, the monthly evaporative demand of the atmosphere (represented by ET_o) reported by Edraki et al. (2003) was ~ 10 – 20% greater than what it was in 2010/11. Additionally, crop water use (represented by ET_c) in 1998/99 was almost double that of crop water use in 2010/11. As presented in Table 6.3, the total observed rainfall in 2010/11 was much greater than in 1998/99, particularly during the months of November and February.

Table 6.3 Monthly reference, potential evapotranspiration (ET_o and ET_c; mm) and rainfall (P; mm) of maize grown in the CIA in 1998/99 and 2010/11 (adapted from Edraki et al., 2003).

Month	*1998/99*			*2010/11*		
	ET_o	ET_c	P	ET_o	ET_c	P
November	215.2	107.6	48.0	273.0	73.0	113.5
December	306.9	214.8	16.0	280.4	110.0	24.4
January	319.3	271.4	15.0	264.0	126.1	56.1
February	243.0	206.6	2.0	222.9	104.0	203.5

Whilst evapotranspiration values of the two summer crops grown in the CIA in 2010/11 were consistently higher than previously reported values, it is difficult to say whether or not the values of evapotranspiration of wheat observed in the CIA in 2011 were typical of wheat grown in the area in other years. Table 6.4 presents the monthly ET_o and ET_c values of wheat grown in 1999 (Edraki et al., 2003) and 2011. As illustrated, monthly ET_o and ET_c values of wheat grown in 2011 were greater than those reported for 1999 in the first few months of the growing season (June – September), and less in the latter part of the season.

Table 6.4 Monthly reference, potential evapotranspiration (ET_o and ET_c; mm) and rainfall (P; mm) of wheat grown in the CIA in 1999 and 2011 (adapted from Edraki et al., 2003).

Month	*1999*			*2011*		
	ET_o	ET_c	P	ET_o	ET_c	P
June	30.0	18.0	51.0	93.3	56.0	14.2
July	36.9	33.2	8.0	92.7	83.4	29.0
August	62.5	68.8	45.0	90.6	95.2	62.0
September	103.8	114.2	24.0	119.8	125.7	34.3
October	155.6	124.5	42.0	129.4	103.5	18.52
November	209.2	104.6	38.0	154.3	77.1	38.6

6.3 Carbon Dioxide Fluxes

6.3.1 Partitioning of carbon dioxide flux into gross primary productivity and total ecosystem respiration

Whilst eddy covariance methodologies provide a direct measure of carbon dioxide flux (F_c) between the land surface and the atmosphere, further modelling of EC data is required to partition F_c into its constituent fluxes that are associated with distinct biophysical processes (Scanlon & Kustas, 2010). By partitioning F_c into its assimilatory (gross primary productivity; *GPP*) and respiratory (total ecosystem respiration; *Re*) components, a greater understanding of the processes that drive carbon cycling within the irrigated agricultural environment can be achieved.

Firstly, a friction velocity (*u**) threshold for each dataset was set to ensure turbulence intensity, whereby any data not meeting the criterion was deemed unreliable and removed from the dataset. The *u** threshold and the percentage of the 30 minute averaged CO_2 flux data that was subsequently selected for further analysis are given in Table 6.5.

Table 6.5 The *u threshold and percentage of night-time data used to determine the empirical model for each flux tower location.**

Crop	*u* (m/s)*	*% Data Selected*
Maize	0.15	32.3
Rice	0.17	16.5
Wheat	0.33	3.0
Mixed	0.17	19.3

The remaining data were then used to determine the empirical exponential models required to partition CO_2 fluxes by fitting an exponential function to night-time CO_2 fluxes plotted against

corresponding night-time soil temperatures. Furthermore, previous studies of CO_2 fluxes of rice crops reveal that it is necessary to separate flooded periods from drained periods, because CO_2 transport from the soil surface to the atmosphere is diffused during periods of permanent irrigation water application (e.g. Miyata et al., 2000; Saito et al., 2005). However, in this study it was difficult to establish a meaningful relationship between F_c and T_s during drained conditions given the small sample set of data representative this period (n = 5).

Secondly, an exponential function was fitted to the data. The resulting empirical models and corresponding coefficients of determination (r^2) for each flux tower location are given by:

$$\boldsymbol{F_{c_{maize}} = 0.0471\exp(0.0576Ts)}; \qquad r^2 = 0.14 \quad (24)$$

$$\boldsymbol{F_{c_{rice}} = 0.00127\exp(0.234Ts)}; \qquad r^2 = 0.14 \quad (25)$$

$$\boldsymbol{F_{c_{wheat}} = 0.0807\exp(0.0658Ts)}; \qquad r^2 = 0.53 \quad (26)$$

$$\boldsymbol{F_{c_{mixed}} = 0.0502\exp(0.0404Ts)}; \qquad r^2 = 0.61 \quad (27)$$

Based on these results, the empirical models developed to determine the relationship between carbon dioxide flux and soil/air temperature represent a marginal fit of the data, as emphasised by the low values of r^2. This is not uncommon in eddy covariance studies where the r^2 is often reported to be less than 0.2 (Baldocchi, 2003). In this study, the relationship between carbon flux and T_s of all cropping systems was weak to moderate (r^2 = 0.14 – 0.61). Therefore, it is likely that the computed values of *Re* and *GPP* contain considerable error. This is not unexpected, given the multiple number of processes not included in standard respiration models that may influence CO_2 flux, e.g. the physical displacement of CO_2 following a rainfall event or the biological activity of both aboveground and belowground autotrophic biomass (Scott et al., 2006).

6.3.2 Cumulative totals and seasonal distribution of net ecosystem exchange, gross primary productivity and total ecosystem respiration

The cumulative totals of partitioned CO_2 fluxes are given in Table 6.6. In this case, a negative value of *NEE* represents a flux of CO_2 from the atmosphere (i.e. carbon uptake).

Table 6.6 Cumulative totals of partitioned CO_2 fluxes.

Crop	*NEE (g C/m^2)*	*GPP (g C/m^2)*	*Re (g C/m^2)*
Maize	-1327	1952	625
Rice	-826	1514	689
Wheat	-388	1367	979
Mixed	-674	1247	572

In addition to climatic drivers of CO_2 flux, which are discussed in detail in Section 6.3, the magnitude of atmospheric carbon uptake or release of a plant is influenced by the nature of the photosynthetic pathway. As a C4 plant, maize has a greater photosynthetic capacity compared to its C3 counterparts such as rice, wheat and canola (McGinn & King, 1990; Suyker et al., 2005). As such, the maize crop exhibited the greatest capacity for carbon uptake (*NEE* = -1327 g C/m^2) over the respective observation periods. In contrast, the winter wheat crop had the least capacity for net carbon capture with a cumulative *NEE* total of -388 g C/m^2.

The daily distribution of average daily rates of *NEE*, *GPP* and *Re* for the summer and winter crops are presented in Figure 6.7 and Figure 6.8, respectively. Maize exhibited the greatest rate of net carbon capture, as the average rate of *NEE* peaked at -21.3 g C/m^2/day on December 14, 2010. The winter wheat crop had the least affinity for net carbon capture where maximum average rate of *NEE* reached only -8.7 g C/m^2/day on October 10, 2011.

(a)

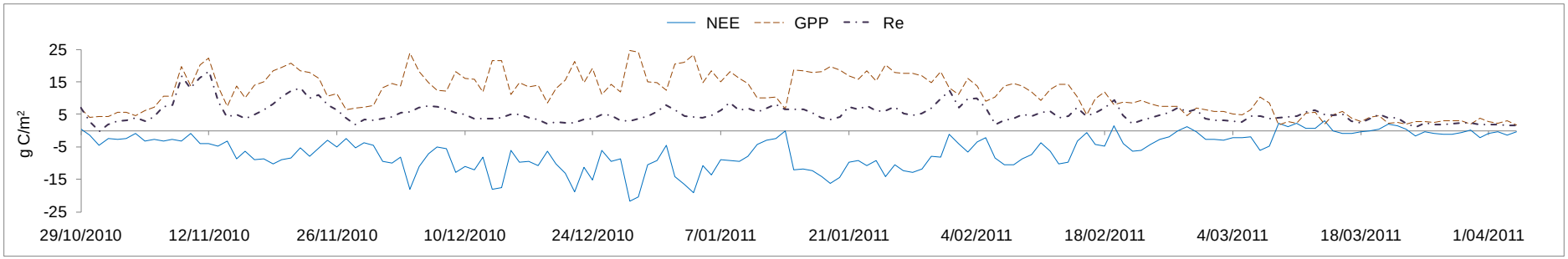

(b)

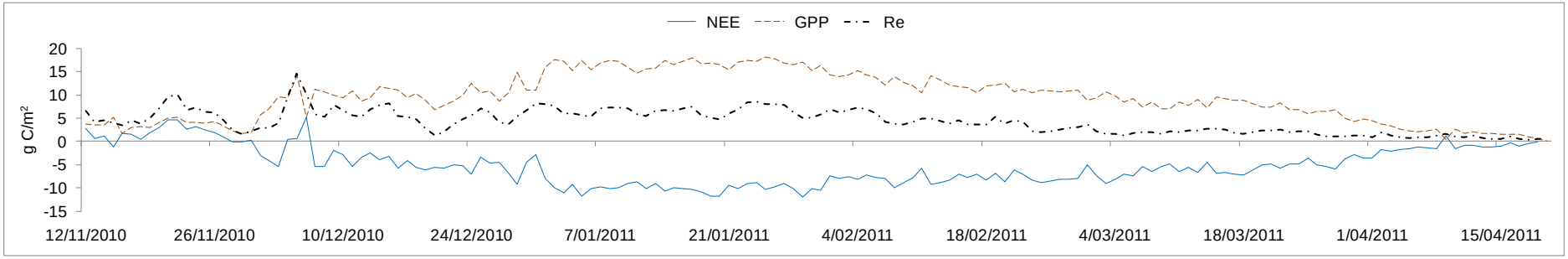

Figure 6.7 Seasonal distributions of *NEE*, *GPP* and total *Re* of the summer (a) maize and (b) rice crops.

(a)

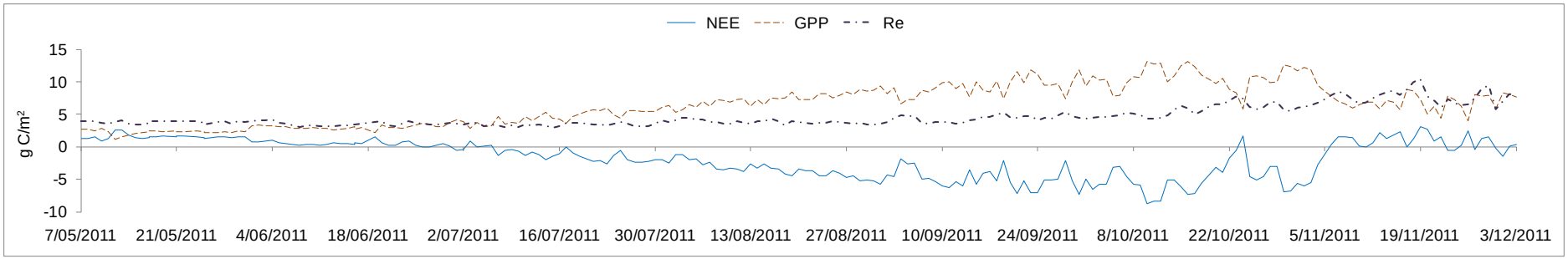

(b)

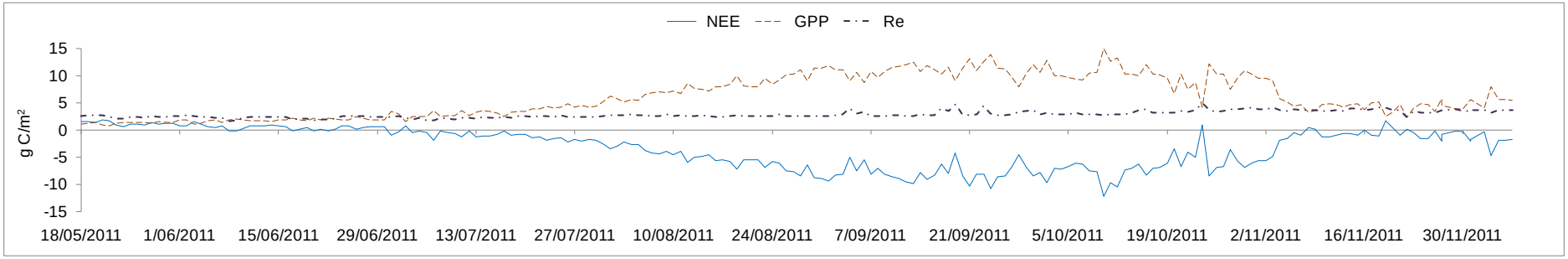

Figure 6.8 Seasonal distributions of *NEE*, *GPP* and *Re* of the winter (a) wheat crop and (b) mixed cropping system.

Whilst all four cropping systems acted as a carbon sink for the majority of the growing season, positive values of *NEE* (i.e. carbon release) were experienced at the beginning of the growing season for rice, wheat and the mixed cropping system, thus becoming a net carbon source during this period. This is due to the relatively small amount of photosynthetic material available for carbon assimilation, particularly at the beginning of the growing season. Because of this, respiration rates of CO_2 (*Re*) directly from the soil surface to the atmosphere account for the majority of the flux, especially at night. For example, in June, 2011, the cumulative total of *Re* estimated over the wheat crop was 105.6 g C/m^2. In comparison, the cumulative totals of *NEE* and *GPP* were 14.7 g C/m^2 and 90.9 g C/m^2, respectively.

The rate of *NEE* during the early vegetative growth stage of the two winter cropping systems was further affected, because the ratio between exposed soil surface and vegetation during this stage was also relatively large. The land preparation prior to sowing also had an influence on *Re* for these two sites. As illustrated in Figure 6.9 and Figure 6.10, the wheat crop was sown directly into the stubble of the previous maize crop. At the alternate winter site, the stubble of the previous crop was burnt prior to sowing. This meant that there was a larger volume of organic material available for decomposition at the former flux tower location, which led to higher average daily rates of *Re* during the vegetative stages of growth (3.6 g C/m^2/day versus 2.3 g C/m^2/day).

Note that early growing season data for the maize crop was not available. Therefore, an assessment of carbon uptake/release during the early vegetative stages of growth was not made for this crop.

Figure 6.9 Early vegetative stages of growth of the wheat crop.

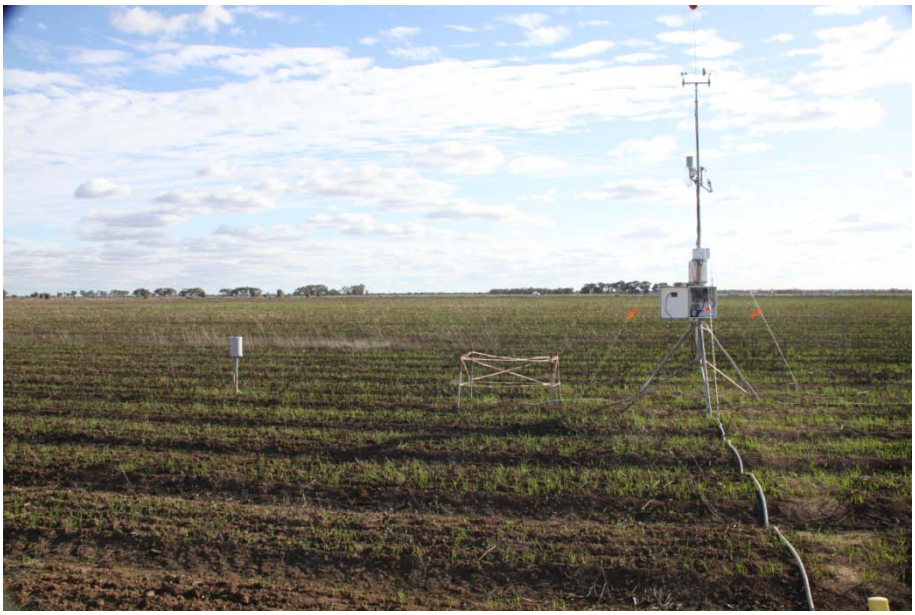

Figure 6.10 Early vegetative stages of growth of the mixed cropping system.

As the crops grew, the volume of photosynthetic material increased thereby increasing the rate of net carbon uptake. For all four cropping systems the maximum average rate of *NEE* occurred during the reproductive stage (see Table 6.7). The lowest average values occurred once physiological maturity had been reached and leaf senescence had begun to occur. Whilst acting as a net carbon sink during this period, pulses of CO_2 into the atmosphere were recorded towards the end of the growing season for the maize, wheat and the mixed cropping systems. These generally coincided with lower levels of incoming solar radiation, as depicted by Figure 6.11, which illustrates fluxes of *NEE* in response to incoming solar radiation levels for the maize crop in June, 2011.

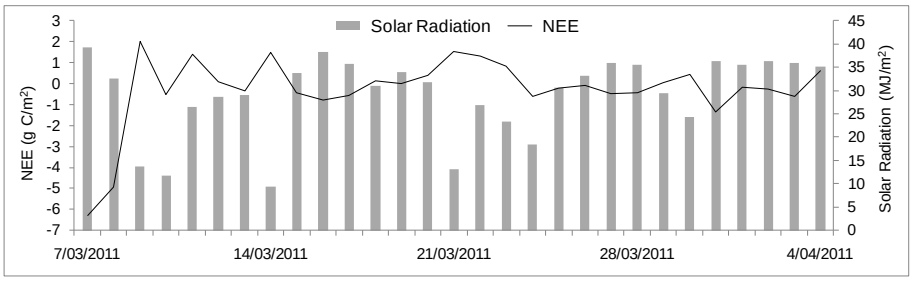

Figure 6.11 Fluxes of *NEE* in response to incoming solar radiation estimated for the maize crop in June, 2011.

Previous studies of CO_2 fluxes of rice crops have found that daily rates of NEE remained positive (i.e. a net carbon source) prior to harvest, generally as a result of a rapid loss of CO_2 from the soil surface due to the draining of the rice field (e.g. Hatala et al., 2012a; Miyata et al., 2000; Saito et al., 2005). In this study, daily rates of *NEE* remained mostly negative after the rice field was drained (March 28, 2011).

Table 6.7 Average daily and seasonal rates of partitioned CO_2 fluxes per phenological period (g C/m^2/day).

Crop	*Vegetative*			*Reproductive*			*Physiological Maturity & Ripening*			*Seasonal*		
	NEE	*Re*	*GPP*	*NEE*	*Re*	*GPP*	*NEE*	*Re*	*GPP*	*NEE*	*Re*	*GPP*
Maize	-8.5	4.0	12.5	-16.9	4.1	21.0	-5.1	3.9	8.9	-8.4	4.0	12.4
Rice	-2.7	5.7	8.4	-9.0	5.6	14.6	-4.1	1.6	5.8	-5.2	4.3	9.5
Wheat	-0.8	3.6	4.4	-4.9	5.0	10.0	0.5	7.7	7.2	-1.8	4.6	6.5
Mixed	-1.2	2.3	3.5	-7.5	3.0	10.5	-1.8	3.6	5.4	-3.3	2.8	6.1

The total amount of carbon fixed as biomass through photosynthesis (represented as *GPP*) was similar the winter cropping systems, ranging between 1247 – 1367 g C/m^2 (see Table 6.6). The cumulative total of *GPP* of rice was greater (1514 g C/m^2) and can be attributed to the greater amount of photosynthetic activity as a result of increased solar radiation during the summer months. Overall, maize exhibited the greatest affinity for carbon assimilation (*GPP* = 1952 g C/m^2). This is to be expected, considering maize is a C4 plant, therefore having a greater capacity for carbon capture. This is also reflected in the maximum average daily rates of *GPP*, which was 25.7 g C/m^2/day for maize compared to 18.2 g C/m^2/day for the rice crop.

The wheat crop appeared to fix the least amount of CO_2 having a maximum daily *GPP* rate of only 13.1 g C/m^2/day. This is also reflected in the biometric measures, represented by the harvest index, sampled just prior to harvest. For example, the harvest index for the wheat crop was 0.61, whereas the harvest index of the wheat planted within the mixed cropping system was 0.68. Decreased rates of *GPP* of winter cropping systems can be partially attributed to lower incoming rates of solar radiation and mean air temperatures. This is discussed further in Section 6.3.

All four cropping systems exhibited similar temporal changes in *GPP*, whereby the rate of increase in *GPP* was slow during the early stages of vegetative growth and increased rapidly during the adult vegetative and reproductive phases (see Figure 6.9 and Figure 6.10). Once physiological maturity had been reached, *GPP* began to decline; this was directly related to the decreased photosynthetic activity that occurs as a result of decreasing chlorophyll content due to leaf senescence (Rossini et al., 2010; Steduto et al., 2007; Suyker & Verma, 2010).

Of the two summer crops, rice exhibited the greatest amount of respiration over the observation period with a cumulative total of 689 g C/m^2 and represented 45.5% of the carbon budget. For the winter

wheat crop, the cumulative season total of *Re* was 979 g C/m^2 which represented 71.6% of the carbon budget. In contrast, maize had a total cumulative total *Re* of 625 g C/m^2 which accounted for 32.0% of the carbon budget; this is reflected in the average daily rates of *Re* throughout the growing season (see Table 6.7) where respiration rates of rice and wheat were consistently higher than those of maize. Decreased respiration rates of maize can be partially attributed to the fact that photorespiration (i.e. respiration during the photosynthetic process) is greatly reduced in C4 plants (e.g. maize) by inhibiting the enzymatic oxygenation activity (Kennedy, 1976; Lara & Andreo, 2011).

6.4 Water and carbon dioxide flux response to environmental drivers

The relationships between ET_a, *GPP* and the various environmental variables (R_n, T_a, *VPD*, *U*, *P* and ET_a) were investigated through the application of geostatistical regression based on model selection methods (specifically, Bayes Information Criterion; BIC). The regression coefficient ($\widehat{\boldsymbol{\beta}}$) of each of the standardised covariates in the geostatistical model of 'best-fit' for each flux tower location are given in Table 6.8. The coefficient of determination (r^2) of each model is also presented. Note that each covariate has been standardised to a mean of zero and a standard deviation of one, in order to compare the regression coefficients of the covariates, as per Yadav et al. (2010).

Table 6.8 Regression coefficients ($\widehat{\boldsymbol{\beta}}$) of the best-fit geostatistical regression model and associated coefficient of determination (r^2).

Flux	*Crop*	R_n	T_a	*VPD*	*U*	*P*	ET_a	r^2
ET_a	Maize	6.62	10.59	—	5.37	-0.82	N/A	0.22
	Rice	22.98	26.69	-16.00	15.29	4.63	N/A	0.67
	Wheat	11.65	—	4.71	6.84	0.66	N/A	0.44
	Mixed	-12.39	14.90	-10.36	5.32	1.27	N/A	0.46
GPP	Maize	0.59	—	—	-0.72	—	1.82	0.42
	Rice	—	—	—	-0.90	—	1.41	0.39
	Wheat	1.10	—	-0.46	—	—	—	0.33
	Mixed	1.08	-1.09	—	—	—	—	0.18

With respect to ET_a flux response to the environmental drivers listed in Table 6.8, the common variables selected for the GR model of maize and rice were R_n, *Ta*, *U* and *P*. However, the extent to which each variable influenced ET_a varied between the two sites. This was indicated by magnitude and sign convention of the regression coefficient. For the maize crop, air temperature had the greatest influence on daily ET_a rates of the maize crop ($\widehat{\boldsymbol{\beta}}$ = 10.6) and rain had the least ($\widehat{\boldsymbol{\beta}}$ = -0.8). For the rice crop, T_a also proved to have the greatest influence on ET_a rates ($\widehat{\boldsymbol{\beta}}$ = 26.9) and *P* also had the least ($\widehat{\boldsymbol{\beta}}$ = 4.6). Note, however, that ET_a of the rice crop was positively correlated to *P* and negatively correlated with that observed over the maize crop. This indicated that rates of ET_a of the maize slightly decreased following a rainfall event. The major difference between the GR models of the two crops was that *VPD* was also selected as a covariate for the GR model of the rice crop ($\widehat{\boldsymbol{\beta}}$ = -16.0) and had a negative influence on ET_a rates.

For the winter crops, the common variables that influenced daily rates of ET_a were R_n, *VPD*, *U* and *P*. T_a appeared only to affect evapotranspiration rates of the mixed cropping system where it also had the largest influence ($\widehat{\boldsymbol{\beta}}$ = 14.90). In this particular case, R_n and *VPD* were negatively correlated to evapotranspiration rates. For the wheat crop, all selected variables had a positive correlation to daily rates of ET_a and net radiation had the greatest influence ($\widehat{\boldsymbol{\beta}}$ = 11.65). Like the summer crops, *P* had the least influence on ET_a rates of the winter cropping systems ($\widehat{\boldsymbol{\beta}}$ = 0.66 and 1.27 for the wheat and mixed system, respectively).

In terms of CO_2 flux response, ET_a was included as an additional variable to investigate *GPP* rates as a function of plant water use (see Table 6.8). As shown, the two common variables selected for the GR model at the two summer flux tower locations were wind speed and evapotranspiration. Both variables had a comparable influence on rates of daily *GPP*, having similar regression coefficients. In both

cases, ET_a was positively correlated to *GPP*, suggesting that an increase in ET_a rates generally led to an increase in carbon uptake for both maize and rice crops. A negative correlation between wind speed and *GPP* was also consistent at both sites. The GR model of the maize crop included net radiation as an additional variable which was positively correlated with carbon uptake. The results of the BIC/GR analysis have also shown that ET_a, having the largest regression coefficient ($\widehat{\boldsymbol{\beta}}$ = 1.8 and 1.4, respectively), had the greatest influence on the variability of daily rates of *GPP* of both maize and rice.

For the winter crops, R_n was the only common variable selected for the GR model at either site and its influence on daily *GPP* rates was similar ($\widehat{\boldsymbol{\beta}}$ = 1.10 and 1.08). *GPP* rates of the wheat crop were negatively influenced by *VPD* ($\widehat{\boldsymbol{\beta}}$ = -0.46). For the mixed cropping system air temperature had a negative effect on the rate of carbon uptake ($\widehat{\boldsymbol{\beta}}$ = -1.09). Unlike the summer crops, ET_a was not selected as a variable for either winter cropping systems and therefore had no effect on daily rates of *GPP*. This is most likely the result of lower evaporative demand and increased residual moisture within the soil during and the winter months.

At all four experimental sites, observed rainfall did not have an effect on the rates of *GPP*, contrary to what would usually be expected in a semi-arid climate (Krishnan et al., 2012) as plant water availability was unusually high for the most part of the growing season due to unusually high rainfall. This was also reflected in ET_a flux response, where, although rainfall did have an effect, it was minimal in comparison to the other selected variables of each GR model.

In terms of model performance, the ability of the selected variables to explain variability in daily rates of ET_a and *GPP* was weak to moderate (r^2 values and ranged from 0.2 – 0.7).

6.5 Water and carbon dioxide flux response to biophysical crop characteristics in the CIA

Due to budgetary restrictions, accurate LAI measurements were collated for the summer crops only. For the purpose of this exercise, each phenological stage of growth of each crop, as determined by field observations, was examined in relation to ET_a and *GPP* rates; LAI measurements were incorporated where available.

Figure 6.12 and Figure 6.13 present the average daily rates of ET_a and *GPP* per phenological stage of the crop. These stages have been broken down into three broad categories of growth for comparative assessment across each site. Figure 6.12 also includes LAI measurements recorded for the maize crop. Note that the LAI data recorded for the rice crop was not included as it was unreliable.

(a)

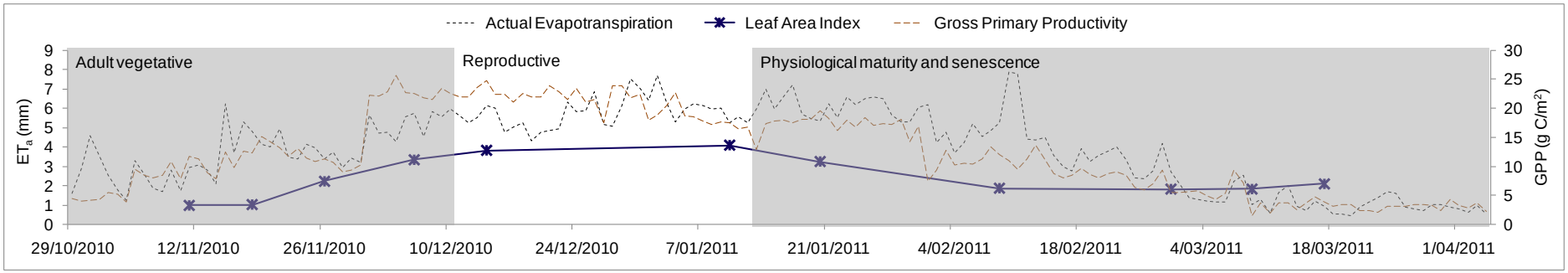

(b)

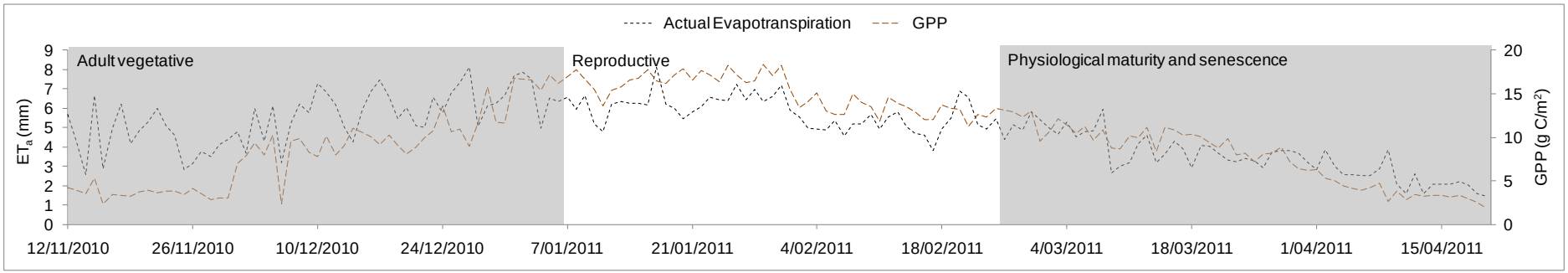

Figure 6.12 Daily ET_a and *GPP* rates and phenological stages of the (a) maize and (b) rice crops. The blue line in (a) represents the LAI of maize.

(a)

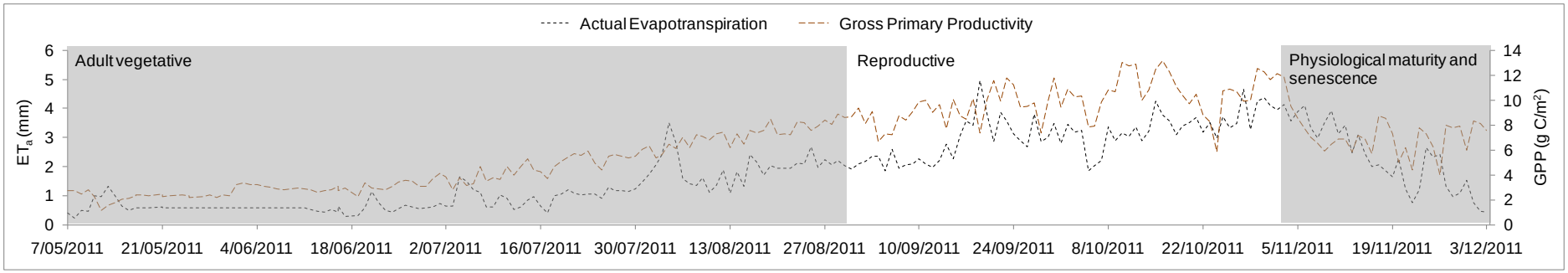

(b)

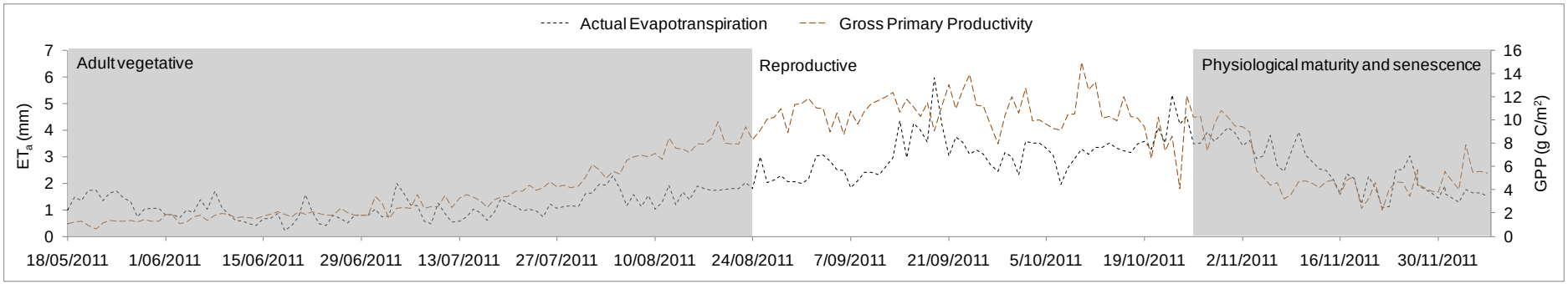

Figure 6.13 Daily ET_a and *GPP* rates and phenological stages of (a) the wheat crop and (b) the mixed cropping systems.

As illustrated in Figure 6.12 and Figure 6.13, ET_a and *GPP* steadily increased throughout the vegetative growth stage although the magnitude between summer and winter crops was quite different. For instance, the maximum average daily rate of ET_a of the winter wheat crop during this period was 3.5 mm/day whereas the maximum average ET_a during the vegetative stage of maize was 6.2 mm/day. The increased rate of evapotranspiration can be attributed, in part, to the increased amount of solar radiation and increased temperatures and, thus, increased evaporative demand experienced during the summer months in the CIA.

Generally, ET_a and *GPP* were greatest during the reproductive growth phase for all cropping systems with the exception the ET_a of the maize crop. According to previous studies (e.g. Jans et al., 2010; Suyker & Verma, 2010), this largely coincides with maximum values of LAI when the volume of photosynthetic and transpiring material is generally greatest (Greco & Baldocchi, 1996). Although this cannot be confirmed for all experimental sites in this study, Figure 6.12, which illustrates maximum LAI values that corresponded with maximum rates of ET_a of the maize crop, is consistent with the findings of the previous studies.

As mentioned previously, ET_a rates generally reach a peak during the reproductive phase of growth. According to the results displayed in Figure 6.12, the maximum average rate of ET_a reached during the reproductive stage of maize was 7.7 mm/day. The maximum average rate of ET_a throughout the entire observation period was 7.9 mm/day and occurred on February 10, 2011. At this point in time the crop had reached physiological maturity, therefore it was expected that ET_a rates were less than those experienced during the reproductive growth phase. Although this appeared to be an anomaly in the data, further investigation revealed that this had been preceded by the largest rainfall event during the growing season (77.7 mm was recorded on February 5, 2011) which resulted in the majority of the energy being partitioned as latent heat flux.

For all four cropping systems, relatively high rates of ET_a and carbon accumulation persisted during the ripening period. For the summer crops, it was for about three weeks and for the winter crops, it was for approximately two weeks. Once physiological maturity had been reached and leaf senescence (and thus decreasing levels of chlorophyll) began to occur, ET_a and *GPP* rates steadily decreased for all four cropping systems due to decreased rates of photosynthesis.

Overall, the general trend in average daily rates of *GPP* followed that of ET_a.

6.6 Water Productivity

As a function of biomass production (i.e. that is related to photosynthetic activity), WP can be defined as the amount of carbon accumulated (as *GPP* or above-ground biomass) per unit of $\boldsymbol{ET_a}$ over the length of the growing season (g C/m^2) (Suyker & Verma, 2010). As above-ground biomass was not measured regularly at any of the experimental sites throughout the growing season, therefore seasonal water productivity was calculated by using estimated values of *GPP* only. To better compare values of WP for different cropping systems, daily ET_a values were normalised by daily reference evapotranspiration values (ET_o) and the crop water productivity calculated for each cropping system is given in Table 6.9. Water productivity of the winter mixed cropping system was not calculated as irrigation and yield information for the canola and faba bean was unavailable. Therefore, it was difficult to make a true assessment of this particular system and was excluded from further analysis.

Table 6.9 Crop water productivity (g C/m^2) of maize, rice and wheat for each growing season.

Crop	*WP (g C/m^2)*
Maize	14.4
Rice	8.1
Wheat	2.1

With respect to carbon assimilation per unit of evapotranspiration of the summer crops, maize displayed the greatest WP (14.2 g C/m^2) and rice displayed the least (10.2 g C/m^2). Maize (and all C4 plants) possess an enzyme, not evident in C3 plants, that has a greater affinity for CO_2 absorption (Keller & Seckler, 2005). As less efficient assimilators of CO_2, C3 plants' stomata tend to be open for longer under the same atmospheric conditions, increasing the amount of water lost and subsequently decreasing water productivity (Keller & Seckler, 2005). Of the three specific crops, winter wheat was the least productive (WP = 2.1 g C/m^2) which can be attributed to lower biomass production of winter crops as a result of lower levels of incoming solar radiation and mean air temperatures that occur during the winter months.

It is difficult to comprehensively compare the WP of results obtained in this study to other studies due to the non-standard methodology used to compute WP. For example, most studies of irrigated crops report WP in terms of yield per unit of irrigation water applied (kg/ML) or yield per unit of evapotranspiration (kg/m^3) (e.g. Molden et al., 2010; Zwart & Bastiaanssen, 2004). This study estimates WP as total biomass accumulation (*GPP*) per unit of evapotranspiration (g C/m^2). Where published results of photosynthetic WP were available, it appeared that WP of irrigated maize in the CIA was less than irrigated maize produced in Nebraska, USA. (mean WP ranged between 17.6 – 18.6 g C/m^2).

6.7 Regional Estimation of Fluxes

6.7.1 Land cover/land use classification

In order to determine the regional estimation of atmospheric fluxes of energy, water vapour and carbon dioxide it was necessary to obtain information as to the land use of the CIA for each cropping season. This was achieved by conducting a land cover/land use (LCLU) classification of the region by incorporating satellite-derived information with ground-truth data and other seasonal water delivery information to identify the crops grown and their geographic location within the boundaries of the CIA.

To accurately assess the land cover/land use characteristics, cloud-free imagery was required. The specific Landsat 5 image acquisition dates for the summer and winter growing seasons were January 5, 2011 and September 18, 2011, respectively. A supervised classification procedure was performed on each image. The accuracy of each classified image was assessed using a confusion matrix built using standard ENVI® 5.0 tools. For this, a combination of ground-truth observations and water delivery information was used as a secondary source of LCLU information.

The LCLU maps for summer 2010/11 and winter 2011 are illustrated in Figure 6.14 and Figure 6.15, respectively. The confusion matrices for each classification are presented in Table 6.10 and Table 6.11.

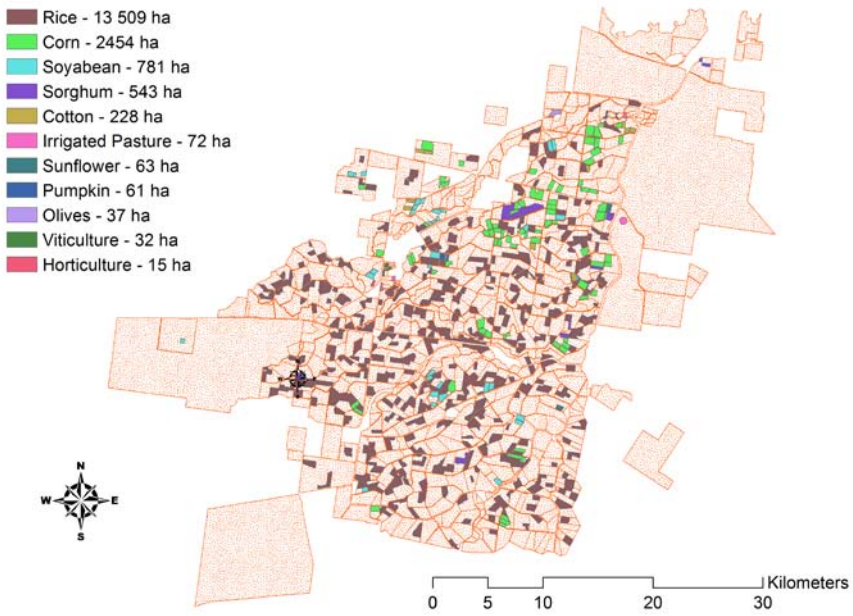

Figure 6.14 Land cover/land use map for the CIA – summer 2010/11.

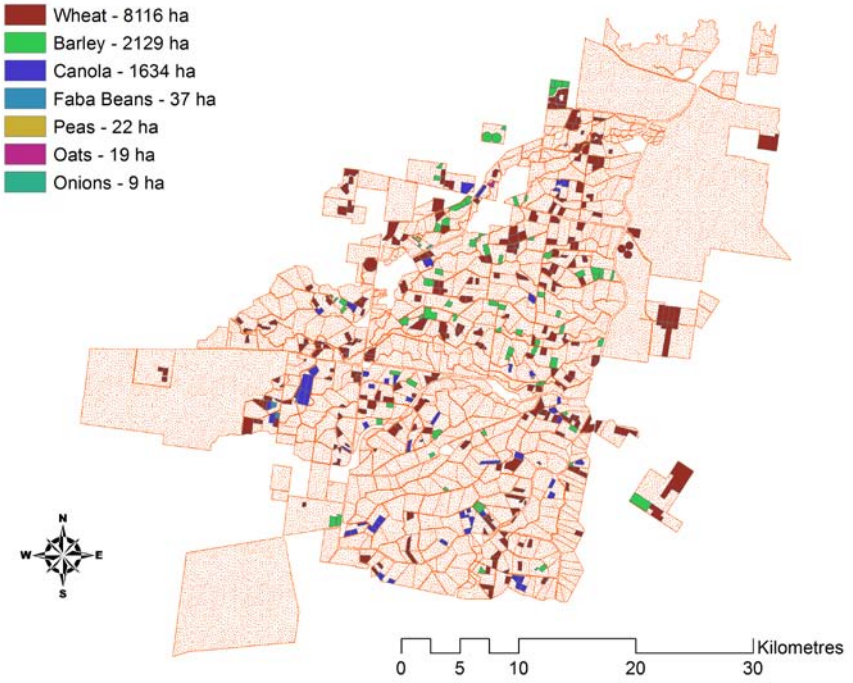

Figure 6.15 Land cover/land use map for the CIA – winter 2011.

Table 6.10 Confusion matrix for CIA land cover/land use classification – summer 2010/11

Class	*Commission (%)*	*Omission (%)*	*Producers Accuracy (%)*	*Users Accuracy (%)*
Rice	0.01	0.00	100.00	99.99
Maize	0.01	8.58	91.42	99.99
Soyabean	0.00	0.00	100.00	100.00
Sorghum	39.02	0.00	100.00	60.98
Cotton	100.00	100.00	0.00	0.00
Pumpkin	100.00	100.00	0.00	0.00
Viticulture	100.00	100.00	0.00	0.00
Irrigated Pasture	100.00	100.00	0.00	0.00
Sunflower	100.00	100.00	0.00	0.00
Horticulture	0.00	0.00	100.00	100.00
Olives	0.00	0.00	100.00	100.00
Overall accuracy:	95.72 %			
Kappa coefficient:	0.89			

Table 6.11 Confusion matrix for CIA land cover/land use classification – winter 2011

Class	*Commission (%)*	*Omission (%)*	*Producers Accuracy (%)*	*Users Accuracy (%)*
Barley	29.28	72.85	27.15	70.72
Canola	0.16	22.36	77.64	99.84
Faba Beans	99.96	98.91	1.09	0.04
Oats	0.00	100.00	0.00	0.00
Onions	100.00	100.00	0.00	0.00
Peas	0.00	100.00	0.00	0.00
Triticale	0.00	100.00	0.00	0.00
Wheat	4.51	25.90	74.10	95.49
Overall accuracy:	68.10%			
Kappa coefficient:	0.44			

As illustrated in Figure 6.14, the major summer crop grown in the CIA in summer 2010/11 was rice with total plantings of 13 509 ha. Maize was second largest planting and accounted for 2454 ha. The major crop grown in winter 2011 was wheat, with 8116 ha planted. Barley and canola accounted for the second and third largest winter plantings with 2129 ha and 1634 ha, respectively. Note that land dedicated to winter pastures has not been identified due to the difficulty of distinguishing between winter pastures and remnant winter vegetation. Since pastures were not the subject of this investigation, identification of these particular cropping systems was superfluous to the requirements of this study.

The confusion matrices presented in Table 6.10 and Table 6.11 provide insight into the accuracy of the supervised classifications. As demonstrated, the overall accuracy was greatest for the summer classification (95.7%) and least for the winter classification (68.1%). The Kappa coefficient ($\widehat{K}$) is another measure agreement between the classification and ground-truthing data (Jensen, 2005). The results of Kappa analysis showed that there was good agreement between ground-truthing information and the summer LCLU classification ($\widehat{K}$ = 0.89) and moderate agreement for the winter LCLU ($\widehat{K}$ = 0.44). Reasons for the lesser degree of accuracy and agreement of winter LCLU classification can be partially attributed to the similarities between spectral reflectance properties of winter crops and remnant vegetation and native grasslands. Therefore, it is difficult to distinguish between crops and other land covers.

With the exception of sorghum and barley, the classification accuracies for each summer and winter crop were generally high, with a reliability (or 'Users Accuracy') that ranged between 95.5% – 100.0%. The reliability of sorghum and barley was 61.0% and 70.7%, respectively, and was most likely attributable to the lower quality of the reference (or ground-truthing) data for these particular cultivars.

6.7.2 Regional upscaling of water and carbon dioxide fluxes

LCLU was further classified by identifying the maize, rice and wheat crops that were grown on the dominate soil type, transitional red-brown earth (TRBE), found at each of the experimental sites. The area of maize, rice and wheat planted on TRBE soils and the percentage of the total area of crop plantings are given in Table 6.12. Cumulative totals of the ET_a and *GPP* based on the area of each crop planted on TRBE soils are also presented here.

Table 6.12 Area and cumulative total of actual evapotranspiration (ET_a) and total carbon capture (represented by *GPP* given as kiloton C; kt = 10^6 kg) of maize, rice and wheat planted on transitional red-brown earth in the CIA 2010/11.

Crop	*Area on TRBE (ha)*	*Percentage of total area (%)*	*Cumulative ET_a (ML)*	*Cumulative GPP (kt C)*
Maize	943	38	5885	18
Rice	7549	56	59 106	123
Wheat	2978	37	11 586	41
Total			76 578	182

Figure 6.16 and Figure 6.17 illustrate the spatial distribution of cumulative season totals of ET_a proportional to planting area for the summer crops (maize and rice) and the winter wheat crop respectively.

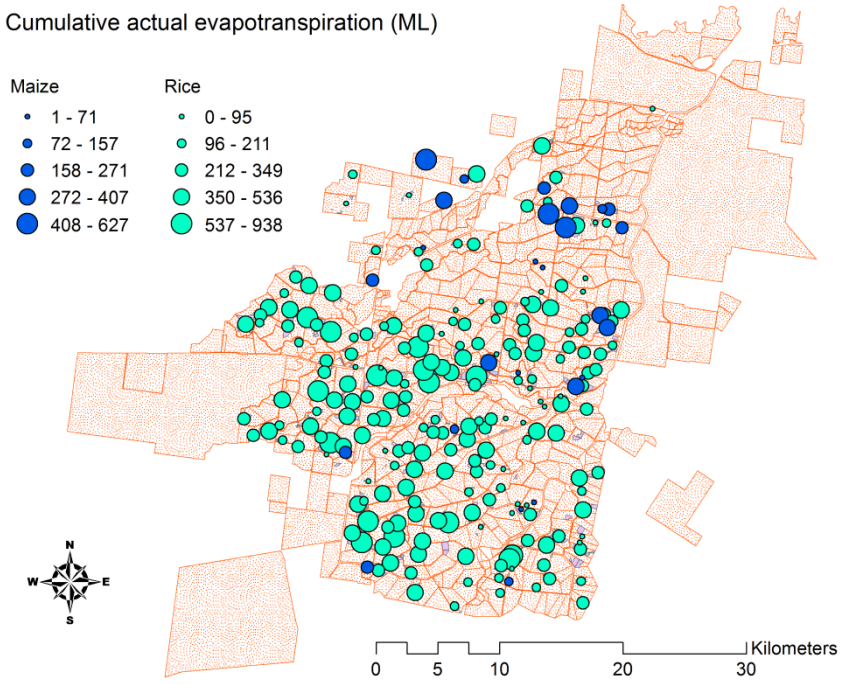

Figure 6.16 Distribution of cumulative totals of ET_a (ML) of the summer maize and rice crops.

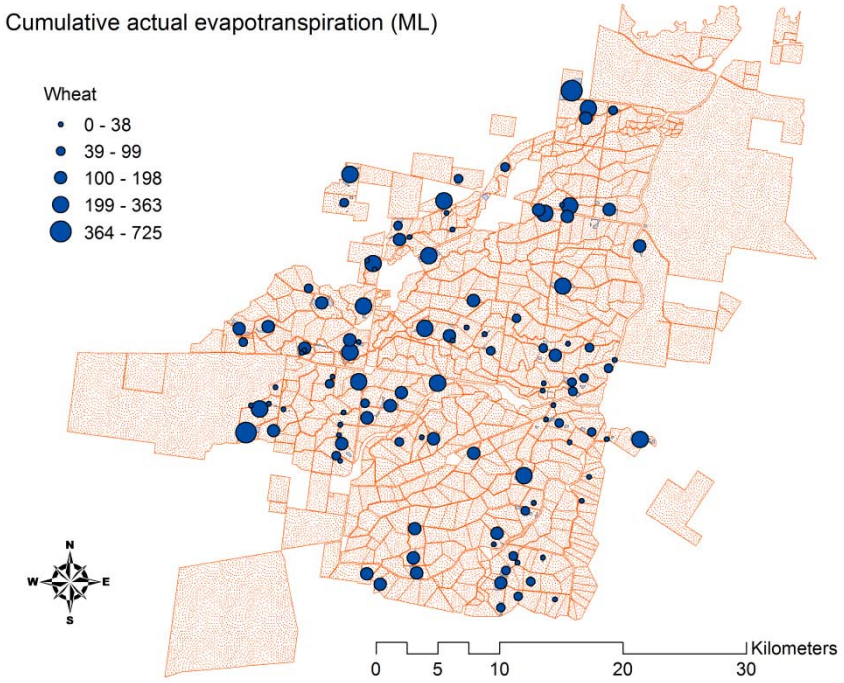

Figure 6.17 Distribution of cumulative totals of ET_a (ML) of the winter wheat crops.

The largest percentage of crops planted on TBRE soils in 2010/11 was rice which accounted for ~ 56% of total rice plantings (see Table 6.12. Maize and wheat had a similar proportion of total crop-specific cultivation area whereby plantings on TBRE soils represented ~ 37 – 38%, respectively. As discussed in Section 6.2, rice had the greatest cumulative season total of ET_a over the growing season (783 mm). Rice also represented the largest cultivation on TBRE soils during the study period. As such, the total amount of ET_a that resulted from rice growing in the CIA in 2010/11 was 59 106 ML. In contrast, total cumulative ET_a of maize production on TBRE soils was only 5885 ML. In total, the amount water lost to the atmosphere through the process of evapotranspiration of maize, rice and wheat production on these particular soils was 76 578 ML.

Figure 6.18 and Figure 6.19 illustrate the spatial distribution of cumulative season totals of *GPP* proportional to planting area for the summer crops (maize and rice) and the winter wheat crop, respectively.

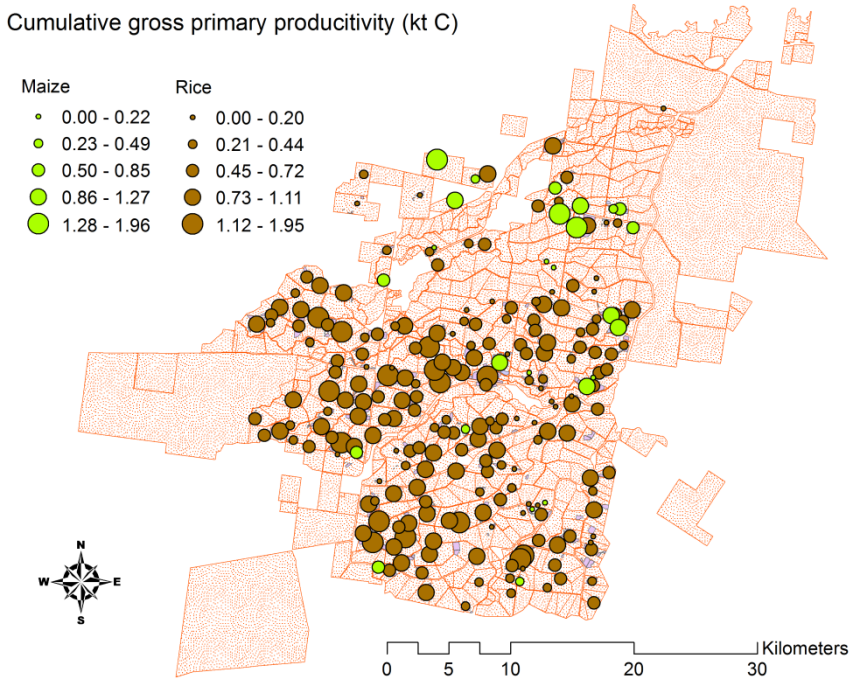

Figure 6.18 Distribution of cumulative totals of *GPP* (kt C) of the summer maize and rice crops.

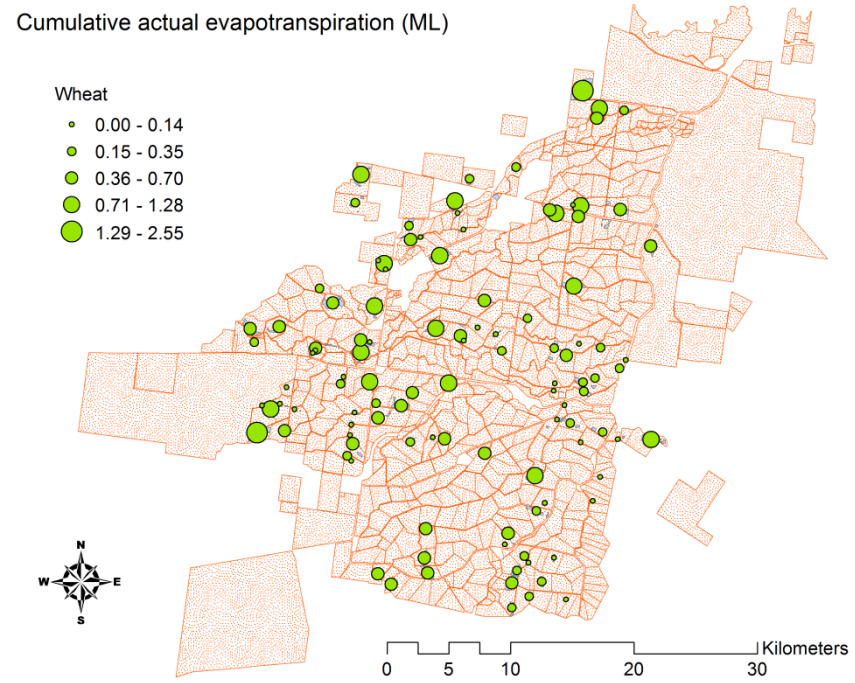

Figure 6.19 Distribution of cumulative totals of *GPP* (kt C) of the winter wheat crops.

Despite having the greatest capacity for carbon capture over the observation period (*GPP* = 1952 g C/m^2), the total cultivation of maize crops grown on TBRE in the CIA in 2010/11 accounted for less than 10% of the total carbon accumulated by all three crops (see Table 6.12). As presented in Table 6.12, further illustrated in Figure 6.18 and Figure 6.19, the number of plantings of maize was much less than the plantings of both rice and wheat in the CIA in 2010/11 and therefore contributed least to total *GPP*. Rice had the largest percentage of total area planted on TBRE soils and subsequently accounted for the greatest amount of total carbon accumulation (total *GPP* = 123 kt C). In total, the three crops planted on the specified soil type had a total carbon accumulation of 182 kt C over the summer and winter growing seasons of 2010/11.

7 DISCUSSION

7.1 Comparative analysis of eddy covariance studies

As a comprehensive review of land-surface interactions between Australian irrigated broad-acre cropping systems and the atmosphere through EC applications is yet to be reported, it is necessary to compare the results of this study to those of similar studies conducted elsewhere. As plant water use (evapotranspiration) and gross primary production (carbon capture) are two of the major defining factors of land-surface exchange (Gilmanov et al., 2003; Suyker & Verma, 2012), only these two components of mass and energy exchange will be discussed in this section.

7.1.1 Actual evapotranspiration

7.1.1.1 Maize

Previous eddy covariance studies of irrigated maize grown in various parts of the conterminous USA reveal that daily ET_a rates and cumulative season totals of ET_a are similar to those found in this study (see Suyker & Verma, 2008; Suyker & Verma, 2010, 2012). Irrigated maize crops grown in the arid northwest regions of China were found to have had a similar range of average daily ET_a rates (0.4 – 7.0 mm/day), as found by Ji et al. (2011). The length of the growing season was 162 days and the cumulative growing season total of ET_a was 562 mm. These values are less than those found in the CIA during 2010/11 despite the length of the growing season being similar. Differences in ET_a between the two studies are most likely related to differences in net radiation due to latitudinal differences between the study areas, although this cannot be confirmed as Ji et al. (2011) did not report these specific values.

The cumulative totals of seasonal ET_a of maize crops in Europe were found to be significantly lower than the integrated total estimated in the CIA. For instance, in the temperate climate of southwest France,

Tallec et al. (2013) estimated the cumulative growing season ET_a total to be only 351 mm. The lower ET_a can be partially attributed to lower levels of incoming radiation, lower mean air temperature and lower vapour pressure deficit (*VPD*). For example, the maximum air temperature reported by Tallec et al. (2013) was 29.2°C and the maximum values of *VPD* during the summer growing season in 2006 and 2007 were 2.8 kPa and 2.2 kPa, respectively. In comparison, air temperatures reached a maximum of 40.0°C and *VPD* peaked at 4.9 kPa in the CIA during the summer growing season of 2010/11.

7.1.1.2 Rice

Recent studies of the mass and energy exchanges of irrigated rice in the Philippines found the average rate of ET_a to be 4.3 mm/day (Alberto et al., 2011). Comparable values for rates of daily ET_a have been found for irrigated rice crops in both Taiwan (Tsai et al., 2007) and Japan (Harazono et al., 1998). The average observed daily rate of ET_a in the CIA was 4.9 mm/day. Despite having similar average daily rates of ET_a during the cultivation period, the integrated season total ET_a in the CIA (783 mm) was significantly different to that found by Alberto et al. (2011) which was 395 mm. Greater evaporative demand was experienced in the CIA due to its drier, semi-arid climatic conditions compared to the tropical, humid climate in the Philippines. Cumulative ET_a rates are further compounded by shorter growing seasons of rice crops in tropical Asia. For instance, the average length of the dry growing season in the Philippines in 2008 was about 102 days (Alberto et al., 2011); the cultivation period of rice grown in the CIA in 2010/11 was 160 days.

In Bangladesh, Hossen et al. (2012) found that average daily rates of ET_a of rice grown during the summer period of 2007 ranged from 2.9 – 3.3 mm/day, depending on variety, which is lower than the daily ET_a average observed in the CIA. Again, the differences in ET_a can be attributed to differences in weather conditions, e.g., the peak rate of daily ET_a, as found by Hossen et al. (2012), was found to be just over

6 mm/day. At peak ET_a in the Bangladeshi study, net radiation exceeded 800 W/m^2, and *VPD* was greater than 2.0 kPa. In the CIA, the peak average daily rate of ET_a was estimated to be 8.1 mm/day. In this case, net radiation also exceeded 800 W/m^2 (R_n = 856 W/m^2) but VPD was greater (VPD ~ 3.0 kPa). Like the studies conducted in east and south-east Asia, cumulative totals of seasonal ET_a of rice crops grown in Bangladesh were 307 – 370 mm (Hossen et al., 2012) and were much less than those estimated in the CIA. Again, this is a result of lower daily ET_a rates experienced in the sub-tropics, shorter growing seasons (n = 114 – 140 days) and variety selection.

7.1.1.3 Wheat

The cultivation period for winter wheat grown in the CIA in 2011 was 210 days. Recent studies of winter wheat cultivated in southwest France found that the total number of days during the growing season was 245 days (Tallec et al., 2013). Despite the reduced number of days, the season total of ET_a was similar to that estimated by Tallec et al. (2013), e.g. the cumulative ET_a in southwest France ranged between 355 – 403 mm over the cultivation period; in the CIA, this was 389 mm. This can be partly attributed to the difference in meteorological conditions experienced at each site. For example, the average winter temperatures in southwest France were 7.4° C and 4.6°C for the years 2007 and 2006, respectively. In the CIA, the average air temperature over the cultivation period in 2011 was 14.6°C. In addition, the *VPD* observed during the French study peaked at ~ 2.0 kPa. In the CIA, the maximum *VPD* was ~ 4.0 kPa. Although the average daily rates of ET_a are not given by Tallec et al. (2013), increases in air temperature and *VPD* are generally associated with greater rates of ET_a. Because both mean air temperature and *VPD* observed by Tallec et al. (2013) were less than those observed in the CIA, one can assume that the daily rates of ET_a of winter wheat crops grown in southwest France are less than those estimated in this study.

In the CIA, maximum daily rates of ET_a were 5.0 mm/day. This is slightly more than those observed in Thuringia, Germany where the maximum values of ET_a of winter wheat crops ranged between ~ 3 – 4 mm/day (Anthoni et al., 2004). Again, this can be directly related to the cooler climatic conditions and the reduced amount of net radiation observed in the northern latitudes of Europe compared to Australian conditions.

Elsewhere, studies in the North China Plain during 2002 – 2004 found that the average maximum daily rate of ET_a was 5.0 mm/day (Zhao et al., 2007). This is similar to that of winter wheat grown in the CIA in 2011. However, more recent findings have shown that, in 2009, the daily rate of ET_a had increased, peaking at 6.1 mm/day (Zhang et al., 2011b). This increase in daily rates of ET_a is consistent with the findings of a 30 year study conducted in the same region, whereby ET_a has been gradually increasing since the 1980's (Zhang et al., 2011a). According to Zhang et al. (2011a), this increase can partly be attributed to increased stomatal conductance of modern cultivars, which have been genetically improved to increase the harvest index, biomass production and, ultimately, grain yield.

7.1.2 Gross Primary Production

7.1.2.1 Maize

The maximum daily rate of *GPP* of the maize crop grown in the CIA in 2010/11 was 25.7 g C/m^2/day, comparable to the maximum daily *GPP* values of irrigated maize grown in Western Europe. For example, Jans et al. (2010) derived maximum *GPP* estimates of 24.7 g C/m^2/day. In the central parts of northern China, maximum daily values of *GPP* during the growing season have been reported to be slightly lower, with Wang et al. (2012) finding maximum *GPP* rates of irrigated maize to be 21.0 g C/m^2/day and 22.3 g C/m^2/day in 2008 and 2009, respectively. As photosynthetic activity, and thus carbon assimilation, is dependent on both light intensity and temperature

(Farquhar & Sharkey, 1982), the lower *GPP* rates estimated by Wang et al. (2012) can partially be attributed to the lower annual average temperatures experienced in the northwest arid regions of China which was 7.0°C in 2008 and 7.8°C in 2009. The average annual temperature in the CIA is almost 10°C higher (17.7°C; Bureau of Meteorology, 2012a).

With lower daily rates of *GPP* occurring in northern China, one would also expect the integrated season total of *GPP* to be lower. Comparisons of integrated *GPP* showed of irrigated maize grown in northern China and the CIA proved this to be true. For instance, in 2003 and 2004, Yan et al. (2009a) found cumulative totals of *GPP* for maize to be 789 g C/m^2 and 1170 g C/m^2, respectively. In addition to the different mean air temperatures experienced, lower rates of *GPP* can also attributed to lower levels of incoming radiation generally experienced in northern China where the mean annual global solar radiation was reported to be 5225 MJ/m^2 (Yan et al., 2009a). In the CIA, the mean annual global solar radiation is 6450 MJ/m^2 (Bureau of Meteorology, 2012b) .

In the north central regions of the USA, maximum daily rates of *GPP* of irrigated maize crops are reported to be greater than irrigated maize crops grown in the CIA during this study. For instance, peaks values of *GPP* between 2002 and 2008 in Nebraska were 28 – 30 g C/m^2/day (Suyker & Verma, 2012). Similar results were found by Peng et al. (2011) and Gitelson et al.(2012), with *GPP* values that peaked at ~ 31 C/m^2/day. According to Wilhelmi et al. (2002), Nebraska experiences similar semi-arid climatic conditions to the CIA; therefore the increased rates of *GPP* in the aforementioned studies can be attributed in part to increased planting density and thus, increased overall biomass production in the USA. For example, Gitelson et al. (2012) reported that the planting density of irrigated maize in these areas was approximately 75,000 plants/ha. In the CIA, the planting density was approximately 68,000 plants/ha. Despite this, the integrated season totals were similar. In the CIA, the cumulative total of *GPP* was 1952

g C/m^2 in 2010/11 and in the USA, the average season total (2002 – 2008) was 1796 ± 92 g C/m^2 (Suyker & Verma, 2012). Differences in the distribution of LAI and photosynthetically active radiation (PAR), which can be affected by the length of the growing season, cloud cover and the effect of dry periods, effect these differences in *GPP* (Suyker & Verma, 2012).

7.1.2.2 Rice

Maximum average daily rates of *GPP* for rice monitored in this study (18.4 g C/m^2/day) were greater than others reported for irrigated rice crops elsewhere. In Japan, Saito et al. (2005) estimated the maximum daily rate of *GPP* to be 13.6 g C/m^2/day; in the Philippines, Alberto et al. (2009) reported this to be 14.5 g C/m^2/day. The difference between maximum daily rates of *GPP* found in the CIA and those estimated in the Asian studies can be directly related to the amount of increased photosynthetically active biomass, as indicated by the difference in crop yields. For instance, in this study the yield was 10.1 t/ha, whereas studies conducted by Alberto et al. (2011; 2009) recorded yields of 5.1 – 7.3 t/ha for irrigated rice crops.

The difference between daily rates of *GPP* is also reflected in the cumulative season *GPP* totals. In the CIA in 2010/11, the cumulative total *GPP* was 1624 g C/m^2. In the Philippines, total *GPP* was 778 g C/m^2 (Alberto et al., 2009), and in south western regions of Korea, the integrated season total *GPP* was 567 g C/m^2 (Kwon et al., 2010). Similar to maize production, the increased *GPP* totals for rice in this study can be attributed to increased photosynthetic activity because of climatic conditions that are more favourable to rice production in Australia. For instance, studies in Korea found monthly solar radiation values averaged between 1971 and 2000 to have a maximum value of approximately 18 MJ/m^2/day (Kwon et al., 2010). In our study, the average solar radiation value over the rice growing season was 35.2 MJ/m^2/day. Additionally, increased yield potentials due to the genetic composition of rice varieties grown in the CIA compared to rice

varieties traditionally grown in Asia will also affect the amount of carbon fixed as biomass.

7.1.2.3 Wheat

Studies of winter wheat grown in the western parts of Germany showed that daily *GPP* rates and cumulative season totals were greater than those found in the CIA, e.g. Schmidt et al. (2012) estimated the maximum daily rate of *GPP* to be ~ 18 – 19 g C/m^2/day and the average cumulative season *GPP* total over two consecutive growing seasons to be 1229 g C/m^2. In the CIA, daily rates of *GPP* peaked at 13.1 C/m^2/day and the cumulative total was 1367 g C/m^2. A little further afield, studies in Belgium have shown that cumulative season totals of *GPP* are greater than those recorded in Germany. For instance, a study of three winter wheat crops between 2004/05 and 2008/09 grown in Belgium revealed that seasonal *GPP* ranged from 1568 g C/m^2 to 1716 g C/m^2 (Dufranne et al., 2011). Similar results were found by Aubinet et al. (2009), where the season *GPP* total ranged between 1580 – 1680 g C/m^2. As highlighted by Schmidt et al. (2012), the difference in *GPP* totals for the two European countries is quite surprising, considering the relative proximity of the neighbouring countries and the similarities between climatic conditions, soil properties and grain yield. In terms of this study, the difference between estimated *GPP* of the European studies and those found in the CIA also remains unclear. Given the difference in mean air temperatures and levels of incoming global solar radiation between Western Europe (see, for example, Dufranne et al., 2011; Schmidt et al., 2012) and south-eastern Australia during the winter, one can assume that *GPP* levels would be greater in the CIA; however, this is not the case. Therefore, the difference in *GPP* must be related to biomass production through variety selection and planting density. This can be partially confirmed by comparing the grain yield of the winter wheat crops grown in both regions, e.g. in Germany, winter wheat crops yielded 7.5 t/ha – 9.1 t/ha (see Schmidt et al., 2012). In the CIA, winter wheat crops yielded 5.0 – 5.5 t/ha.

With respect to integrated season totals of *GPP*, the values found in the CIA were much greater than those found elsewhere in the world. For example, Gilmanov et al. (2003) found that the season total of *GPP* of winter wheat grown in Oklahoma, USA was 778 g C/m^2. Similar results have been found in China where the integrated total of *GPP* over the cultivation period was 790 g C/m^2 (Lei et al., 2011). This large difference can be primarily related to the difference in meteorological conditions experienced at each site, including air temperature and net radiation, which, as mentioned previously, can have a direct effect on photosynthesis rates, and thus carbon uptake of a plant. For instance, the mean air temperature during the coldest winter month (January) is 0.4°C in Ponca, City, Oklahoma, USA (Gilmanov et al., 2003); in the CIA, the mean air temperature during the coldest winter month (July) is 9.6°C (Bureau of Meteorology, 2012a).

7.2 Impact of increased rice production in a water-limited irrigation area

In 2010/11, production levels of rice had increased by 93% from the previous season and ranked third in terms of gross value of irrigated agricultural production ($174 million; ABS, 2012a). As an industry, increased rice production can have many positive socio-economic impacts on regional communities where rice is grown (e.g. more direct and in-direct employment opportunities, alternative income streams of by-products, good return on investment), but environmentally, the impacts of increased rice production may not be so attractive.

As discussed in Section 6.2, 6.3 and 7.1, rice is the largest consumer of water of all three crops commonly grown in the CIA. Of the summer crops, it is also the least productive in terms of total and net carbon capture (*GPP* is ~ 20% less than *GPP* of maize; and *NEE* is ~ 40% less than *NEE* of maize). In a water-short basin such as the CIA, the decision to increase rice production in years where there is adequate water supply could have negative effects on the system as a

whole. From the quantitative empirical assessment of carbon capture and water use in this study, the most obvious environmental impacts of increased rice production compared to maize production are: decreased carbon sequestration; and increased water loss to the atmosphere.

7.3 Experimental impact evaluation

The potential sources of experimental and instrumentation error and the consequences of failing to meet the assumptions of EC methodologies have been discussed earlier (see Section 3.3.1 – 3.3.3). However, there are a number of key elements of experimental design and implementation identified it this study that could remarkably decrease the uncertainty of CO_2 and H_2O flux estimates of future studies of irrigated broad-acre crops in the CIA. The key sources of error and the implications they may have had on flux estimation are listed in Table 7.1. Except for the cross-calibration of EC sensors, all suggestions made in this table should theoretically improve the degree of energy balance closure; and thus the level of confidence in the reported results.

Table 7.1 Key sources of error identified in this study and the implications they have on EC flux estimation and energy balance closure.

Source of error	*Implications*	*Future considerations*
• Appropriate gas analyser selection to suit weather conditions	Sensors not suited to local conditions can lead to large data gaps e.g. open path sensors should only be used in areas with low rainfall.	If long-term weather forecasts of the CIA predict above average rainfall, alternative gas analysers should be considered e.g. the enclosed CO_2/H_2O analyser is able to make contiguous measurements through rain, snow and fog (LI-7200, LI-COR Inc., USA).
• Failure to cross-calibrate EC sensors at each flux tower location	Systematic bias of observations by site and by crop.	Ensure all sensors are cross-calibrated so that results are comparable across space and time.
• Inaccurate placement of EC sensors	Flux footprint is not representative of area of interest for all conditions; therefore, an increased number of contaminated fluxes must be removed from the time series.	As identified in Section 5.2.1, there is no distinct prevailing wind during the summer or winter growing seasons; instead, the winds generally swing from NE – SW. Therefore, future placements of the flux towers should aim to be centred within the field of interest to minimise data loss.
• Two dimensional rotation into the natural wind coordinate	Impracticably large rotation angles in periods of low turbulence and $v'\overline{w}' \neq 0$ (Lee et al., 2004a) which may contribute to energy imbalance.	Application of the planar fit method to compute a single set of sonic anemometer tilt angles that are less likely to be affected by sampling errors (Wilczak et al., 2001). This method may not be suitable if the sonic anemometer requires re-positioning often.

Table 7.1 (cont) Key sources of error identified in this study and the implications they have on EC flux estimation and energy balance closure.

Source of error	*Implications*	*Future considerations*
• Failure to measure soil moisture content over time	Large errors in *G* as the isothermal latent heat component is grossly neglected (Mayocchi & Bristow, 1995).	Include additional sensors to accurately measure soil moisture content over time.
• Failure to measure temperature of standing water (rice crop only)	As above.	Include additional sensors to accurately measure temperatures of the standing water over time.
• Periods of low turbulence and advection	Failure to measure low-frequency fluxes of large eddies as a result of stable conditions; or generated by a change in land use or temperature/moisture gradient between irrigated and non-irrigated fields.	Direct measurement of advection terms based on the CO_2 mass balance equation (Aubinet et al., 2010) which may be expensive and impractical.
• *u** threshold used to estimate *Re* and thus, *GPP*	Site-specific systematic bias of *Re* and *GPP* estimations	Use an objective threshold determination (e.g. Moving point test, Gu et al., 2005) ; or light-response curves to calculate *NEE* (e.g. Lasslop et al., 2010; Zhang et al., 2012).

8 SUMMARY AND CONCLUSIONS

There are very few studies that have reported an integrated quantitative assessment of energy, water vapour and carbon dioxide fluxes of Australian irrigated broad-acre agricultural cropping systems. For the first time, this study presents a detailed analysis of the estimation and seasonal distribution of energy, water vapour and carbon dioxide fluxes of three of the major irrigated crops grown in inland Australia; maize, rice and wheat.

The first objective of this study was to determine whether irrigated agro-ecosystems in Australian semi-arid climate zones are net sources or sinks of carbon dioxide. Overall, it was found that all four cropping systems acted as a net carbon sink over each growing season, although small pulses of CO_2 into the atmosphere were observed in the early vegetative stages of growth and at times during leaf senescence. Carbon uptake (*NEE* and *GPP*) of all four cropping systems was greatest during the reproductive growth stage.

The second objective was to determine which of the common broad-acre cropping systems (i.e. maize, rice and wheat) grown in these environments were most productive. In terms of total carbon accumulation per unit of evapotranspiration, it appeared that maize was the most productive consumer of water. Rice was generally the least productive consumer of water. This can be partially attributed to the fact that the energy budget for rice was predominately driven by latent heat exchange with a seasonal actual evapotranspiration budget that was 25% greater than that of maize. This is directly related to the water management strategies of both crops, i.e. a permanent water application throughout the cultivation period versus intermittent irrigation applications as required. The presence of the permanent water applied to the rice crop, particularly during the early vegetative growth stages prior to canopy closure led to increased rates of evaporation from the directly exposed water surface.

With respect to carbon capture, represented by the total amount of carbon fixed as biomass (*GPP*), maize exhibited the greatest affinity for carbon assimilation. The cumulative seasonal total *GPP* was ~ 20 – 40% greater than for rice, wheat and mixed cropping systems. This is to be expected, given that maize has a C4 photosynthetic pathway. As a crop species, maize exhibited the greatest seasonal net carbon capture (*NEE*), followed by rice. Like *GPP*, this can be attributed to the greater affinity of the C4 photosynthetic pathway of maize and the reduced loss of carbon dioxide through greater stomatal control. As a crop, wheat exhibited the least net carbon capture. This can be attributed in part to the smaller amount of biomass production relative to the summer crops as reflected by the smaller grain yield.

Based on crop varieties grown on soil types similar to those of the experimental sites of this study, regional estimations of ET_a during the summer and winter growing seasons of 2010/11 revealed that the largest proportion of the total of water lost through ET_a was a result of rice production; ET_a of rice accounted for 59 106 ML of a total 76 578 ML). With respect to total carbon capture, the results revealed that rice represented the largest component of net carbon capture. The cumulative total *GPP* of rice (123 kt C) was three times that of wheat (41 kt C), which was the second largest component. As both rice and wheat were the predominant crops grown in summer and winter, representing 13 509 ha and 11 040 ha, respectively, one would expect that they would account for the largest distribution of net carbon capture in comparison to other crops grown in the CIA. Maize had the least representation (943 ha; 18 kt C).

Photosynthetic water productivity revealed that summer crops are generally more productive than winter wheat (WP = 14.4 g C/m^2, 8.1 g C/m^2 and 2.1 g C/m^2 for maize, rice and wheat respectively).

The third objective of this study was to investigate the flux response to various environmental signals within the CIA. From the results of the geostatistical regression analysis, it was found that air temperature, net

radiation, wind speed and rainfall had an influence on the daily ET_a rates of both summer crops. However, the extent to which each variable influenced ET_a varied between the two sites. This was indicated by the magnitude and sign of the regression coefficient. For the maize crop, T_a had the greatest influence on daily ET_a rates of the maize crop ($\widehat{\boldsymbol{\beta}}$ = 10.6) and rain had the least ($\widehat{\boldsymbol{\beta}}$ = -0.8). For the rice crop, T_a also proved to have the greatest influence on ET_a rates ($\widehat{\boldsymbol{\beta}}$ = 26.9) and P also had the least ($\widehat{\boldsymbol{\beta}}$ = 4.6). Note, however, that ET_a of the rice crop was positively correlated to P and negatively correlated with that observed over the maize crop, indicating that rates of E ET_a of the maize slightly decreased following a rainfall event. The major difference between the GR models of the two crops was that *VPD* was also selected as a covariate for the GR model of the rice crop ($\widehat{\boldsymbol{\beta}}$ = -16.0) and had a negative influence on ET_a rates. For the winter crops, the common variables that influenced daily rates of ET_a were R_n, *VPD*, *U* and *P*. T_a appeared only to affect evapotranspiration rates of the mixed cropping system where it also had the largest influence ($\widehat{\boldsymbol{\beta}}$ = 14.90). In this particular case, R_n and *VPD* were negatively correlated to evapotranspiration rates. For the wheat crop, all selected variables had a positive correlation to daily rates of ET and R_n had the greatest influence ($\widehat{\boldsymbol{\beta}}$ = 11.65). Like the summer crops, *P* had the least influence on ET_a rates of the winter cropping systems ($\widehat{\boldsymbol{\beta}}$ = 0.66 and 1.27 for the wheat and mixed system, respectively).

In terms of CO_2 flux response, ET_a was included as an additional variable to investigate *GPP* rates as a function of plant water use. In conjunction with estimates of water productivity, this served to partially satisfy the third objective to examine the relationship between water and carbon dioxide flux. The two common variables selected for the GR model at the two summer flux tower locations were wind speed and evapotranspiration. Both variables had a comparable influence on rates of daily *GPP*, having similar regression coefficients. In both cases, ET_a was positively correlated to *GPP* ($\widehat{\boldsymbol{\beta}}$ = 1.82 and 1.41 for maize and rice, respectively), which suggested that

an increase in ET_a rates generally led to an increase in carbon uptake for both maize and rice crops. A negative correlation between wind speed and *GPP* was also consistent at both sites ($\widehat{\boldsymbol{\beta}}$ = -0.72 and -0.90, respectively). The GR model of the maize crop included R_n as an additional variable which was positively correlated with carbon uptake ($\widehat{\boldsymbol{\beta}}$ = 0.59). The results of the BIC/GR analysis indicated that ET_a, having the largest regression coefficient ($\widehat{\boldsymbol{\beta}}$ = 1.8 and 1.4, respectively), had the greatest influence on the variability of daily rates of GPP of both maize and rice.

For the winter crops, R_n was the only common variable selected for the GR model at both sites, and its influence on daily GPP rates was similar ($\widehat{\boldsymbol{\beta}}$ = 1.10 and 1.08). GPP rates of the wheat crop were negatively influenced by VPD ($\widehat{\boldsymbol{\beta}}$ = -0.46). For the mixed cropping system, T_a had a negative effect on the rate of carbon uptake ($\widehat{\boldsymbol{\beta}}$ = -1.09). Unlike the summer crops, ET_a was not selected as a variable for either winter cropping systems and therefore had no apparent effect on daily rates of *GPP*, which may be attributable to lower evaporative demand and increased residual soil moisture during the winter months. In terms of model performance, the ability of the selected variables to explain variability in daily rates of ET and GPP was weak to moderate (r^2 values ranged from 0.2 – 0.7).

8.1 Future research priorities

The results of this study serve to fill the knowledge gap with respect to the mass and energy exchange of broad-acre cropping systems in Australian dryland irrigation areas. By doing this we can begin to understand the influence of irrigated agriculture on the daily fluxes of carbon dioxide, water vapour and energy and the way in which it affects the local and regional climate.

It is acknowledged that studies of atmospheric land-surface interactions for single growing seasons or years are insufficient when trying to understand the long-term processes that drive agro-

ecosystem functions. Therefore, it is necessary to conduct long-term experiments using eddy covariance technologies to compare the interannual variability of different cropping systems and the influence of varying meteorological conditions and agricultural management practices.

Furthermore, point-based eddy covariance methods can only provide information regarding the atmospheric land-surface exchange within a finite area. In order to quantify the mass and energy balance at greater spatial scales, upscaling eddy covariance data via numerical modelling in conjunction with remote sensing data from satellites designed specifically to measure atmospheric water and carbon dioxide (e.g. GOSAT) could assist in the closing of regional and global water and carbon budgets. Information derived from these studies can then be used to inform policy and shape current and future water-saving and climate change adaption initiatives.

9 REFERENCES

ABS. (2012a). *Gross Value of Irrigated Agricultural Production, 2010-11*. (4610.0.55.008). Canberra: Australian Bureau of Statistics Retrieved from http://abs.gov.au/ausstats/abs@.nsf/Latestproducts/4610.0.55.008Main%20Features12010-11?opendocument&tabname=Summary&prodno=4610.0.55.008&issue=2010-11&num=&view=.

ABS. (2012b). *Value of Agricultural Commodities Produced, Australia, 2010-11*. (7503.0). Canberra: Australian Bureau of Statistics Retrieved from http://www.abs.gov.au/AUSSTATS/abs@.nsf/mf/7503.0.

ABS. (2012c). *Water Account Australia: 2010 - 2011*. (4610.0). Canberra: Australian Bureau of Statistics Retrieved from http://www.abs.gov.au/ausstats/abs@.nsf/mf/4610.0.

Alberto, M. C. R., Wassmann, R., Hirano, T., Miyata, A., Hatano, R., Kumar, A., Padre, A., & Amante, M. (2011). Comparisons of energy balance and evapotranspiration between flooded and aerobic rice fields in the Philippines. *Agric. Water Manage., 98*(9), 1417-1430. doi: 10.1016/j.agwat.2011.04.011

Alberto, M. C. R., Wassmann, R., Hirano, T., Miyata, A., Kumar, A., Padre, A., & Amante, M. (2009). CO2/heat fluxes in rice fields: Comparative assessment of flooded and non-flooded fields in the Philippines. *Agric. For. Meteorol., 149*(10), 1737-1750. doi: 10.1016/j.agrformet.2009.06.003

Allen, R. G., Pereira, L. S., Raes, D., & Smith, M. . (1988). Crop evapotranspiration - Guidelines for computing crop water requirements *FAO Irrigation and drainage paper* (Vol. 300, pp. 1 -15): Food and Agriculture Organization (FAO).

Anderson, D. E., & Verma, S. B. (1986). Carbon dioxide, water vapor and sensible heat exchanges of a grain sorghum canopy. *Boundary-Layer Meteorol., 34*(4), 317-331. doi: 10.1007/bf00120986

Anthoni, P. M., Freibauer, A., Kolle, O., & Schulze, E.-D. (2004). Winter wheat carbon exchange in Thuringia, Germany. *Agric. For. Meteorol., 121*(1–2), 55-67. doi: 10.1016/s0168-1923(03)00162-x

Aubinet, M., Feigenwinter, C., Heinesch, B., Bernhofer, C., Canepa, E., Lindroth, A., Montagnani, L., Rebmann, C., Sedlak, P., & Van Gorsel, E. (2010). Direct advection measurements do not help to solve the night-time CO2 closure problem: Evidence from three different forests. *Agric. For. Meteorol., 150*(5), 655-664. doi: 10.1016/j.agrformet.2010.01.016

Aubinet, M., Heinesch, B., & Yernaux, M. (2003). Horizontal and Vertical CO2 Advection In A Sloping Forest. *Boundary-Layer Meteorol., 108*(3), 397-417. doi: 10.1023/a:1024168428135

Aubinet, M., Moureaux, C., Bodson, B., Dufranne, D., Heinesch, B., Suleau, M., Vancutsem, F., & Vilret, A. (2009). Carbon sequestration by a crop over a 4-year sugar beet/winter

wheat/seed potato/winter wheat rotation cycle. *Agric. For. Meteorol., 149*(3–4), 407-418. doi: 10.1016/j.agrformet.2008.09.003

Baker, J. M., & Griffis, T. J. (2005). Examining strategies to improve the carbon balance of corn/soybean agriculture using eddy covariance and mass balance techniques. [Article]. *Agric. For. Meteorol., 128*(3-4), 163-177. doi: 10.1016/j.agrformet.2004.11.005

Baldocchi, D. (2008). Turner Review No. 15. 'Breathing' of the terrestrial biosphere: lessons learned from a global network of carbon dioxide flux measurement systems. *Aust. J. Bot., 56*(1), 1 - 26. doi: 10.1071/BT07151

Baldocchi, D., Falge, E., Gu, L. H., Olson, R., Hollinger, D., Running, S., Anthoni, P., Bernhofer, C., Davis, K., Evans, R., Fuentes, J., Goldstein, A., Katul, G., Law, B., Lee, X. H., Malhi, Y., Meyers, T., Munger, W., Oechel, W., U, K. T. P., Pilegaard, K., Schmid, H. P., Valentini, R., Verma, S., Vesala, T., Wilson, K., & Wofsy, S. (2001). FLUXNET: A new tool to study the temporal and spatial variability of ecosystem-scale carbon dioxide, water vapor, and energy flux densities. [Review]. *Bull. Am. Meteorol. Soc., 82*(11), 2415-2434.

Baldocchi, D., & Meyers, T. (1998). On using eco-physiological, micrometeorological and biogeochemical theory to evaluate carbon dioxide, water vapor and trace gas fluxes over vegetation: a perspective. [Review]. *Agric. For. Meteorol., 90*(1-2), 1-25.

Baldocchi, D. D. (2003). Assessing the eddy covariance technique for evaluating carbon dioxide exchange rates of ecosystems: past, present and future. *Global Change Biol., 9*(4), 479-492. doi: 10.1046/j.1365-2486.2003.00629.x

Baldocchi, D. D., Hincks, B. B., & Meyers, T. P. (1988). Measuring Biosphere-Atmosphere Exchanges of Biologically Related Gases with Micrometeorological Methods. *Ecology, 69*(5), 1331-1340.

Barnhart, B. L., Eichinger, W. E., & Prueger, J. H. (2012). Introducing an Ogive method for discontinuous data. *Agric. For. Meteorol., 162–163*(0), 58-62. doi: 10.1016/j.agrformet.2012.04.003

Barr, A. G., Morgenstern, K., Black, T. A., McCaughey, J. H., & Nesic, Z. (2006). Surface energy balance closure by the eddy-covariance method above three boreal forest stands and implications for the measurement of the CO2 flux. [Article]. *Agric. For. Meteorol., 140*(1-4), 322-337. doi: 10.1016/j.agrformet.2006.08.007

Barr, A. G., van der Kamp, G., Black, T. A., McCaughey, J. H., & Nesic, Z. (2011). Energy balance closure at the BERMS flux towers in relation to the water balance of the White Gull Creek watershed 1999-2009. *Agric. For. Meteorol., 153*, 3-13. doi: 10.1016/j.agrformet.2011.05.017

Beringer, J., Hutley, L. B., Hacker, J. M., Neininger, B., & Paw U, K. T. (2011). Patterns and processes of carbon, water and energy cycles across northern Australian landscapes: From point to region. *Agric. For. Meteorol., 151*(11), 1409-1416. doi: 10.1016/j.agrformet.2011.05.003

Brouwer, C., & Heibloem, M. (1986). *Irrigation Water Management*. Rome: Food and Agriculture Organization of the United Nations.

Brutsaert, W. (1982). *Evaporation into the atmosphere: theory, history, and applications*: Reidel.

Burba, G. (2013). *Eddy Covariance Method for Scientific, Industrial, Agricultural, and Regulatory Applications.* Lincoln, Nebraksa, USA: LI-COR Biosciences.

Burba, G. G., & Anderson, D. J. (2010). *A Brief Practical Guide to Eddy Covariance Flux Measurements: Principles and Workflow Examples for Scientific and Industrial Applications* Lincoln, USA: LI-COR Biosciences.

Bureau of Meteorology. (2005). Australian climatic zones (based on temperature and humidity) Retrieved 18th July, 2012, from http://reg.bom.gov.au/climate/environ/travel/IDCJCM0000_tmp_rh_climaticzones.shtml

Bureau of Meteorology. (2010a). Mean sea level pressure analysis for the Australian region valid at 0000 UTC October 30, 2010.

Bureau of Meteorology. (2010b). Mean sea level pressure analysis for the Australian region valid at 0600 UTC December 7, 2010.

Bureau of Meteorology. (2011). Mean sea level pressure analysis for the Australian region valid at 0000 UTC July 4, 2011.

Bureau of Meteorology. (2012a, 18th April 2012). Climate statistics for Australian locations - Griffith Airport AWS 075041 Retrieved 18th April, 2012, from http://www.bom.gov.au/climate/averages/tables/cw_075041.shtml

Bureau of Meteorology. (2012b). Solar exposure data derived from satellite imagery processed by the Bureau of Meteorology from the Geostationary Meteorological Satellite and MTSAT series operated by Japan Meteorological Agency and from GOES-9 operated by the National Oceanographic & Atmospheric Administration (NOAA) for the Japan Meteorological Agency. Retrieved 18/07/2012, from Bureau of Meteorology http://www.bom.gov.au/jsp/ncc/cdio/weatherData/av?p_display_type=dataSGraph&p_stn_num=074249&p_nccObsCode=193&p_month=13&p_startYear=2012

Cabral, O. M. R., Gash, J. H. C., Rocha, H. R., Marsden, C., Ligo, M. A. V., Freitas, H. C., Tatsch, J. D., & Gomes, E. (2010). Fluxes of CO2 above a plantation of Eucalyptus in southeast Brazil. *Agric. For. Meteorol., 151*(1), 49 - 59.

Cai, X., Molden, D., Mainuddin, M., Sharma, B., Ahmad, M.-u.-D., & Karimi, P. (2011). Producing more food with less water in a changing world: assessment of water productivity in 10 major

river basins. *Water International, 36*(1), 42-62. doi: 10.1080/02508060.2011.542403

Campbell Scientific Inc. (2007). Model HFP01SC Self-calibrating soil heat flux plate - Instruction Manual (8/07 ed.). Logan, Utah, U.S.A.: Campbell Scientific, Inc.

Chen, J. M., Rich, P. M., Gower, S. T., Norman, J. M., & Plummer, S. (1997). Leaf area index of boreal forests: Theory, techniques, and measurements. [Article]. *Journal of Geophysical Research-Atmospheres, 102*(D24), 29429-29443. doi: 10.1029/97jd01107

CICL. (2008). Annual Compliance Report 2008 (pp. 84): Coleambally Irrigation Cooperative Ltd.

CICL. (2009). Annual Compliance Report 2009 (pp. 84): Coleambally Irrigation Cooperative Ltd.

CICL. (2010). Annual Compliance Report 2010 (pp. 86): Coleambally Irrigation Cooperative Ltd.

CICL. (2011). Annual Compliance Report 2011 (pp. 84): Coleambally Irrigation Cooperative Ltd.

CICL. (2012). Annual Compliance Report 2012 (pp. 84): Coleambally Irrigation Cooperative Ltd.

Clay, J. (2011). Freeze the footprint of food. [10.1038/475287a]. *Nature, 475*(7356), 287-289.

Clement, R. (1999). EdiRe (Version 1.5.0.28): University of Edinburgh, U.K. Retrieved from http://www.geos.ed.ac.uk/abs/research/micromet/EdiRe/

Davin, E. L., & de Noblet-Ducoudre, N. (2010a, November). Biogeophysical processes behind the climatic influence of deforestation. *iLeaps Newsletter*, 44.

Davin, E. L., & de Noblet-Ducoudre, N. (2010b). Climatic Impact of Global-Scale Deforestation: Radiative versus Nonradiative Processes. *J. Clim., 23*(1), 97-112. doi: doi:10.1175/2009JCLI3102.1

Davis, K. J., Bakwin, P. S., Yi, C. X., Berger, B. W., Zhao, C. L., Teclaw, R. M., & Isebrands, J. G. (2003). The annual cycles of CO2 and H2O exchange over a northern mixed forest as observed from a very tall tower. *Global Change Biol., 9*(9), 1278-1293. doi: 10.1046/j.1365-2486.2003.00672.x

DCCEE. (2011). *Australian National Greenhouse Accounts: National Inventory Report 2009*. Department of Climate Change and Energy Efficiency Retrieved from http://www.climatechange.gov.au/en/climate-change/emissions.aspx.

De Datta, S. K. (1987). *Principles and practices of rice production*. Malabar, Fla.: Krieger.

Delpierre, N., Soudani, K., François, C., Le Maire, G., Bernhofer, C., Kutsch, W., Misson, L., Rambal, S., Vesala, T., & Dufrêne, E. (2012). Quantifying the influence of climate and biological drivers on the interannual variability of carbon exchanges in European forests through process-based modelling.

Agricultural and Forest Meteorology, 154-155(0), 99-112. doi: 10.1016/j.agrformet.2011.10.010

Denmead, O. T., Harper, L. A., Freney, J. R., Griffith, D. W. T., Leuning, R., & Sharpe, R. R. (1998). A mass balance method for non-intrusive measurements of surface-air trace gas exchange. *Atmos. Environ., 32*(21), 3679-3688. doi: 10.1016/s1352-2310(98)00091-0

Department of Climate Change. (2008). Carbon Pollution Reduction Scheme. Australia's Low Pollution Future. (D. o. C. Change, Trans.) *White Paper* (Vol. 1). Canberra, ACT.

Desjardins, R. L., Buckley, D. J., & Amour, G. S. (1984). Eddy flux measurements of CO2 above corn using a microcomputer system. *Agric. For. Meteorol., 32*(3-4), 257-265. doi: 10.1016/0168-1923(84)90053-4

Domingo, F., Serrano-Ortiz, P., Were, A., Villagarcía, L., García, M., Ramírez, D. A., Kowalski, A. S., Moro, M. J., Rey, A., & Oyonarte, C. (2011). Carbon and water exchange in semiarid ecosystems in SE Spain. *J. Arid Environ., 75*(12), 1271-1281. doi: 10.1016/j.jaridenv.2011.06.018

Donald, C. M., & Hamblin, J. (1976). The Biological Yield and Harvest Index of Cereals as Agronomic and Plant Breeding Criteria. In N. C. Brady (Ed.), *Advances in Agronomy* (Vol. Volume 28, pp. 361-405): Academic Press.

Dufranne, D., Moureaux, C., Vancutsem, F., Bodson, B., & Aubinet, M. (2011). Comparison of carbon fluxes, growth and productivity of a winter wheat crop in three contrasting growing seasons. *Agric., Ecosyst. Environ., 141*(1 - 2), 133 - 142. doi: 10.1016/j.agee.2011.02.023

Easterling, W. E., Aggarwal, P. K., Batima, P., Brander, K. M., Erda, L., Howden, S. M., Kirilenko, A., Morton, J., Soussana, J.-F., Schmidhuber, J., & Tubiello, F. N. (2007). Food, fibre and forest products. In M. L. Parry, O. F. Canziani, P. J.P, P. J. van der Linden & C. E. Hanson (Eds.), *Climate Change 2007: Impacts, Adaptation and Vulnerability. Contribution of Working Group II to the Fourth Assessment Report of the Intergovernmental Panel on Climate Change* (pp. 273 - 313). Cambridge, UK: Cambridge University Press

Edraki, M., Smith, D., Humphreys, E., Khan, S., O'Connell, N., & Xevi, E. (2003). Validation of the SWAGMAN Farm and SWAGMAN Destiny models *Technical Report*: CSIRO Land and Water, Griffith.

Evans, G. N. (1971). Evaporation from rice at griffith, New South Wales. *Agricultural Meteorology, 8*(0), 117-127. doi: http://dx.doi.org/10.1016/0002-1571(71)90101-4

Falge, E., Baldocchi, D., Olson, R., Anthoni, P., Aubinet, M., Bernhofer, C., Burba, G., Ceulemans, R., Clement, R., Dolman, H., Granier, A., Gross, P., Grünwald, T., Hollinger, D., Jensen, N.-O., Katul, G., Keronen, P., Kowalski, A., Lai, C. T., Law, B. E., Meyers, T., Moncrieff, J., Moors, E., Munger, J. W., Pilegaard, K., Rannik, Ü., Rebmann, C.,

Suyker, A., Tenhunen, J., Tu, K., Verma, S., Vesala, T., Wilson, K., & Wofsy, S. (2001a). Gap filling strategies for defensible annual sums of net ecosystem exchange. *Agric. For. Meteorol., 107*(1), 43-69.

Falge, E., Baldocchi, D., Olson, R., Anthoni, P., Aubinet, M., Bernhofer, C., Burba, G., Ceulemans, R., Clement, R., Dolman, H., Granier, A., Gross, P., Grünwald, T., Hollinger, D., Jensen, N.-O., Katul, G., Keronen, P., Kowalski, A., Ta Lai, C., Law, B. E., Meyers, T., Moncrieff, J., Moors, E., William Munger, J., Pilegaard, K., Rannik, Ü., Rebmann, C., Suyker, A., Tenhunen, J., Tu, K., Verma, S., Vesala, T., Wilson, K., & Wofsy, S. (2001b). Gap filling strategies for long term energy flux data sets. *Agric. For. Meteorol., 107*(1), 71-77. doi: 10.1016/S0168-1923(00)00235-5

Farquhar, G. D., & Sharkey, T. D. (1982). Stomatal conductance and photosynthesis. *Annual Review of Plant Physiology and Plant Molecular Biology, 33*, 317-345. doi: 10.1146/annurev.pp.33.060182.001533

Finnigan, J. J., Clement, R., Malhi, Y., Leuning, R., & Cleugh, H. A. (2003). A Re-Evaluation of Long-Term Flux Measurement Techniques Part I: Averaging and Coordinate Rotation. [Article]. *Boundary-Layer Meteorol., 107*(1), 1-48.

Foken, T., Göockede, M., Mauder, M., Mahrt, L., Amiro, B., & Munger, W. (2004). Post-Field Data Quality Control. In X. Lee, W. Massman & B. Law (Eds.), *Handbook of Micrometeorology* (Vol. 29, pp. 181-208): Springer Netherlands.

Foken, T., & Leclerc, M. Y. (2004). Methods and limitations in validation of footprint models. *Agric. For. Meteorol., 127*(3-4), 223-234.

Foken, T., Mauder, M., Liebethal, C., Wimmer, F., Beyrich, F., Leps, J.-P., Raasch, S., DeBruin, H., Meijninger, W., & Bange, J. (2010). Energy balance closure for the LITFASS-2003 experiment. *Theor. Appl. Climatol.*

Foken, T., & Wichura, B. (1996). Tools for quality assessment of surface-based flux measurements. *Agric. For. Meteorol., 78*(1-2), 83-105. doi: 10.1016/0168-1923(95)02248-1

Foken, T., Wimmer, F., Mauder, M., Thomas, C., & Liebethal, C. (2006). Some aspects of the energy balance closure problem. *Atmospheric Chemistry and Physics, 6*(12), 8. doi: 10.5194/acp-6-4395-2006

Foley, J. A., DeFries, R., Asner, G. P., Barford, C., Bonan, G., Carpenter, S. R., Chapin, F. S., Coe, M. T., Daily, G. C., Gibbs, H. K., Helkowski, J. H., Holloway, T., Howard, E. A., Kucharik, C. J., Monfreda, C., Patz, J. A., Prentice, I. C., Ramankutty, N., & Snyder, P. K. (2005). Global Consequences of Land Use. *Science, 309*(5734), 570-574. doi: 10.1126/science.1111772

Forster, M. R. (2000). Key concepts in model selection: Performance and generalizability. *J. Math. Psychol., 44*, 205-231.

Franssen, H. J. H., Stöckli, R., Lehner, I., Rotenberg, E., & Seneviratne, S. I. (2010). Energy balance closure of eddy-covariance data: A multisite analysis for European FLUXNET stations. *Agric. For. Meteorol., 150*(12), 1553-1567. doi: 10.1016/j.agrformet.2010.08.005

Gallant, J. C., Dowling, T. I., Read, A. M., Wilson, N., Tickle, P., & Inskeep, C. (2011). 1 second STRM Level 2 Derived Digital Elevation Model. In G. Australia (Ed.), (1.0 ed.). Canberra.

Garratt, J. R. (1984). The measurement of evaporation by meteorological methods. *Agric. Water Manage., 8*(1-3), 99-117. doi: 10.1016/0378-3774(84)90048-9

Gash, J. H. C. (1986). A note on estimating the effect of a limited fetch on micrometeorological evaporation measurements. *Boundary-Layer Meteorol., 35*(4), 409-413. doi: 10.1007/bf00118567

Giambelluca, T. W., Scholz, F. G., Bucci, S. J., Meinzer, F. C., Goldstein, G., Hoffmann, W. A., Franco, A. C., & Buchert, M. P. (2009). Evapotranspiration and energy balance of Brazilian savannas with contrasting tree density. *Agric. For. Meteorol., 149*(8), 1365-1376. doi: 10.1016/j.agrformet.2009.03.006

Gilmanov, T. G., Aires, L., Barcza, Z., Baron, V. S., Belelli, L., Beringer, J., Billesbach, D., Bonal, D., Bradford, J., Ceschia, E., Cook, D., Corradi, C., Frank, A., Gianelle, D., Gimeno, C., Gruenwald, T., Guo, H., Hanan, N., Haszpra, L., Heilman, J., Jacobs, A., Jones, M. B., Johnson, D. A., Kiely, G., Li, S., Magliulo, V., Moors, E., Nagy, Z., Nasyrov, M., Owensby, C., Pinter, K., Pio, C., Reichstein, M., Sanz, M. J., Scott, R., Soussana, J. F., Stoy, P. C., Svejcar, T., Tuba, Z., & Zhou, G. (2010). Productivity, Respiration, and Light-Response Parameters of World Grassland and Agroecosystems Derived From Flux-Tower Measurements. *Rangeland Ecol. Manage., 63*(1), 16-39. doi: 10.2111/rem-d-09-00072.1

Gilmanov, T. G., Verma, S. B., Sims, P. L., Meyers, T. P., Bradford, J. A., Burba, G. G., & Suyker, A. E. (2003). Gross primary production and light response parameters of four Southern Plains ecosystems estimated using long-term CO2-flux tower measurements. *GBioC, 17*(2). doi: 107110.1029/2002gb002023

Gitelson, A. A., Peng, Y., Masek, J. G., Rundquist, D. C., Verma, S., Suyker, A., Baker, J. M., Hatfield, J. L., & Meyers, T. (2012). Remote estimation of crop gross primary production with Landsat data. *Remote Sensing of Environment, 121*(0), 404-414. doi: 10.1016/j.rse.2012.02.017

Göckede, M. (2004). *Adoption of footprint methods for the quality control of eddy covariance measurements.* Dr. Rer. Nat., University of Bayreuth, Bayreuth.

Göckede, M., Rebmann, C., & Foken, T. (2004). A combination of quality assessment tools for eddy covariance measurements with footprint modelling for the characterisation of complex

sites. *Agric. For. Meteorol., 127*(3-4), 175-188. doi: 10.1016/j.agrformet.2004.07.012

Goulden, M. L., McMillan, A. M. S., Winston, G. C., Rocha, A. V., Manies, K. L., Harden, J. W., & Bond-Lamberty, B. P. (2011). Patterns of NPP, GPP, respiration, and NEP during boreal forest succession. *Global Change Biol., 17*(2), 855-871. doi: 10.1111/j.1365-2486.2010.02274.x

Goulden, M. L., Munger, J. W., Fan, S. M., Daube, B. C., & Wofsy, S. C. (1996). Measurements of carbon sequestration by long-term eddy covariance: Methods and a critical evaluation of accuracy. [Article]. *Global Change Biol., 2*(3), 169-182.

Greco, S., & Baldocchi, D. D. (1996). Seasonal variations of CO2 and water vapour exchange rates over a temperate deciduous forest. [Article]. *Global Change Biol., 2*(3), 183-197.

Gu, L. H., Falge, E. M., Boden, T., Baldocchi, D. D., Black, T. A., Saleska, S. R., Suni, T., Verma, S. B., Vesala, T., Wofsy, S. C., & Xu, L. K. (2005). Objective threshold determination for nighttime eddy flux filtering. [Article]. *Agric. For. Meteorol., 128*(3-4), 179-197. doi: 10.1016/j.agrformet.2004.11.006

Harazono, Y., Kim, J., Miyata, A., Choi, T., Yun, J. I., & Kim, J. W. (1998). Measurement of energy budget components during the International Rice Experiment (IREX) in Japan. *Hydrological Processes, 12*(13-14), 2081-2092. doi: 10.1002/(sici)1099-1085(19981030)12:13/14<2081::aid-hyp721>3.0.co;2-m

Hatala, J. A., Detto, M., & Baldocchi, D. D. (2012a). Gross ecosystem photosynthesis causes a diurnal pattern in methane emission from rice. *Geophys. Res. Lett., 39*(6), L06409. doi: 10.1029/2012gl051303

Hatala, J. A., Detto, M., Sonnentag, O., Deverel, S. J., Verfaillie, J., & Baldocchi, D. D. (2012b). Greenhouse gas (CO2, CH4, H2O) fluxes from drained and flooded agricultural peatlands in the Sacramento-San Joaquin Delta. *Agric., Ecosyst. Environ., 150*(0), 1-18. doi: 10.1016/j.agee.2012.01.009

Hollinger, D. Y., & Richardson, A. D. (2005). Uncertainty in eddy covariance measurements and its application to physiological models. *Tree Physiol., 25*(7), 873-873.

Hornbuckle, J., Christen, E., Thacker, J., Muirhead, W., & Stein, T. M. (2008). Soils of the Murrumbidgee, Coleambally and Murray Irrigation Areas of Australia II: *Physical properties CSIRO Land and Water Science Report*: CSIRO and IF Technologies Pty Ltd.

Horst, T. W., & Weil, J. C. (1992). Footprint Estimation for Scalar Flux Measurements in the Atmospheric Surface Layer. *Boundary-Layer Meteorol., 59*, 18.

Hossen, M. S., Mano, M., Miyata, A., Baten, M. A., & Hiyama, T. (2012). Surface energy partitioning and evapotranspiration over a double-cropping paddy field in Bangladesh. *Hydrol. Processes, 26*(9), 1311-1320. doi: 10.1002/hyp.8232

Howden, S. M., Soussana, J.-F. o., Tubiello, F. N., Chhetri, N., Dunlop, M., & Meinke, H. (2007). Adapting agriculture to

climate change. *Proceedings of the National Academy of Sciences, 104*(50), 19691-19696. doi: 10.1073/pnas.0701890104

Hui, D. F., Wan, S. Q., Su, B., Katul, G., Monson, R., & Luo, Y. Q. (2004). Gap-filling missing data in eddy covariance measurements using multiple imputation (MI) for annual estimations. [Article]. *Agric. For. Meteorol., 121*(1-2), 93-111. doi: 10.1016/s0168-1923(03)00158-8

Humphreys, E., Meyer, W., Prathapar, S., & Smith, D. (1994). Estimation of evapotranspiration from rice in southern New South Wales: a review. *Australian Journal of Experimental Agriculture, 34*(7), 1069-1078. doi: http://dx.doi.org/10.1071/EA9941069

Huntzinger, D. N., Gourdji, S. M., Mueller, K. L., & Michalak, A. M. (2011). A systematic approach for comparing modeled biospheric carbon fluxes across regional scales. *Biogeosciences, 8*, 1579-1593. doi: 10.5194/bg-8-1579-2011

Hutley, L. B., Leuning, R., Beringer, J., & Cleugh, H. A. (2005). The utility of the eddy covariance techniques as a tool in carbon accounting: tropical savanna as a case study. [Article]. *Aust. J. Bot., 53*(7), 663-675. doi: 10.1071/bt04147

Inagaki, A., Letzel, M. O., Raasch, S., & Kanda, M. (2006). Impact of Surface Heterogeneity on Energy Imbalance: A Study Using LES. *Journal of the Meteorological Society of Japan. Ser. II, 84*(1), 187-198.

IPCC. (2007). Climate Change 2007: Synthesis Report. Contribution of Working Groups I, II and III to the Fourth Assessment Report of the Intergovernmental Panel on Climate Change. In R. K. Pachauri & A. Reisinger (Eds.). Geneva, Switzerland.

Isaac, P. (2004). *Estimating Surface-Atmosphere Exchange at Regional Scales.* Doctor of Philosophy, The Flinders University of South Australia, Adelaide, S.A.

Isaac, P., & Cleverly, J. (2011). OzFlux QC (Version 1.5). Canberra, Australia: CSIRO. Retrieved from http://www.ozflux.org.au/

Isaac, P. R., Leuning, R., Hacker, J. M., Cleugh, H. A., Coppin, P. A., Denmead, O. T., & Raupach, M. R. (2004). Estimation of regional evapotranspiration by combining aircraft and ground-based measurements. [Article]. *Boundary-Layer Meteorol., 110*(1), 69-98.

Jackson, T. M. (2009). *An appraisal of the on-farm water and energy nexus in irrigated agriculture.* Doctor of Philosophy, Charles Sturt University, Wagga Wagga.

Jackson, T. M., Khan, S., & Hafeez, M. (2010). A comparative analysis of water application and energy consumption at the irrigated field level. *Agricultural Water Management, 97*(10), 1477-1485. doi: 10.1016/j.agwat.2010.04.013

Jacobs, J. M., Mergelsberg, S. L., Lopera, A. F., & Myers, D. A. (2002). Evapotranspiration from a wet prairie wetland under drought conditions: Paynes Prairie Preserve, Florida, USA.

Wetlands, 22(2), 374-385. doi: 10.1672/0277-5212(2002)022[0374:efawpw]2.0.co;2

Jans, W. W. P., Jacobs, C. M. J., Kruijt, B., Elbers, J. A., Barendse, S., & Moors, E. J. (2010). Carbon exchange of a maize (Zea mays L.) crop: Influence of phenology. *Agric., Ecosyst. Environ., 139*(3), 316-324. doi: 10.1016/j.agee.2010.06.008

Jensen, J. R. (2005). *Introductory Digital Image Processing: a remote sensing perspective* (3rd ed.). Upper Saddle River, N.J., U.S.A.: Pearson Prentice Hall.

Ji, X.-B., Zhao, W.-Z., Kang, E.-S., Zhang, Z.-H., Jin, B.-W., & Zhao, L.-W. (2011). Carbon Dioxide Exchange in an Irrigated Agricultural Field within an Oasis, Northwest China. [Article]. *Journal of Applied Meteorology & Climatology, 50*(11), 2298-2308. doi: 10.1175/2011jamc2614.1

Kaimal, J. C., & Finnigan, J. J. (1994). *Atmospheric boundary layer flows: their structure and measurement*: Oxford University Press.

Kalfas, J. L., Xiao, X., Vanegas, D. X., Verma, S. B., & Suyker, A. E. (2011). Modelling gross primary production of irrigated and rain-fed maize using MODIS imagery and CO2 flux tower data. *Agric. For. Meteorol., 151*(12), 1514-1528. doi: 10.1016/j.agrformet.2011.06.007

Kanniah, K. D., Beringer, J., & Hutley, L. B. (2011). Environmental controls on the spatial variability of savanna productivity in the Northern Territory, Australia. *Agric. For. Meteorol., 151*(11), 1429-1439. doi: 10.1016/j.agrformet.2011.06.009

Keller, A., & Seckler, D. (2005). Limits to the Productivity of Water in Crop Production (D. o. W. Resources, Trans.) *California Water Plan Update*: State of California.

Kelly, K. (2013, 09/09/2013). [Surface water irrigation and associated land preparation methods in the CIA].

Kennedy, R. A. (1976). Photosynthesis and photorepiration in C3 and C4 plant-tissue cultures - Significance of Kranz Anatomy to operation of C4 pathway. *Plant Physiology, 57*(5), 53-53.

Khan, S., & Hanjra, M. A. (2009). Footprints of water and energy inputs in food production - Global perspectives. *Food Policy, 34*(2), 130-140.

Kidston, J., Bruemmer, C., Black, T. A., Morgenstern, K., Nesic, Z., McCaughey, J. H., & Barr, A. G. (2010). Energy Balance Closure Using Eddy Covariance Above Two Different Land Surfaces and Implications for CO2 Flux Measurements. *Boundary-Layer Meteorol., 136*(2), 193-218. doi: 10.1007/s10546-010-9507-y

Kilinc, M., Beringer, J., Hutley, L. B., Haverd, V., & Tapper, N. (2012). An analysis of the surface energy budget above the world's tallest angiosperm forest. *Agric. For. Meteorol., 166–167*(0), 23-31. doi: 10.1016/j.agrformet.2012.05.014

Kljun, N., Kormann, R., Rotach, M. W., & Meixer, F. X. (2003). Comparison of the Langrangian footprint model LPDM-B with

an analytical footprint model. *Boundary-Layer Meteorol., 106*(2), 349-355.

Kominami, Y., Jomura, M., Dannoura, M., Goto, Y., Tamai, K., Miyama, T., Kanazawa, Y., Kaneko, S., Okumura, M., Misawa, N., Hamada, S., Sasaki, T., Kimura, H., & Ohtani, Y. (2008). Biometric and eddy-covariance-based estimates of carbon balance for a warm-temperate mixed forest in Japan. [Article]. *Agric. For. Meteorol., 148*(5), 723-737. doi: 10.1016/j.agrformet.2008.01.017

Kormann, R., & Meixner, F. X. (2001). An analytical footprint model for non-neutral stratification. *Boundary-Layer Meteorol., 99*(2), 207-224.

Krishnan, P., Meyers, T. P., Scott, R. L., Kennedy, L., & Heuer, M. (2012). Energy exchange and evapotranspiration over two temperate semi-arid grasslands in North America. *Agric. For. Meteorol., 153*(0), 31-44. doi: 10.1016/j.agrformet.2011.09.017

Kueppers, L., & Snyder, M. (2012). Influence of irrigated agriculture on diurnal surface energy and water fluxes, surface climate, and atmospheric circulation in California. *Clim. Dyn., 38*(5), 1017-1029. doi: 10.1007/s00382-011-1123-0

Kurbanmuradov, O., & Sabelfeld, K. (2000). Lagrangian stochastic models for turbulent dispersion in the atmospheric boundary layer. *Boundary-Layer Meteorol., 97*(2), 191-218.

Kwon, H., Kim, J., Hong, J., & Lim, J. H. (2010). Influence of the Asian monsoon on net ecosystem carbon exchange in two major ecosystems in Korea. [Article]. *Biogeosciences, 7*(5), 1493-1504. doi: 10.5194/bg-7-1493-2010

Lara, M. V., & Andreo, C. S. (2011). C4 Plants Adaptation to High Levels of CO2 and to Drought Environments. In A. Shanker & B. Venkateswarlu (Eds.), *Abiotic Stress in Plants - Mechanisms and Adaptations*: InTech.

Lasslop, G., Reichstein, M., Papale, D., Richardson, A. D., Arneth, A., Barr, A., Stoy, P., & Wohlfahrt, G. (2010). Separation of net ecosystem exchange into assimilation and respiration using a light response curve approach: critical issues and global evaluation. [Article]. *Global Change Biol., 16*(1), 187-208. doi: 10.1111/j.1365-2486.2009.02041.x

Leahy, P., & Kiely, G. (2012). The effect of introducing a winter forage rotation on CO2 fluxes at a temperate grassland. *Agric., Ecosyst. Environ., 156*(0), 49-56. doi: 10.1016/j.agee.2012.05.001

Leclerc, M. Y., Shen, S., & Lamb, B. (1997). Observations and large-eddy simulation modelling of footprints in the lower convective boundary layer. *Journal of Geophysical Research D: Atmospheres, 102*(8), 9323-9334.

Leclerc, M. Y., & Thurtell, G. W. (1990). Footprint prediction of scalar fluxes using a Markovian analysis. *Boundary-Layer Meteorology, 52*, 12.

Lecoeur, J., & Sinclair, T. R. (2001). Harvest index increase during seed growth of field pea. *European Journal of Agronomy, 14*(3), 173-180. doi: 10.1016/s1161-0301(00)00091-5

Lee, X. (1998). On micrometeorological observations of surface-air exchange over tall vegetation. *Agric. For. Meteorol., 91*(1-2), 39-49. doi: 10.1016/s0168-1923(98)00071-9

Lee, X., Finnigan, J. J., & Paw U, K. T. (2004a). Coordinate systems and flux bias error. In X. Lee, W. J. Massman & B. Law (Eds.), *Handbook of Micrometeorology: A Guide for Surface Flux Measurement and Analysis* (pp. 33-66): Springer Netherlands.

Lee, X., & Hu, X. (2002). Forest-Air Fluxes Of Carbon, Water And Energy Over Non-Flat Terrain. *Boundary-Layer Meteorol., 103*(2), 277-301. doi: 10.1023/a:1014508928693

Lee, X., Law, B., & Massman, W. (2004b). *Handbook of Micrometeorology: A Guide for Surface Flux Measurement and Analysis*: Springer Netherlands.

Lei, H., Yang, D., Shen, Y., Liu, Y., & Zhang, Y. (2011). Simulation of evapotranspiration and carbon dioxide flux in the wheat-maize rotation croplands of the North China Plain using the Simple Biosphere Model. *Hydrol. Processes, 25*(20), 3107-3120. doi: 10.1002/hyp.8026

Leuning, R. (2004). Measurements of trace gas fluxes in the atmosphere using eddy covariance: WPL corrections revisited. In X. Lee, W. J. Massman & B. Law (Eds.), *Handbook of Micrometeorology: A guide for surface flux measurement and analysis* (pp. 119-132): Springer Netherlands.

Leuning, R., Cleugh, H. A., Zegelin, S. J., & Hughes, D. (2005). Carbon and water fluxes over a temperate Eucalyptus forest and a tropical wet/dry savanna in Australia: measurements and comparison with MODIS remote sensing estimates. *Agric. For. Meteorol., 129*(3-4), 151-173.

Leuning, R., Raupach, M. R., Coppin, P. A., Cleugh, H. A., Isaac, P., Denmead, O. T., Dunin, F. X., Zegelin, S., & Hacker, J. (2004). Spatial and temporal variations in fluxes of energy, water vapour and carbon dioxide during OASIS 1994 and 1995. *Boundary-Layer Meteorol., 110*, 3-38.

LI-COR, I. (1992). LAI-2000 Plant Canopy Analyser - Operating Manual. Lincoln, Nebraska, USA.

LI-COR, I. (2001). Open Path CO2/H2O Analyzer - Instruction Manual. Lincoln, Nebraska, USA.

Li, S., Kang, S. H., Li, F. S., & Zhang, L. (2008). Evapotranspiration and crop coefficient of spring maize with plastic mulch using eddy covariance in northwest China. [Article]. *Agric. Water Manage., 95*(11), 1214-1222. doi: 10.1016/j.agwat.2008.04.014

Liu, S. M., Xu, Z. W., Wang, W. Z., Jia, Z. Z., Zhu, M. J., Bai, J., & Wang, J. M. (2011). A comparison of eddy-covariance and large aperture scintillometer measurements with respect to the energy balance closure problem. *Hydrological and Earth*

System Sciences, 15(4), 1291 - 1306. doi: 10.5194/hess-15-1291-2011

Lloyd, J., & Taylor, J. A. (1994). On the Temperature Dependence of Soil Respiration. *Funct. Ecol., 8*(3), 315-323.

Loescher, H. W., Law, B. E., Mahrt, L., Hollinger, D. Y., Campbell, J., & Wofsy, S. C. (2006). Uncertainties in, and interpretation of, carbon flux estimates using the eddy covariance technique. *Journal of Geophysical Research-Atmospheres, 111*(D21). doi: D21s9010.1029/2005jd006932

Loescher, H. W., Ocheltree, T., Tanner, B., Swiatek, E., Dano, B., Wong, J., Zimmerman, G., Campbell, J., Stock, C., Jacobsen, L., Shiga, Y., Kollas, J., Liburdy, J., & Law, B. E. (2005). Comparison of temperature and wind statistics in contrasting environments among different sonic anemometer–thermometers. *Agric. For. Meteorol., 133*(1–4), 119-139. doi: http://dx.doi.org/10.1016/j.agrformet.2005.08.009

Long, K. D. (2008). *Methane fluxes from a northern peatland: Mechanisms controlling diurnal and seasonal variation and the magnitude of aerobic methanogensis.* Master of Science, University of Lethbridge, Lethbridge, Alberta, Canada.

Malhi, Y., McNaughton, K., & Von Randow, C. (2004). Low frequency atmospheric transport and surface flux measurement. In X. Lee, W. J. Massman & B. Law (Eds.), *Handbook of Micrometeorology: A Guide for Surface Flux Measurement and Analysis* (pp. 77): Springer Netherlands.

Massman, W. J. (2000). A simple method for estimating frequency response corrections for eddy covariance systems. [Article]. *Agric. For. Meteorol., 104*(3), 185-198.

Massman, W. J. (2001). Reply to comment by Rannik on “A simple method for estimating frequency response corrections for eddy covariance systems”. *Agric. For. Meteorol., 107*(3), 247-251. doi: http://dx.doi.org/10.1016/S0168-1923(00)00237-9

Massman, W. J., & Clement, R. (2004). Uncertainty in eddy covariance flux estimates resulting from spectral attenuation. In X. Lee, W. Massman & B. Law (Eds.), *Handbook of Micrometeorology* (pp. 67-99): Springer Netherlands.

Matsoukas, C., Benas, N., Hatzianastassiou, N., Pavlakis, K. G., Kanakidou, M., & Vardavas, I. (2011). Potential evaporation trends over land between 1983-2008: driven by radiative fluxes or vapour-pressure deficit? *Atmospheric Chemistry and Physics, 11*(15), 7601-7616. doi: 10.5194/acp-11-7601-2011

Mauder, M., Oncley, S. P., Vogt, R., Weidinger, T., Ribeiro, L., Bernhofer, C., Foken, T., Kohsiek, W., De Bruin, H. A. R., & Liu, H. (2007). The energy balance experiment EBEX-2000. Part II: Intercomparison of eddy-covariance sensors and post-field data processing methods. [Article]. *Boundary-Layer Meteorol., 123*(1), 29-54. doi: 10.1007/s10546-006-9139-4

Mayocchi, C. L., & Bristow, K. L. (1995). Soil surface heat flux: some general questions and comments on measurements. *Agric. For. Meteorol., 75*(1-3), 43-50.

McGinn, S. M., & King, K. M. (1990). Simultaneous measurements of heat, water vapour and CO2 fluxes above alfalfa and maize. *Agric. For. Meteorol., 49*(4), 331-349. doi: 10.1016/0168-1923(90)90005-q

McVicar, T., & Van Niel, T. (2012). Coleambally: An Agricultural Time Series Site Retrieved 26th July, 2012, from http://www.eoc.csiro.au/hswww/oz_pi/colly_site/key.htm

Meyer, W. S., Smith, D. J., & Shell, G. (1999). Estimating reference evaporation and crop evapotranspiration from weather data and crop coefficients: An addendum to AWRAC Research Project 84/162 - Quantifying components of the water balance under irrigated crops CSIRO Land and Water.

Miranda, A. C., Miranda, H. S., Lloyd, J., Grace, J., Francey, R. J., McIntyre, J. A., Meir, P., Riggan, P., Lockwood, R., & Brass, J. (1997). Fluxes of carbon, water and energy over Brazilian cerrado: An analysis using eddy covariance and stable isotopes. [Article]. *Plant Cell and Environment, 20*(3), 315-328.

Miyata, A., Leuning, R., Denmead, O. T., Kim, J., & Harazono, Y. (2000). Carbon dioxide and methane fluxes from an intermittently flooded paddy field. [Article]. *Agric. For. Meteorol., 102*(4), 287-303.

Moffat, A. M., Papale, D., Reichstein, M., Hollinger, D. Y., Richardson, A. D., Barr, A. G., Beckstein, C., Braswell, B. H., Churkina, G., Desai, A. R., Falge, E., Gove, J. H., Heimann, M., Hui, D. F., Jarvis, A. J., Kattge, J., Noormets, A., & Stauch, V. J. (2007). Comprehensive comparison of gap-filling techniques for eddy covariance net carbon fluxes. [Article]. *Agric. For. Meteorol., 147*(3-4), 209-232. doi: 10.1016/j.agrformet.2007.08.011

Molden, D., Oweis, T., Steduto, P., Bindraban, P., Hanjra, M. A., & Kijne, J. (2010). Improving agricultural water productivity: Between optimism and caution. *Agricultural Water Management, 97*(4), 528-535.

Moncrieff, J., Clement, R., Finnigan, J., & Meyers, T. (2004). Averaging, Detrending, and Filtering of Eddy Covariance Time Series. In X. Lee, W. Massman & B. Law (Eds.), *Handbook of Micrometeorology* (Vol. 29, pp. 7-31): Springer Netherlands.

Moore, C. J. (1986). Frequency response corrections for eddy correlation systems. *Boundary-Layer Meteorol., 37*(1), 17-35. doi: 10.1007/bf00122754

Mudge, P. L., Wallace, D. F., Rutledge, S., Campbell, D. I., Schipper, L. A., & Hosking, C. L. (2011). Carbon balance of an intensively grazed temperate pasture in two climatically contrasting years. *Agric., Ecosyst. Environ., 144*(1), 271-280. doi: 10.1016/j.agee.2011.09.003

Mueller, K. L., Yadav, V., Curtis, P. S., Vogel, C., & Michalak, A. M. (2010). Attributing the variability of eddy-covariance CO2 flux measurements across temporal scales using geostatistical

regression for a mixed northern hardwood forest. *Global Biogeochem. Cycles, 24*(3), GB3023. doi: 10.1029/2009gb003642

Murrumbidgee Irrigation Ltd. (2013). Rice water use in the Murrumbidgee Irrigation Area Retrieved March 25, 2013, from http://www.mirrigation.com.au/Customers/Rice-Water-Use-Targets

Murrumbidgee Irrigation Ltd. (2012a). Historical Allocation Availability Retrieved 8th August, 2012, from http://www.mirrigation.com.au/Content/Documents/Historical-Allocation-Availability

Murrumbidgee Irrigation Ltd. (2012b). History Retrieved 18/07/2012, from http://www.mirrigation.com.au/Centenary/History

Neftel, A., Spirig, C., & Ammann, C. (2008). Application and test of a simple tool for operational footprint evaluations. *Environ. Pollut., 152*(3), 644-652.

Ohtaki, E. (1980). Turbulent transport of carbon dioxide over a paddy field. *Boundary-Layer Meteorol., 19*(3), 315-336. doi: 10.1007/bf00120595

Oncley, S. P., Foken, T., Vogt, R., Kohsiek, W., DeBruin, H. A. R., Bernhofer, C., Christen, A., van Gorsel, E., Grantz, D., Feigenwinter, C., Lehner, I., Liebethal, C., Liu, H., Mauder, M., Pitacco, A., Ribeiro, L., & Weidinger, T. (2007). The Energy Balance Experiment EBEX-2000. Part I: overview and energy balance. *Boundary-Layer Meteorol., 123*(1), 1-28.

Oncley, S. P., & Friehe, C. A. (1996). Surface-layer fluxes, profiles, and turbulence measurements over uniform terrain under near-neutral conditions. [Article]. *Journal of the Atmospheric Sciences, 53*(7), 1029.

Pasquill, F. (1972). Some aspects of boundary layer description. *Quart.J. Roy. Meteorol. Soc., 98*(417), 469-494. doi: 10.1002/qj.49709841702

Pasquill, F., & Smith, F. B. (1983). *Atmospheric Diffusion* (Third ed.). New York: Wiley.

Peng, Y., Gitelson, A. A., Keydan, G., Rundquist, D. C., & Moses, W. (2011). Remote estimation of gross primary production in maize and support for a new paradigm based on total crop chlorophyll content. *Remote Sensing of Environment, 115*(4), 978-989. doi: 10.1016/j.rse.2010.12.001

Ramankutty, N., Evan, A. T., Monfreda, C., & Foley, J. A. (2008). Farming the planet: 1. Geographic distribution of global agricultural lands in the year 2000. *Global Biogeochem. Cycles, 22*(1), GB1003. doi: 10.1029/2007gb002952

Rao, P. (2008). *Agricultural Meteorology*. New Delhi, India: Prentice-Hall of India Pty. Ltd.

Rebmann, C., Göckede, M., Foken, T., Aubinet, M., Aurela, M., Berbigier, P., Bernhofer, C., Buchmann, N., Carrara, A., Cescatti, A., Ceulemans, R., Clement, R., Elbers, J. A., Granier, A., Grünwald, T., Guyon, D., Havránková, K., Heinesch, B., Knohl, A., Laurila, T., Longdoz, B., Marcolla,

B., Markkanen, T., Miglietta, F., Moncrieff, J., Montagnani, L., Moors, E., Nardino, M., Ourcival, J. M., Rambal, S., Rannik, Ü., Rotenberg, E., Sedlak, P., Unterhuber, G., Vesala, T., & Yakir, D. (2005). Quality analysis applied on eddy covariance measurements at complex forest sites using footprint modelling. *Theor. Appl. Climatol., 80*(2), 121-141. doi: 10.1007/s00704-004-0095-y

Reynolds, O. (1895). On the Dynamical Theory of Incompressible Viscous Fluids and the Determination of the Criterion. *Philosophical Transactions of the Royal Society of London. A, 186*(ArticleType: research-article / Full publication date: 1895 / Copyright © 1895 The Royal Society), 123-164.

Richardson, A. D., & Hollinger, D. Y. (2005). Statistical modelling of ecosystem respiration using eddy covariance data: Maximum likelihood parameter estimation, and Monte Carlo simulation of model and parameter uncertainty, applied to three simple models. *Agric. For. Meteorol., 131*(3-4), 191-208. doi: 10.1016/j.agrformet.2005.05.008

Rocha, A. V., & Goulden, M. L. (2009). Why is marsh productivity so high? New insights from eddy covariance and biomass measurements in a Typha marsh. *Agric. For. Meteorol., 149*(1), 159-168. doi: 10.1016/j.agrformet.2008.07.010

Rosenberg, N. J. (1974). *Microclimate - The Biological Environment* (First ed.). New York, London, Sydney, Toronto: Wiley-Interscience Publications.

Rossini, M., Cogliati, S., Meroni, M., Migliavacca, M., Galvagno, M., Busetto, L., Cremonese, E., Julitta, T., Siniscalco, C., Morra di Cella, U., & Colombo, R. (2010). Remote sensing-based estimation of gross primary production in a subalpine grassland. *Biogeosciences Discuss., 9*(2). doi: 10.5194/bgd-9-1711-2012

Rowan, T. S. C., Maier, H. R., Connor, J., & Dandy, G. C. (2011). An integrated dynamic modelling framework for investigating the impact of climate change and variability on irrigated agriculture. *Water Resour. Res., 47*(7), W07520. doi: 10.1029/2010wr010195

Sadras, V., & McDonald, G. (2012). Water use efficiency of grain crops in Australia: principles, benchmarks and management: Grains Research and Development Corporation, South Australian Research and Development Institute and University of Adelaide.

Saiki, E. M., Moeng, C.-H., & Sullivan, P. P. (2000). Large-Eddy Simulation Of The Stably Stratified Planetary Boundary Layer. *Boundary-Layer Meteorol., 95*(1), 1-30. doi: 10.1023/a:1002428223156

Saito, M., Miyata, A., Nagai, H., & Yamada, T. (2005). Seasonal variation of carbon dioxide exchange in rice paddy field in Japan. *Agric. For. Meteorol., 135*(1-4), 93-109. doi: 10.1016/j.agrformet.2005.10.007

Scanlon, T. M., & Kustas, W. P. (2010). Partitioning carbon dioxide and water vapor fluxes using correlation analysis. *Agric. For. Meteorol., 150*(1), 89-99. doi: 10.1016/j.agrformet.2009.09.005

Schmid, H. P. (2002). Footprint modelling for vegetation atmosphere exchange studies: a review and perspective. *Agric. For. Meteorol., 113*(1-4), 159-183. doi: 10.1016/s0168-1923(02)00107-7

Schmidt, M., Reichenau, T. G., Fiener, P., & Schneider, K. (2012). The carbon budget of a winter wheat field: An eddy covariance analysis of seasonal and inter-annual variability. *Agric. For. Meteorol., 165*(0), 114-126. doi: 10.1016/j.agrformet.2012.05.012

Schultz, T. (2011). fcnwindrose: Mathworks, Inc.

Schwarz, G. (1978). Estimating the Dimension of a Model. *Annals of Statistics, 6*(2), 461-464. doi: 10.1214/aos/1176344136

Scott, R. L., Huxman, T. E., Cable, W. L., & Emmerich, W. E. (2006). Partitioning of evapotranspiration and its relation to carbon dioxide exchange in a Chihuahuan Desert shrubland. *Hydrol. Processes, 20*(15), 3227-3243. doi: 10.1002/hyp.6329

Scott, R. L., Serrano-Ortiz, P., Domingo, F., Hamerlynck, E. P., & Kowalski, A. S. (2012). Commonalities of carbon dioxide exchange in semiarid regions with monsoon and Mediterranean climates. *J. Arid Environ., 84*(0), 71-79. doi: 10.1016/j.jaridenv.2012.03.017

Smith, D. (2013, March 25). [Rice water use in the CIA].

Smith, M., & Nayar, M. (2008). *The first stage of Coleambally Water Smart Australia Project: Building on CICL's adoption of Total Channel Control (TCC)*. Paper presented at the Irrigation Australia National Conference and Exhibition, Melbourne, Australia.

Spiertz, H. (2012). Avenues to meet food security. The role of agronomy on solving complexity in food production and resource use. *European Journal of Agronomy, 43*(0), 1-8. doi: 10.1016/j.eja.2012.04.004

Spirig, C., & Neftel, A. (2007). The Art Footrpint Tool (Version 11.3.2007).

Steduto, P., Hsiao, T. C., & Fereres, E. (2007). On the conservative behavior of biomass water productivity. *Irrigation Science, 25*(3), 189-207. doi: 10.1007/s00271-007-0064-1

Stoy, P. C., Katul, G. G., Siqueira, M. B. S., Juang, J. Y., McCarthy, H. R., Kim, H., Oishi, A. C., & Oren, R. (2005). Variability in net ecosystem exchange from hourly to inter-annual time scales at adjacent pine and hardwood forests: a wavelet analysis. *Tree Physiology, 25*, 887-902.

Stoy, P. C., Katul, G. G., Siqueira, M. B. S., Juang, J. Y., Novick, K. A., Uebelherr, J. M., & Oren, R. (2006). An evaluation of models for partitioning eddy covariance-measured net ecosystem exchange into photosynthesis and respiration.

[Article]. *Agric. For. Meteorol., 141*(1), 2-18. doi: 10.1016/j.agrformet.2006.09.001

Stoy, P. C., Mauder, M., Foken, T., Marcolla, B., Boegh, E., Ibrom, A., Arain, M. A., Arneth, A., Aurela, M., Bernhofer, C., Cescatti, A., Dellwik, E., Duce, P., Gianelle, D., van Gorsel, E., Kiely, G., Knohl, A., Margolis, H., McCaughey, H., Merbold, L., Montagnani, L., Papale, D., Reichstein, M., Saunders, M., Serrano-Ortiz, P., Sottocornola, M., Spano, D., Vaccari, F., & Varlagin, A. (2013). A data-driven analysis of energy balance closure across FLUXNET research sites: The role of landscape scale heterogeneity. *Agric. For. Meteorol., 171–172*(0), 137-152. doi: http://dx.doi.org/10.1016/j.agrformet.2012.11.004

Stoy, P. C., Richardson, A. D., Baldocchi, D. D., Katul, G. G., Stanovick, J., Mahecha, M. D., Reichstein, M., Detto, M., Law, B. E., Wohlfahrt, G., Arriga, N., Campos, J., McCaughey, J. H., Montagnani, L., U, K. T. P., Sevanto, S., & Williams, M. (2009). Biosphere-atmosphere exchange of CO2 in relation to climate: a cross-biome analysis across multiple time scales. [Article]. *Biogeosciences, 6*(10), 2297-2312.

Sulman, B. N., Desai, A. R., Schroeder, N. M., Ricciuto, D., Barr, A., Richardson, A. D., Flanagan, L. B., Lafleur, P. M., Tian, H., Chen, G., Grant, R. F., Poulter, B., Verbeeck, H., Ciais, P., Ringeval, B., Baker, I. T., Schaefer, K., Luo, Y., & Weng, E. (2012). Impact of hydrological variations on modelling of peatland CO2 fluxes: Results from the North American Carbon Program site synthesis. *J. Geophys. Res., 117*(G1), G01031. doi: 10.1029/2011jg001862

Suyker, A. E., & Verma, S. B. (2008). Interannual water vapor and energy exchange in an irrigated maize-based agroecosystem. *Agric. For. Meteorol., 148*(3), 417-427. doi: 10.1016/j.agrformet.2007.10.005

Suyker, A. E., & Verma, S. B. (2010). Coupling of carbon dioxide and water vapor exchanges of irrigated and rainfed maize-soybean cropping systems and water productivity. *Agric. For. Meteorol., 150*(4), 553-563.

Suyker, A. E., & Verma, S. B. (2012). Gross primary production and ecosystem respiration of irrigated and rainfed maize–soybean cropping systems over 8 years. *Agric. For. Meteorol., 165*(0), 12-24. doi: 10.1016/j.agrformet.2012.05.021

Suyker, A. E., Verma, S. B., Burba, G. G., & Arkebauer, T. J. (2005). Gross primary production and ecosystem respiration of irrigated maize and irrigated soybean during a growing season. *Agric. For. Meteorol., 131*(3-4), 180-190. doi: 10.1016/j.agrformet.2005.05.007

Tallec, T., Béziat, P., Jarosz, N., Rivalland, V., & Ceschia, E. (2013). Crops' water use efficiencies in temperate climate: Comparison of stand, ecosystem and agronomical approaches. *Agric. For. Meteorol., 168*(0), 69-81. doi: 10.1016/j.agrformet.2012.07.008

The MathWorks Inc. (2010). MATLAB (Version 7.10.0 (R2010a)). Natick, MA, USA: The MathWorks Inc.

Thom, A. S. (1975). *Momentum, Mass and Heat Exchange of Plant Communities: edited by J.L. Monteith*.

Tsai, J.-L., Tsuang, B.-J., Lu, P.-S., Yao, M.-H., & Yuan, S. (2007). *Surface Energy Components and Land Characteristics of a Rice Paddy* (Vol. 46). Boston, MA, U.S.A.: American Meteorological Society.

Twine, T. E., Kustas, W. P., Norman, J. M., Cook, D. R., Houser, P. R., Meyers, T. P., Prueger, J. H., Starks, P. J., & Wesely, M. L. (2000). Correcting eddy-covariance flux underestimates over a grassland. *Agric. For. Meteorol., 103*(3), 279-300.

Ullah, M. K. (2011). *A Geoinformatics Approach for Spatial Water Accounting and Irrigation Demand Forecasting for a Gravity Irrigation System.* Doctor of Philosophy, Charles Sturt University, Wagga Wagga.

Van Dijk, A., & Dolman, A. J. (2004). Estimates of CO2 uptake and release among European forests based on eddy covariance data. [Article]. *Global Change Biol., 10*(9), 1445-1459. doi: 10.1111/j.1365-2486.2004.00831.x

Vermeulen, S. J., Aggarwal, P. K., Ainslie, A., Angelone, C., Campbell, B. M., Challinor, A. J., Hansen, J. W., Ingram, J. S. I., Jarvis, A., Kristjanson, P., Lau, C., Nelson, G. C., Thornton, P. K., & Wollenberg, E. (2012). Options for support to agriculture and food security under climate change. *Environmental Science and Policy, 15*(1), 136-144. doi: 10.1016/j.envsci.2011.09.003

Vesala, T., Kljun, N., Rannik, Ü., Rinne, J., Sogachev, A., Markkanen, T., Sabelfeld, K., Foken, T., & Leclerc, M. Y. (2008). Flux and concentration footprint modelling: State of the art. *Environ. Pollut., 152*(3), 653-666. doi: 10.1016/j.envpol.2007.06.070

Vickers, D., & Mahrt, L. (1997). Quality Control and Flux Sampling Problems for Tower and Aircraft Data. [Article]. *Journal of Atmospheric & Oceanic Technology, 14*(3), 512.

Von Randow, C., Kruijt, B., Holtslag, A. A. M., & de Oliveira, M. B. L. (2008). Exploring eddy-covariance and large-aperture scintillometer measurements in an Amazonian rain forest. [Article]. *Agric. For. Meteorol., 148*(4), 680-690. doi: 10.1016/j.agrformet.2007.11.011

Vourlitis, G. L., Priante, N., Hayashi, M. M. S., Nogueira, J. D., Caseiro, F. T., & Campelo, J. H. (2001). Seasonal variations in the net ecosystem CO2 exchange of a mature Amazonian transitional tropical forest (cerradao). *Funct. Ecol., 15*(3), 388-395. doi: 10.1046/j.1365-2435.2001.00535.x

Wang, X., Ma, M., Huang, G., Veroustraete, F., Zhang, Z., Song, Y., & Tan, J. (2012). Vegetation primary production estimation at maize and alpine meadow over the Heihe River Basin, China. *IJAEO, 17*(0), 94-101. doi: 10.1016/j.jag.2011.09.009

Ward, P. R., Micin, S. F., & Fillery, I. R. P. (2012). Application of eddy covariance to determine ecosystem-scale carbon balance and evapotranspiration in an agroforestry system. *Agric. For. Meteorol.*, *152*(0), 178-188. doi: 10.1016/j.agrformet.2011.09.016

Watson, R. T., & IPCC. (2000). *Land use, land-use change, and forestry : a special report of the Intergovernmental Panel on Climate Change*. Cambridge: Cambridge University Press.

Watt, J. (2008). *The effect of irrigation on surface-groundwater interactions: Quantifying time-dependent spatial dynamics in irrigation systems.* Doctor of Philosophy, Charles Sturt University, Wagga Wagga.

Webb, E. K., Pearman, G. I., & Leuning, R. (1980). Correction of flux measurements for density effects due to heat and water vapour transfer. *Quart.J. Roy. Meteorol. Soc.*, *106*(447), 85-100. doi: 10.1002/qj.49710644707

Wilczak, J. M., Oncley, S. P., & Stage, S. A. (2001). Sonic Anemometer Tilt Correction Algorithms. [Article]. *Boundary-Layer Meteorol.*, *99*(1), 127-150.

Wilhelmi, O. V., Hubbard, K. G., & Wilhite, D. A. (2002). Spatial representation of agroclimatology in a study of agricultural drought. *International Journal of Climatology*, *22*(11), 1399-1414. doi: 10.1002/joc.796

Wilson, K., Goldstein, A., Falge, E., Aubinet, M., Baldocchi, D., Berbigier, P., Bernhofer, C., Ceulemans, R., Dolman, H., Field, C., Grelle, A., Ibrom, A., Law, B. E., Kowalski, A., Meyers, T., Moncrieff, J., Monson, R., Oechel, W., Tenhunen, J., Valentini, R., & Verma, S. (2002a). Energy balance closure at FLUXNET sites. *Agric. For. Meteorol.*, *113*(1-4), 223-243.

Wilson, K. B., Baldocchi, D. D., Aubinet, M., Berbigier, P., Bernhofer, C., Dolman, H., Falge, E., Field, C., Goldstein, A., Granier, A., Grelle, A., Halldor, T., Hollinger, D., Katul, G., Law, B. E., Lindroth, A., Meyers, T., Moncrieff, J., Monson, R., Oechel, W., Tenhunen, J., Valentini, R., Verma, S., Vesala, T., & Wofsy, S. (2002b). Energy partitioning between latent and sensible heat flux during the warm season at FLUXNET sites. *Water Resour. Res.*, *38*(12). doi: 1294.10.1029/2001wr000989

Wohlfahrt, G., Bahn, M., Haslwanter, A., Newesely, C., & Cernusca, A. (2005). Estimation of daytime ecosystem respiration to determine gross primary production of a mountain meadow. *Agric. For. Meteorol.*, *130*(1–2), 13-25. doi: 10.1016/j.agrformet.2005.02.001

Wohlfahrt, G., & Widmoser, P. (2013). Can an energy balance model provide additional constraints on how to close the energy imbalance? *Agric. For. Meteorol.*, *169*(0), 85-91. doi: http://dx.doi.org/10.1016/j.agrformet.2012.10.006

World Bank. (2007). *World Development Report 2008: Agriculture for Development*. Washington, DC: World Bank.

Wu, Q., Christen, E., & Enever, D. (2000). BASINMAN - A water balance model for farms with subsurface pipe drainage and on-farm basin *On-farm and community-scale salt disposal basins on the Riverine Plain*: CSIRO Land and Water.

Xiao, X., Zuo, H. C., Yang, Q. D., Wang, S. J., Wang, L. J., Chen, J. W., Chen, B. L., & Zhang, B. D. (2012). On the factors influencing surface-layer energy closure and their seasonal variability over the semi-arid Loess Plateau of Northwest China. *Hydrol. Earth Syst. Sci.*, *16*(3), 893-910. doi: 10.5194/hess-16-893-2012

Yadav, V., Mueller, K. L., Dragoni, D., & Michalak, A. M. (2010). A geostatistical synthesis study of factors affecting gross primary productivity in various ecosystems of North America. *Biogeosciences*, *7*(9), 2655-2671. doi: 10.5194/bg-7-2655-2010

Yan, H., Fu, Y., Xiao, X., Huang, H. Q., He, H., & Ediger, L. (2009a). Modeling gross primary productivity for winter wheat–maize double cropping system using MODIS time series and CO2 eddy flux tower data. *Agric., Ecosyst. Environ.*, *129*(4), 391-400. doi: 10.1016/j.agee.2008.10.017

Yan, H., Fu, Y., Xiao, X., Huang, H. Q., He, H., & Ediger, L. (2009b). Modelling gross primary productivity for winter wheat–maize double cropping system using MODIS time series and CO2 eddy flux tower data. *Agriculture, Ecosystems & Environment*, *129*(4), 391-400. doi: 10.1016/j.agee.2008.10.017

Yang, R., & Friedl, M. A. (2003). Determination of Roughness Lengths for Heat and Momentum Over Boreal Forests. *Boundary-Layer Meteorol.*, *107*(3), 581-603. doi: 10.1023/a:1022880530523

Yu, Q., Wu, W., Yang, P., Li, Z., Xiong, W., & Tang, H. (2012). Proposing an interdisciplinary and cross-scale framework for global change and food security researches. *Agriculture, Ecosystems & Environment*, *156*(0), 57-71. doi: 10.1016/j.agee.2012.04.026

Zha, T., Barr, A. G., van der Kamp, G., Black, T. A., McCaughey, J. H., & Flanagan, L. B. (2010). Interannual variation of evapotranspiration from forest and grassland ecosystems in western canada in relation to drought. *Agric. For. Meteorol.*, *150*(11), 1476-1484. doi: 10.1016/j.agrformet.2010.08.003

Zhang, P., Chen, S., Zhang, W., Miao, H., Chen, J., Han, X., & Lin, G. (2012). Biophysical regulations of NEE light response in a steppe and a cropland in Inner Mongolia. *Journal of Plant Ecology*, *5*(2), 238-248. doi: 10.1093/jpe/rtr017

Zhang, X., Chen, S., Sun, H., Shao, L., & Wang, Y. (2011a). Changes in evapotranspiration over irrigated winter wheat and maize in North China Plain over three decades. *Agricultural Water Management*, *98*(6), 1097-1104. doi: http://dx.doi.org/10.1016/j.agwat.2011.02.003

Zhang, Y., Shen, Y., Sun, H., & Gates, J. B. (2011b). Evapotranspiration and its partitioning in an irrigated winter

wheat field: A combined isotopic and micrometeorologic approach. *J. Hydrol.*, *408*(3–4), 203-211. doi: 10.1016/j.jhydrol.2011.07.036

Zhang, Z., Jiang, H., Liu, J., Weimin, J., & Xiuying, Z. (2013). Effect of heterogeneous atmospheric CO2 on simulated global carbon budget. *Global Planet. Change*(0). doi: http://dx.doi.org/10.1016/j.gloplacha.2012.12.002

Zhao, F.-H., Yu, G.-R., Li, S.-G., Ren, C.-Y., Sun, X.-M., Mi, N., Li, J., & Ouyang, Z. (2007). Canopy water use efficiency of winter wheat in the North China Plain. *Agric. Water Manage.*, *93*(3), 99-108. doi: 10.1016/j.agwat.2007.06.012

Zhou, Y., Sun, X., Zhu, Z., Zhang, R., Tian, J., Liu, Y., Guan, D., & Yuan, G. (2006). Surface roughness length dynamic over several different surfaces and its effects on modelling fluxes. *Science in China Series D: Earth Sciences*, *49*(0), 262-272. doi: 10.1007/s11430-006-8262-x

Zhu, Z. L., Sun, X. M., Wen, X. F., Zhou, Y. L., Tian, J., & Yuan, G. F. (2006). Study on the processing method of nighttime CO2 eddy covariance flux data in ChinaFLUX. [Article]. *Science in China Series D-Earth Sciences*, *49*, 36-46. doi: 10.1007/s11430-006-8036-5

Zwart, S. J., & Bastiaanssen, W. G. M. (2004). Review of measured crop water productivity values for irrigated wheat, rice, cotton and maize. *Agricultural Water Management*, *69*(2), 115-133. doi: 10.1016/j.agwat.2004.04.007

Zwart, S. J., Bastiaanssen, W. G. M., de Fraiture, C., & Molden, D. J. (2010). A global benchmark map of water productivity for rainfed and irrigated wheat. *Agricultural Water Management*, *97*(10), 1617-1627. doi: http://dx.doi.org/10.1016/j.agwat.2010.05.018